universität wien

MASTERARBEIT / MASTER'S THESIS

Titel der Masterarbeit / Title of the Master's Thesis

„Assessing protein-metal-binding using 'accurate constant via transient incomplete separation' (ACTIS)"

verfasst von / submitted by

Zorica Eric, BSc

angestrebter akademischer Grad / in partial fulfilment of the requirements for the degree of

Master of science (MSc)

Wien, 2024 / Vienna 2024

Studienkennzahl lt. Studienblatt / degree programme code as it appears on the student record sheet:	UA 066 862
Studienrichtung lt. Studienblatt / degree programme as it appears on the student record sheet:	Masterstudium Chemie UG2002
Betreut von / Supervisor:	Univ.-Prof. Dr. Gunda Köllensperger

MASTER'S THESIS

Title of the Master's Thesis

„Assessing protein-metal-binding using 'accurate constant via transient incomplete separation' (ACTIS)"

submitted by

Zorica Eric, BSc

in partial fulfilment of the requirements for the degree of

Master of science (MSc)

This work was performed at the Institute of Analytical Chemistry at BOKU in the group of Prof. Stephan Hann, from March to November 2023, under the guidance of Dr. Sven Kochmann and Dr. Anastassiya Tschaikovsky. I want to thank them for guiding me, offering valuable support, and providing helpful feedback throughout my research.

I would also like to thank Dr. Lisa Fisher, Andreas Brandstätter, and Core Facility Mass Spectrometry Team for their valuable suggestions and technical support in the experimental work.

Abstract (English)

The assessment of biomolecular interactions is one of the main aspects of bioanalytics. All established methods for assessment of protein-compound (PC) binding have inherent sources of inaccuracy. This results in multiple values for the dissociation constant (K_d) differing in few orders of magnitude determined for same model system. Accurate constant via transient incomplete separation (ACTIS) is a recently introduced method, theoretically free from inherent sources of inaccuracy. This method is based on a deterministic process of transient incomplete separation (TIS). The difference in transverse diffusion of free C and PC is the basic for the TIS occurrence. So far ACTIS was only used for assessment of small molecule-protein models. This would be the first protein-metal-binding assessment utilizing ACTIS. To proof our setup, the Humane Serum Albumin (HSA) binding to Fluorescein (FLC) was assessed using ACTIS coupled to fluorescence detector. Furthermore, the compatibility of ACTIS with different detection methods was demonstrated. Our experiments included coupling of ACTIS setup to four different detection methods: fluorescence detection (FLD), time-of-flight mass spectrometry (TOF-MS), inductively coupled plasma mass spectrometry (ICP-MS) and atomic emission spectroscopy (ICP-AES). The binding constant of β-lactoglobulin (BLG) to quercetin-iron (FeQ_2) complex was assessed using ACTIS-TOF-MS. Beside the assessing of K_d, the experiments aiming the improvement of the transient Fe detection with ICP techniques were also conducted. Finally, the impact of the detector configuration, specifically the inner radius of the transfer capillary, was examined *in silico* by employing computer simulations.

Abstract (Deutsch)

Die Bewertung von biomolekularen Interaktionen ist einer der wichtigsten Aspekte der Bioanalytik. Alle etablierten Methoden zur Beurteilung der Bindungsstärke zwischen Protein und einer bindenden Komponente (PC) weisen inhärente Fehlerquellen auf. Dies führ dazu, dass die resultierenden Dissoziationskonstanten (K_d) für dasselbe Modellsystem mehrere Größenordnungen voneinander abweichen. Accurate Constant via Transient Incomplete Separation (ACTIS) ist eine neue Methode zur genauen Bestimmung von K_d, die theoretisch frei von inhärenten Fehlerquellen ist. Diese Methode basiert auf einem deterministischen Prozess der Transient Incomplete Separation (TIS). Die Differenz in der transversalen Diffusion von freiem C und PC ist die Grundlage für das Auftreten von TIS. Bisher wurde ACTIS nur zur Bewertung von Protein-Kleinmolekül-Modellen verwendet. Diese Arbeit stellt den ersten Versuch einer Analyse von Protein-Metall-Bindungen mithilfe von ACTIS dar. Zur Validierung unseres Setups wurde die Bindung von Humanem Serumalbumin (HSA) an Fluorescein (FLC) mithilfe von ACTIS gekoppelt an einem Fluoreszenzdetektor untersucht. Darüber hinaus wurde die Kompatibilität von ACTIS mit verschiedenen Detektionsmethoden demonstriert. Unsere Experimente umfassten die Kopplung des ACTIS-Setups mit vier verschiedenen Detektionsmethoden: Fluoreszenzdetektion (FLD), Flugzeit - Massenspektrometrie (TOF-MS), induktiv gekoppelte Plasma - Massenspektrometrie (ICP-MS) und Atomemissionsspektroskopie (ICP-AES). Die Bindung von Quercetin-Eisen (FeQ_2)-Komplex an β-Lactoglobulin (BLG) wurde mithilfe von ACTIS-TOF-MS untersucht. Neben der K_d – Bestimmung wurden auch Experimente zur Verbesserung der Fe - Detektion mit ICP-Techniken durchgeführt. Abschließend wurde der Einfluss der Detektor-Konfiguration, insbesondere des inneren Radius der Transferkapillare, *in silico* mit Hilfe von Computersimulationen untersucht.

Table of contents

1 Introduction

Molecular interactions of proteins with other biomolecules are crucial for various biochemical reactions and processes. The association and dissociation of protein-compound complexes determines their functionality [1]. Numerous factors including pH value and temperature, can influence the dissociation of such complexes [2]. Thermodynamic stability, which characterizes the tendency of complexes to exist in equilibrium conditions is quantified through the dissociation constant K_d [3].

Dissociation constant is an important characteristic to be evaluated in the pharmacology for drug discovery and design [4]. For instance, the evaluation of drug-receptor binding strength reveals the drugs efficiency. In material chemistry, the dissociation constant of metal complexes is used to predict its redox potential and catalytic properties [5]. More precisely, the dissociation constant provides insights into the stability of metal complexes, which is linked to their ability to undergo redox reactions and catalyze various chemical processes [6].

1.1 Definition of dissociation constant K_d

A reversible chemical reaction of a compound (C) binding to a protein (P) can be described with the following equation:

$$\mathbf{PC} \rightleftarrows \mathbf{P} + \mathbf{C} \qquad (1)$$

At equilibrium, the rates of forward and reverse reactions are equal and all components in the system do not have tendency to change their concentration [7]. Their concentrations at equilibrium define the dissociation constant K_d as follows:

$$\boldsymbol{K_d} = \frac{[\mathbf{P}][\mathbf{C}]}{[\mathbf{PC}]} \qquad (2)$$

$[C]$, $[P]$, and $[PC]$ refer to compound, protein, and complex concentrations at equilibrium, respectively. If we know the starting concentrations of P and C ($[P]_0$ and $[C]_0$) and we are able to determine either the [PC] or [C], the K_d value can be calculated by applying formula (2) on previously calculated or determined [P], [C], and [PC].

Conceptually, determining K_d is relatively simple. In practice, however, it is a challenging task. To find K_d (independent of the starting concentrations), wide range of concentration ratios of $[P]_0$ and $[C]_0$ must be evaluated. The assessment of K_d of a specific PC complex typically involves investigating a mixture with a constant $[C]_0$ and gradually increasing $[P]_0$. For each $[P]_0$, the ratio of [PC] to [C] is determined and K_d is found as the inflection point of the corresponding binding isotherm.

1.2 Established methods for finding K_d

Established methods employed for finding K_d of protein-compound complexes predominantly rely on biosensorics and calorimetric methodologies [8]. The accuracy of K_d may have a high impact on the investigated biochemical or catalyst processes. For example, the detection sensitivity of polymerization-based amplification reactions can be precisely predicted with the K_d value [9]. Moreover, an accurate K_d is crucial for the optimization of drug discovery, with a primary focus on the thermodynamics of the drug-receptor binding [10]. Despite the high impact of accurate K_d values for various applications, obtaining of similar values for one complex may be challenging [11–13]. The most commonly used methods for finding K_d are isothermal titration calorimetry and surface plasmon resonance [14].

Isothermal titration calorimetry (ITC) is considered as gold standard for finding K_d [15]. ITC measures the heat flow between a reference and a measurement cell (Figure 1). The reference cell is filled with the solvent. At the beginning, the measurement cell is filled with the protein or compound solution. Subsequently, the solution of the other complex component is added slowly to the measurement cell while the temperature is kept constant. Any release or absorption of heat is recorded. The heat change corresponds to the change of the fraction of bound compound. With increased compound concentration in the titration cell less heat is absorbed or released and signal saturation occurs. Besides finding K_d, ITC provides direct insight into enthalpy and entropy changes caused by molecular interactions as well as the reaction stoichiometry [16]. These thermodynamic parameters can be used to understand the underlying mechanism of the interaction.

ITC is a direct and label free approach but it possesses some inherent sources of inaccuracy. Very weak binding affinities cause minor heat changes that may not be detected due to instrumental signal-to-noise ratio. Furthermore, even a small amount of impurities as well as nonspecific P-P and C-C binding can have a strong impact on the final results and potentially lead to false conclusions [17].

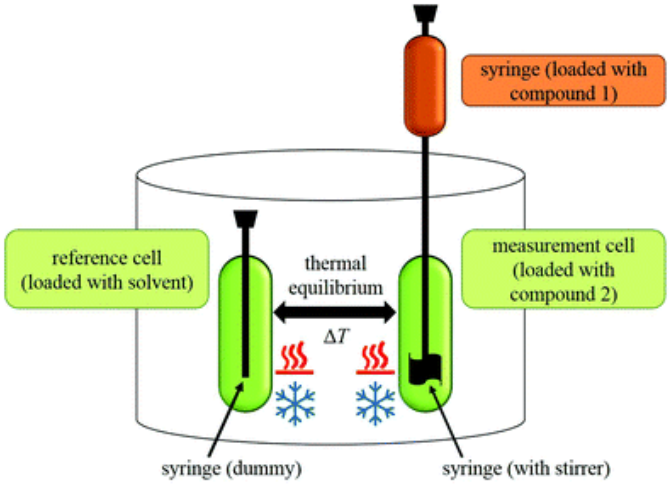

Figure 1: The schematic illustration of ITC. Reproduced from [18] with permission from the Royal Society of Chemistry.

Surface plasmon resonance (SPR) is a biosensorics technique based on a phenomenon known as a surface plasmon resonance [19]. SPR refers to the resonant oscillations of free metal electrons when polarized light strikes a thin metal layer. In SPR protein or compound molecules are immobilized on a thin gold layer fixed on a transparent prism (Figure 2). The thickness of the gold layer is commonly within the range of few hundreds to thousands angstroms (Å) [20]. A microfluidic system is used to continuously propagate the solution of the other complex component on the gold surface and a light source excites the gold from the bottom side. Biomolecular interactions cause the changes in refractive index consequently changing the resonance angle, which is used as SPR signal.

SPR signals can reveal information about binding kinetics and affinity. The main limitation of SPR for finding K_d is its sensitivity. Low mass molecules cause minor changes of the angle of refraction that may not be detectable. The immobilization of biomolecules represents another source of inaccuracy since it can greatly affect the investigated affinity [21].

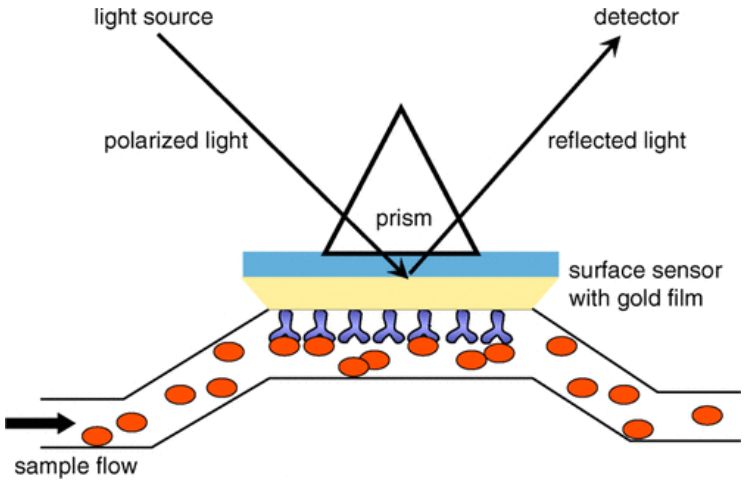

Figure 2: Schematic illustration of SPR. Adapted with permission from [22]. Copyright 2023 American Chemical Society.

Due to such sources of inaccuracies, variations of up to 100-fold in K_d values for the same PC are gained from different determination methods applied by different researchers [23]. Therefore, a new approach with absence of inherent sources of inaccuracy is desired in order to avoid false conclusions caused by unreliable K_d values. A new method that is based on a deterministic phenomenon would have a potential to greatly improve the determination of K_d. Basic advantage of such method would be the possibility to explain and consequently to predict the experimental outcome more reliably. A potential candidate, "Accurate constant via transient incomplete separation" (ACTIS) was introduced as a method based on a deterministic phenomenon and hypothetically free of inherent sources of inaccuracy [24].

1.3 Accurate constant via transient incomplete separation (ACTIS)

ACTIS is a recently introduced method for assessing K_d [24]. Theoretically, this method is free of inherent sources of inaccuracy and thus highly promising to become a reference-standard method for finding K_d values [25].

The principle of transient incomplete separation (TIS) is used in ACTIS to determine unbound C. TIS is a phenomenon that was first described in 1910. [26]. Over the last forty years it was extensively studied in experiments and simulations [27-28]. The concept of TIS is based on a characteristic flow profile of species in laminar pipe flow depending on their transverse diffusion. In a capillary of length l and inner radius r, the liquid is propagated by a pressure gradient between capillary ends. A characteristic parabolic flow profile occurs in this laminar pipe flow [28]. In this flow profile, the maximal velocity lies in the centre of the capillary. With increased distance from the capillary centre, the velocity is reduced gradually until it finally reaches 0 at the capillary walls [29]. Therefore, molecules in the capillary experience a different velocity, depending on their lane as presented in Figure 3.

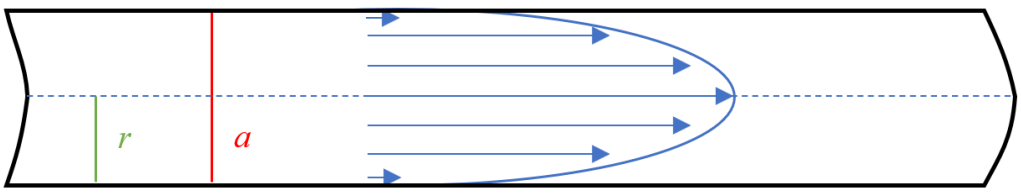

Figure 3: Velocity distribution in parabolic flow profile with r as a variable along the radius a of the capillary, from r = 0 to r = a

The molecules in the capillary centre, experience the maximal flow velocity v_{max}:

$$\boldsymbol{v_{max} = 2 \times v_{mean}} \qquad (3)$$

The average velocity of molecules is determined in dependence of flow rate Q and capillary diameter a:

$$v_{mean} = \frac{Q}{\pi \times a^2} \quad (4)$$

The velocity of all molecules as function of r (the distance of the molecule from the centreline) is described with the following formula:

$$v(r) = v_{max} \times \left(1 - \frac{r^2}{a^2}\right) \quad (5)$$

The flow profile of molecules in a capillary is mainly influenced by how they shift lanes while traveling in a straight line. This shifting movement, known as transverse diffusion, affects how quickly molecules can switch between the centre and the walls of a capillary. In general, molecules at the capillary center move faster compared to those near the capillary wall (Figure 3).

When transverse diffusion is low, molecules move slowly between the capillary center and its walls. With time, variations in velocity became more apparent and this results in a flow profile shown in Figure 4A. On the other hand, high transverse diffusion allows molecules to smoothly change positions within the capillary. Therefore, their velocities became more similar with the time resulting in a more evenly balanced flow profile (Figure 4B).

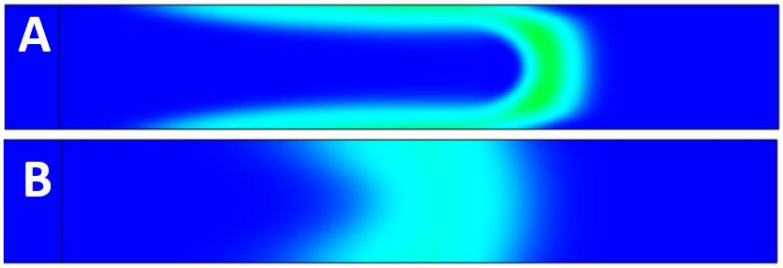

Figure 4: Different flow profiles resulting from different transversal diffusion constants of the molecules. Flow profile of the high (A) and the low (B) diffuse molecules

Different flow profiles caused by difference in a transversal diffusion of molecule species, such as C and PC, result in transient incomplete separation (TIS) [24]. If the difference of transversal diffusions of C and PC is about an order of magnitude, then the propagation of their mixture in a capillary will result in a combination of two different flow profiles. Low transverse diffusion of PC will cause faster propagation around the capillary centre compared to C. C molecules at the capillary centre propagate a bit slower due to a higher rate of transversal position changes. The time point at which the signal of eluted C reaches its maximum is denoted as a characteristic time of transverse diffusion, τ_C. In the short time window around τ_C, denoted as a transitional stage, the small portion of PC moves faster than C molecules while a tail of PC near the capillary walls moves slower than C. As a result, incomplete separation of PC and C occurs, since their concentration profiles overlap (see Figure 5).

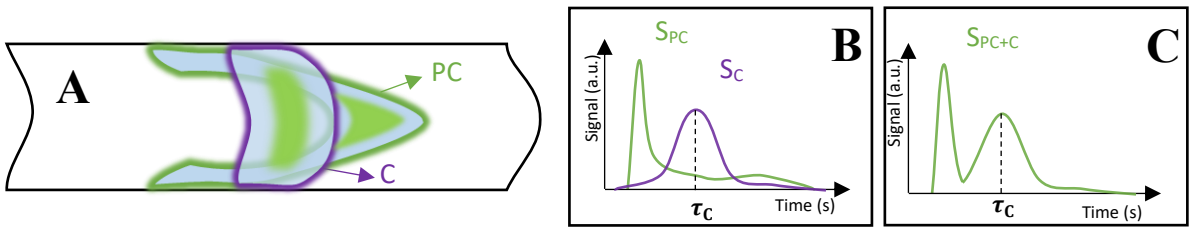

Figure 5: Transitional stage of an equilibrated mixture of P and C propagated through a capillary. Different flow profiles of PC and C fraction occur (A). Overlapping concentration profiles of C from PC and C fractions (B). Resulting cumulative C signal (C).

The diffusion coefficient of C, μ_C and the capillary inner radius r define τ_C as:

$$\boldsymbol{\tau_C = \frac{r^2}{\mu_C}} \tag{6}$$

The flow rate used to propagate the plug of equilibrated mixture of PC, P and C is chosen based on capillary length l and previously calculated τ_C:

$$\boldsymbol{Q = \frac{l}{\tau_C}} \tag{7}$$

At the end of the capillary in which the mixture is propagated, eluted fluid is transferred directly into a detection system, which quantifies the presence of C in it over the time. The resulting signal presents the cumulative C signal of both PC and C fractions. This cumulative C signal over the time is further denoted as a *separagram*. An example of separagram is given in Figure 5C. While separagram includes C signals of the entire ACTIS measurement, the separation peak refers to a segment of the separagram specifically indicating a compound signal during the separation step of the ACTIS measurement.

The following paragraphs describes the application of TIS to assess the K_d of a PC complex in ACTIS. Due to significantly smaller size of C molecules compared to the PC complex, their diffusion is considerably greater, resulting in different flow profiles. Thus, the concept of TIS can be applied to determine the fraction of unbound C in the equilibrium mixture of P, PC, and C. If the initial C and P concentrations are known, the determination of unbound C can be used to find the K_d. The fraction of free C is defined as R:

$$\boldsymbol{R = \frac{[C]}{[C]_0}} \tag{8}$$

Where [C] refers to a concentration of free C molecules in the equilibrium mixture and $[C]_0$ refers to a concentration of C added into the mixture.

When different equilibrated PC mixtures, with constant $[C]_0$ and varying concentration of P added into the mixture ($[P]_0$) are measured, R will also change depending on $[P]_0$ and K_d of PC complex. *Binding isotherm* represents the dependence of R on $[P]_0$ [30]. If we can determine the R values, K_d can be found as the deflection point of the binding isotherm as presented in Figure 6.

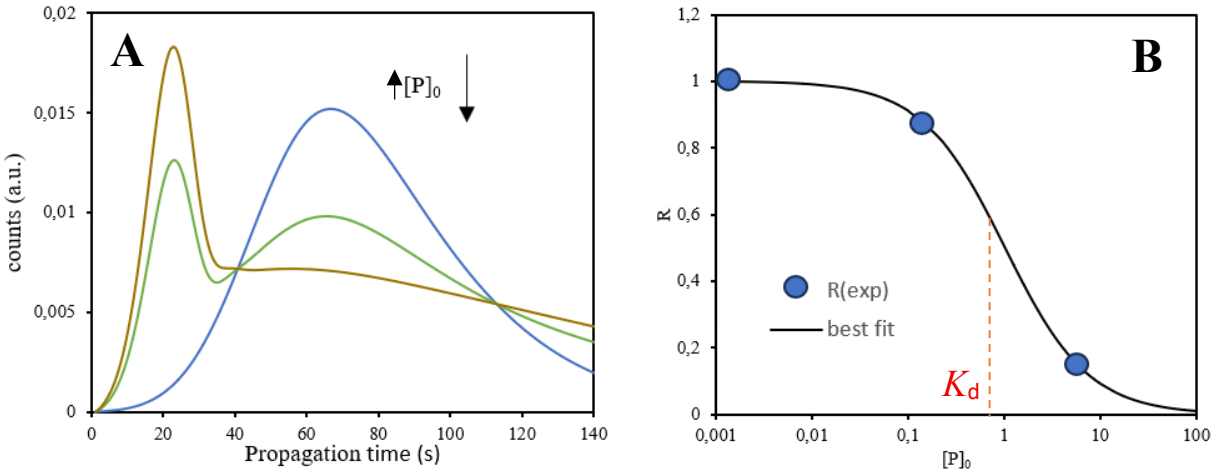

Figure 6: Resulting C signals of three equilibrated mixtures with constant $[C]_0$ and varying $[P]_0$ (A) and the resulting binding isotherm (B).

The cumulative signal of C, S, is calculated from R as follows:

$$\boldsymbol{S = S_C \times R + S_{PC} \times (1 - R)} \qquad (9)$$

where S_C corresponds to pure compound signal and S_{PC} represents the signal of the pure PC complex. The transformation of equation 9 gives the formula for calculation of experimental R, R_{exp} from the corresponding C signals:

$$\boldsymbol{R_{exp} = \frac{S - S_{PC}}{S_C - S_{PC}}} \qquad (10)$$

At very high $[P]_0$ added into a mixture, we assume that nearly all the C molecules are incorporated into the PC complex. Therefore, the compound signal at very high protein concentrations $S_{[P]_0 \gg K_d}$ is approximately equal to the S_{PC}. Analogous to that, compound signal at very low protein concentrations, $S_{[P]_0 \ll K_d}$ is approximately equal to the S_C.

If we measure PC mixtures with constant $[C]_0$ and following $[P]_0$ variations: $[P]_0 \gg K_d$, $[P]_0 \ll K_d$ and an arbitrary $[P]_0$, the equation 10 can be written as:

$$\boldsymbol{R_{exp} \approx \frac{S_{[P]_0} - S_{[P]_0 \gg K_d}}{S_{[P]_0 \ll K_d} - S_{[P]_0 \gg K_d}}} \qquad (11)$$

where $S_{[P]_0}$ refers to a S resulting from measurement of an equilibrated mixture with an arbitrary $[P]_0$ added into it.

Finally, a theoretical R_{theo} function is used to fit the experimental data R_{exp}. The R_{theo} values are calculated by applying following formula in which an arbitrary value is used for K_d as a starting value.

$$\boldsymbol{R_{theo} = -\frac{K_d + [P]_0 - [C]_0}{2[C]_0} + \sqrt{\left(\frac{K_d + [P]_0 - [C]_0}{2[C]_0}\right)^2 + \frac{K_d}{[C]_0}}} \qquad (10)$$

Two essential conditions must be met to achieve accurate K_d values: the reaction should be at equilibrium and the experiment must be done in the so-called binding regime [31-32]. More precisely, the $[C]_0$ is the limiting component and if it is similar to the K_d value, the resulting K_d will be affected by titration. Therefore, the ratio $[C]_0/K_d$ should be optimally 1/100.

Since the TIS relies on a deterministic process, it can be accurately described by using a differential equation system and without empirical coefficients known. Consequently, ACTIS separagrams can be computer-simulated allowing a comprehensive in-silico evaluation of ACTIS performance, including its accuracy [33].

Finally, let's briefly look at the experimental implementation of ACTIS. After a system consisting of P and C is selected for assessment, an appropriate detection system needs to be chosen. The choice of the detection system depends on the PC properties and detection system limitations. If the K_d of the PC is unknown, computer simulations or preliminary experiments can be used to estimate the K_d value. Based on the estimated K_d, the maximum $[C]_0$ can be determined. Subsequently, the mixtures of PC with constant $[C]_0$ and varying $[P]_0$ are prepared. After the equilibration of the PC mixtures, the actual ACTIS experiment is performed. One ACTIS experiment refers to a set of measurements of prepared PC mixtures. Typically, ten PC mixtures are prepared for a single ACTIS experiment. Each prepared mixture has multiple replicates, and each replicate is denoted as an ACTIS run. One run typically lasts about four minutes. In standard experiments, six replicates of each equilibrated mixture are performed. Including the time required for sample changing, the overall time for one whole ACTIS experiment is approximately four hours.

1.4 Thesis scope

ACTIS was firstly introduced in 2019 bringing a significant improvement to analytical methods for finding K_d [34]. Since then, various model systems have been evaluated using ACTIS. Using the fluorescence detector coupled to ACTIS, K_d for bovine serum albumin and fluorescein was determined to be 28 ± 6 µmol L^{-1}. By using MS as the detector, the K_d value for the same model system was found to be 31 ± 6 µmol L^{-1} [24]. ACTIS coupled with MS as the detector assessed K_d of 1.4 ± 0.2 µmol L^{-1} for the alpha-1-acidglycoprotein - alprenolol model system [24]. In further experiment, the investigations of binding of similar-sized molecules were performed. More specifically, K_d value of 0.12 nmol L^{-1} for the Mut-S binding aptamer model system was found [30]. Simultaneously, the computer simulations were investigated and Python script for evaluation was developed. The brief overview of already performed ACTIS investigations is given in Table 1.

Table 1: The overview of reported ACTIS experiments up until now

Protein	Compound	Detection	K_d	*Reference*
BSA	Fluorescein	Fluorescence	22 ± 2 µmol L^{-1}	[24]
BSA	Fluorescein	Mass spectrometry	31 ± 4 µmol L^{-1}	[24]
AGP[1]	Alprenolol	Mass spectrometry	1.4 ± 0.2 µmol L^{-1}	[24]
Mut-S protein[2]	Aptamer	Mass spectrometry	0.12 nmol L^{-1}	[30]

[1]α-1-acid glyco protein, [2]His-tagged recombinant Thermus aquaticus Mut-S protein

Despite the broad range of ACTIS experiments, no experiments have been reported for the assessment of protein-metal binding. Therefore, this work was intended to further explore ACTIS applicability to these systems. This includes the following points:

- The building up and the evaluation of ACTIS setup functionality
- The evaluation of feasibility of selected protein-metal model system for ACTIS experiments
- The actual assessment of K_d of selected protein-metal model system employing ACTIS

The first stage of this work includes establishing an ACTIS setup since no ACTIS instrument existed at BOKU at the start of this project. Notably, ACTIS setup is not commercially available. It is crucial to detailly test the setup's stability and to find optimal solutions for maintaining constant and reproducible flow rates. Moreover, the optimal duration of individual run steps should be determined.

In the next stage, the functionality of the ACTIS setup must be evaluated in terms of actual K_d assessment. To achieve this, experiments using a relatively simple model system, preferably one previously investigated with ACTIS, will be conducted. The similarity of the results with prior ACTIS experiments will serve as a clear indicator of the instrumentation's suitability for further studies.

The selected protein-metal model system should be explored regarding protein and compound stability, solubility, and signal intensity in the chosen detection system. This step also includes first ACTIS experiment on this system in order to further explore its feasibility. Furthermore, the optimal $[C]_0$ for working solution for actual ACTIS experiment will be determined in this step.

Then, all the findings and results from the previously described points should be considered to enable successful assessment of K_d of a protein-metal complex. To the best of our knowledge, this would be the first protein-metal-binding assessment utilizing ACTIS. In addition to the main goal, several additional tasks need be done to enhance ACTIS as a method. In order to improve assessment of protein-metal systems, different detection systems need to be evaluated. In particular, detection methods which enable direct precise metal determination should be explored. Potential issues will be investigated, documented, and assessed with experimental and computational tools.

The possibility of assessing K_d of metal-protein complexes via ACTIS would be a significant extension of the application range. More metal detection systems with even lower LOQs, LODs, and signal-to-noise ratios could be coupled with ACTIS. Lower LOQ, LOD, and signal-to-noise would increase the range of accessible K_d values and, in turn, the range of investigated complexes.

2 Materials and methods

2.1 Model systems

In this work the assessing of K_d of two different model systems was done. The binding pairs: human serum albumin (HSA) and fluorescein (FLC) as well as β-lactoglobulin (BLG), quercetin (Q) and iron (Fe) were investigated by coupling ACTIS to different detection systems. The HSA-FLC system has many benefits regarding the application of ACTIS. Firstly, FLC is fluorometric active, which enables using the fluorescence detector (FLD) as a detection system. Both substances (HAS,FLC) are cost-effective and have great solubility in aqueous solutions [35-36]. Since a similar protein-compound system has already been investigated using ACTIS, our main consideration was to validate our ACTIS instrumentation and detection methods by comparing the results with literature values and our previous experiments.

Compared to HSA-FLC, BLG-FeQ_2 is a more complex system (Figure 7). In this model system the FeQ_2 is the compound in the BLG-FeQ_2 complex. Iron binds to quercetin with very high affinity at a physiologic pH of 7.4 [37-38]. The binding of FeQ_2 complex to BLG was recently investigated in terms of its antiallergenic potential [39]. It was found that the BLG-FeQ_2 complex plays an important role in preventing milk allergies. This study reveals previous unrecognized immune-regulatory effects of BLG-FeQ_2 complex. Additionally, it was found that the affinity of BLG binding to the FeQ_2 is in nmol L^{-1} range. Theoretically, this system is adaptable for various detection systems. This represents a significant advantage for studying the potential of ACTIS by exploring its compatibility to other detection systems. The fluorescence of Q enables the employment of the fluorescence detector. Organic MS methods could be used to detect FeQ_2. Finally, the precise Fe detection over time can be done by applying element analytic methods, such as inductively coupled plasma mass spectrometry (ICP-MS) and atomic emission spectroscopy (ICP-AES).

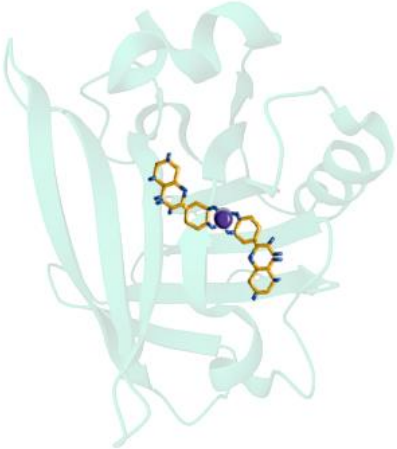

Figure 7: Bovine β-lactoglobulin complex with quercetin and iron

2.2 Reagents and solutions

Following solutions were used in our ACTIS experiments:

stock solutions – concentrated solution of a specific substance used to prepare working solutions;

working solutions – mixture of a specified amount of protein and a compound of investigated model system, measured in ACTIS experiments;

ACTIS running solution (ASR) – used as a background solution to prefill the ACTIS setup and to propagate the sample plug through it.

2.2.1 HSA-FLD solutions

Albumin from human serum (HSA) and fluorescein were purchased from Sigma Aldrich. All solutions were made by using 30 mmol L^{-1} ammonium acetate (NH_4Ac) as a solvent with pH=7.2. NH_4Ac was prepared by weighing 1.2 g of ammonium acetate purchased from Thermo Fisher and dissolving it in 500 mL MQ-H_2O. 1 mol L^{-1} NaOH solution, purchased from Thermo Fisher, was used to adjust the pH of the NH_4Ac to 7.2. The working solutions of HSA and fluorescein prepared with corresponding final concentrations are shown in the Table 2. The HSA-FLC mixtures were prepared by mixing the corresponding amounts of HSA and FLC working solutions as shown in Table 3 and Table 4. The mixtures were incubated for 2 h at room temperature of 22 ^oC before measurements. Each experiment took two days and the mixtures were measured in increasing protein concentrations. Working solutions were stored in the fridge at 4 ^oC.

Table 2: HSA-FLC stock solutions

Stock solution	Mass of component	Added NH_4Ac volume	Final concentration
HSA I	208.0 mg	4 mL	7.8×10^{-1} mmol L^{-1}
HSA II	400.0 mg	3 mL	2.0 mmol L^{-1}
FLC I	3.3 mg	10 mL	1.0 mmol L^{-1}
HSA III	1:100 dilution of HSA I with NH_4Ac solution		7.8×10^{-3} mmol L^{-1}
HSA IV	1:100 dilution of HSA II with NH_4Ac solution		2.0×10^{-2} mmol L^{-1}
FLC II	1:100 dilution of FLC I with NH_4Ac solution		1.0×10^{-2} mmol L^{-1}

Table 3: Table of HSA-FLC solutions made for the first ACTIS-FLD experiment

Nr.	Final HSA concentration (µmol L^{-1})	HSA stock solution	Volume of HSA stock solution added (µL)	FLC stock solution	Volume of FLC stock solution added (µL)	Added NH_4Ac volume (µL)
1	700.00	HSA I	895	FLC II	5	100
2	496.80	HSA I	635	FLC II	5	360
3	101.70	HSA I	130	FLC II	5	865
4	50.00	HSA I	64	FLC II	5	931
5	10.00	HSA I	13	FLC II	5	982
6	5.00	HSA III	639	FLC II	5	360
7	1.00	HSA III	128	FLC II	5	865
8	0.50	HSA III	64	FLC II	5	931
9	0.25	HSA III	32	FLC II	5	963
10	0.10	HSA III	13	FLC II	5	982

Table 4:Table of HSA-FLC solutions made for the second ACTIS-FLD experiment

Nr.	Final HSA concentration (µmol L^{-1})	HSA stock solution	Volume of HSA stock solution added (µL)	FLC stock solution	Volume of FLC stock solution added (µL)	Added NH_4Ac volume (µL)
1	1800.0	HSA II	900	FLC II	5	95
2	1200.0	HSA II	600	FLC II	5	395
3	1000.0	HSA II	500	FLC II	5	495
4	700.0	HSA II	350	FLC II	5	645
5	500.0	HSA II	250	FLC II	5	745
6	250.0	HSA II	125	FLC II	5	870
7	100.0	HSA II	50	FLC II	5	945
8	50.0	HSA II	25	FLC II	5	970
9	10.0	HSA IV	500	FLC II	5	495
10	5.0	HSA IV	250	FLC II	5	745

2.2.2 BLG-FeQ_2 solutions

β-lactoglobulin from bovine milk and quercetin were purchased from Sigma Aldrich. Iron (III) chloride hexahydrate was purchased from PanReach AppliChem. NH_4Ac was prepared by weighing 1.2 g of ammonium acetate purchased from Thermo Fisher and dissolving it in 500 mL MQ-H_2O following by adjusting the pH to 7.2 with 1 mol L^{-1} NaOH. The solubility of BLG and $FeCl_3 \times 6H_20$ in NH_4Ac was very good and all the working solutions were made easily as described in the Table 5. However, the quercetin solubility at pH 7.2 was low. The first quercetin working solution was made by dissolving 17.81 g in 27.960 mL of NH_4Ac followed by homogenization for 10 minutes in an ultrasonic bath. After first FLD measurements of pure quercetin solutions, the yellow solid residuals were observed on the connection part of the syringe and the capillary. The poor repeatability of fluorescence signals implicated that injected quercetin concentration varied. After closer inspection, we noticed that quercetin was not completely dissolved in the solution. The increasing of the pH of the NH_4Ac was found to be an important factor to improve the quercetin solubility. Therefore, a small amount of 1 mol L^{-1} NaOH solution was added to the stock solution, as described in the Table 5.

Table 5 shows the processes of making BLG, Q and Fe stock solutions that were used later to prepare working solutions for ACTIS experiments.

Table 5: Stock solutions used for making BLG-FeQ_2 working solutions for ACTIS measurements

Stock solution	Added mass	Added NH_4Ac volume	Final concentration
BLG I	92.1 mg	2.00 mL	2.5 mmol L^{-1}
Q I	17.8 mg	27.96 mL	2.0 mmol L^{-1}
Fe I	38.3 mg	14.20 mL	10.0 mmol L^{-1}
BLG II	1:10 dilution of BLG I with NH_4Ac solution		2.5×10^{-1} mmol L^{-1}
BLG III	1:10 dilution of BLG II with NH_4Ac solution		2.5×10^{-2} mmol L^{-1}
BLG IV	1:100 dilution of BLG II with NH_4Ac solution		2.5×10^{-3} mmol L^{-1}
BLG V	1:10 dilution of BLG IV with NH_4Ac solution		2.5×10^{-4} mmol L^{-1}
BLG VI	1:10 dilution of BLG V with NH_4Ac solution		2.5×10^{-5} mmol L^{-1}
Q II	1:2 dilution of Q I with NH_4Ac solution with 200 µL of 1M NaOH per 5 mL solution		1.0 mmol L^{-1}
Q III	1:1000 dilution of Q II with NH_4Ac solution		1.0×10^{-3} mmol L^{-1}
Q IV	1:5 dilution of Q III with NH_4Ac solution		2.0×10^{-4} mmol L^{-1}
Q V	1:50 dilution of Q II with NH_4Ac solution		2.0×10^{-2} mmol L^{-1}
Fe II	1:20 dilution of Fe I with NH_4Ac solution		1.0×10^{-2} mmol L^{-1}
Fe III	1:1000 dilution of Fe II with NH_4Ac solution		5.0×10^{-4} mmol L^{-1}

Fe IV	1:5 dilution of Fe III with NH_4Ac solution	1.0×10^{-4} mmol L^{-1}

One set of BLG-FeQ_2 mixtures was measured with ACTIS-FLD, ACTIS-TOF-MS, and ACTIS-AES. Three runs for each mixture were carried out using ACTIS-FLD. In both ACTIS-TOF-MS experiments, six replicates were conducted. Only one run per mixture was performed using ACTIS-AES. The preparation of all the working solutions is shown in the Tables 6-10. Note that in the preparation procedure, the initial mixing of Q and Fe was followed by 15-minutes of incubation at room temperature of 23 ^{o}C. After incubation the proper amount of NH_4Ac and BLG stock solutions were added. The concentration of compound, in this case the FeQ_2 complex, is constant in each solution from one experiment while the protein concentration was varied.

Table 6: BLG-FeQ_2 working solutions prepared for ACTIS-FLD experiment

No.	Final [BLG] (µmol L^{-1})	BLG stock solution	Added volume of BLG stock solution (µL)	Q stock solution	Added volume of Q stock solution (µL)	Fe stock solution	Added volume of Fe stock solution (µL)	Added NH_4Ac volume (µL)
1	750.0	BLG I	450	Q II	150	Fe III	150	750
2	500.0	BLG I	300	Q II	150	Fe III	150	900
3	250.0	BLG I	150	Q II	150	Fe III	150	1050
4	100.0	BLG I	60	Q II	150	Fe III	150	1140
5	50.0	BLG II	300	Q II	150	Fe III	150	900
6	10.0	BLG II	60	Q II	150	Fe III	150	1140
7	5.0	BLG III	300	Q II	150	Fe III	150	900
8	1.0	BLG III	60	Q II	150	Fe III	150	1140
9	0.1	BLG IV	60	Q II	150	Fe III	150	1140
10	0.01	BLG V	60	Q II	150	Fe III	150	1140

Table 7: BLG-FeQ_2 working solutions prepared for the first ACTIS-TOF-MS experiment

No.	Final [BLG] (µmol L^{-1})	BLG stock solution	Added volume of BLG stock solution (µL)	Q stock solution	Added volume of Q stock solution (µL)	Fe stock solution	Added volume of Fe stock solution (µL)	Added NH_4Ac volume (µL)
1	1000	BLG IV	800	Q IV	100	Fe IV	100	1000
2	750.0	BLG IV	600	Q IV	100	Fe IV	100	1200
3	500.0	BLG IV	400	Q IV	100	Fe IV	100	1400
4	250.0	BLG IV	200	Q IV	100	Fe IV	100	1600
5	100.0	BLG IV	80	Q IV	100	Fe IV	100	1720
6	50.0	BLG IV	40	Q IV	100	Fe IV	100	1760
7	25.0	BLG V	200	Q IV	100	Fe IV	100	1600
8	10.0	BLG V	80	Q IV	100	Fe IV	100	1720
9	5.0	BLG VI	400	Q IV	100	Fe IV	100	1400
10	1.0	BLG VI	80	Q IV	100	Fe IV	100	1720

Table 8: BLG-FeQ_2 working solutions prepared for the second ACTIS-TOF-MS experiment

No.	Final [BLG] (nmol L^{-1})	BLG stock solution	Added volume of BLG stock solution (µL)	Q stock solution	Added volume of Q stock solution (µL)	Fe stock solution	Added volume of Fe stock solution (µL)	Added NH_4Ac volume (µL)
1	250.0	BLG IV	200	Q IV	100	Fe IV	100	1600
2	100.0	BLG IV	80	Q IV	100	Fe IV	100	1720
3	75.0	BLG IV	60	Q IV	100	Fe IV	100	1740
4	50.0	BLG IV	40	Q IV	100	Fe IV	100	1760
5	35.0	BLG IV	28	Q IV	100	Fe IV	100	1772
6	25.0	BLG V	200	Q IV	100	Fe IV	100	1600
7	15.0	BLG V	120	Q IV	100	Fe IV	100	1680
8	10.0	BLG V	80	Q IV	100	Fe IV	100	1720
9	5.0	BLG VI	400	Q IV	100	Fe IV	100	1400
10	1.0	BLG VI	80	Q IV	100	Fe IV	100	1720

Table 9: BLG-FeQ_2 Solutions made for the ACTIS-ICP-AES experiment

No.	Final [BLG] (µmol L^{-1})	BLG stock solution	Added volume of BLG stock solution (µL)	Q stock solution	Added volume of Q stock solution (µL)	Fe stock solution	Added volume of Fe stock solution (µL)	Added NH_4Ac volume (µL)
1	1000	BLG I	80	Q V	20	Fe II	20	80
2	500.0	BLG I	40	Q V	20	Fe II	20	120
3	100.0	BLG II	80	Q V	20	Fe II	20	80
4	50.0	BLG II	40	Q V	20	Fe II	20	120
5	10.0	BLG III	80	Q V	20	Fe II	20	80
6	5.0	BLG III	40	Q V	20	Fe II	20	120
7	1.0	BLG IV	80	Q V	20	Fe II	20	80
8	0.5	BLG IV	40	Q V	20	Fe II	20	120
9	0.25	BLG IV	20	Q V	20	Fe II	20	140
10	0.1	BLG V	80	Q V	20	Fe II	20	80

Table 10: Protein concentration ranges and compound concentrations in measured samples for each detection method utilized for assessing K_d of BLG-FeQ_2 model system

Detection method	FLD	TOF-MS		AES
		1st experiment	2nd experiment	
$[BLG]_0$	750.0 – 1.0 × 10^{-2} µmol L^{-1}	1.0 × 10^3 - 1.0 nmol L^{-1}	2.5 × 10^2 – 1.0 nmol L^{-1}	1000 – 0.1 µmol L^{-1}
[FeQ_2]	50.0 µmol L^{-1}	5.0 × 10^{-3} µmol L^{-1}	5.0 × 10^{-3} µmol L^{-1}	1.0 µmol L^{-1}

No K_d assessment was performed using ACTIS-ICP-MS. This technique was evaluated by measuring Fe solutions. The overview of injected solutions with corresponding preparation recipes are given in the Table 11.

Table 11: The Fe solutions prepared for testing of ACTIS-ICP-MS

$[Fe]_0$	Stock solution used for preparation	The solvent used to dilute the stock solution
5.0 µmol L^{-1}	Fe II	30.0 mmol L^{-1} NH_4Ac (pH=7.2)

5.0 µmol L^{-1}	1000 ng g^{-1} Fe solution in 2% HNO_3 and 0.1% HCl	30.0 mmol L^{-1} NH_4Ac (pH=7.2)
5.0 µmol L^{-1}	1000 ng g^{-1} Fe solution in 2% HNO_3 and 0.1% HCl	Sub-boiled H_20

2.3 ACTIS setup

The ACTIS setup consisted of a pump, valve, flow sensor, and five capillaries. The setup scheme is presented in Figure 8. The pump was used to propagate the ACTIS running solution (ARS) and the sample plug through the capillaries. ARS refers to the solution used to prefill the ACTIS setup and to propagate the sample plug through it. The 30 mmol L^{-1} NH_4Ac solution with pH=7.2 was used as ARS in ACTIS experiments in this work. Three pumps were tested for the application in our ACTIS setup. The overview of tested pumps is given at the end of this section. Liquid flow sensor SLF3S-0600F produced by Senserion and purchased from Bartels Mikrotechnik was used to monitor the flow rate. 10-port valve Cheminert C2H-2340D, produced by VICI Valco Instruments, was used to enable the smooth loading of the sample while maintaining constant flow rate. The capillary in which the TIS takes place is referred as a separation capillary. In this setup, a separation capillary with length of 60 cm and an inner diameter of 254 µm was used. The injection capillary was prefilled with sample and later connected via the valve to the separation capillary to load the sample into it. The injection capillary was 15.6 cm long with an inner diameter of 102 µm. Besides separation and injection capillaries, ACTIS setup also had two waste and one sample introduction capillary. Both waste capillaries have inner diameter of 50.8 mm. The sample introduction capillary was connected to a syringe filled with sample solution.

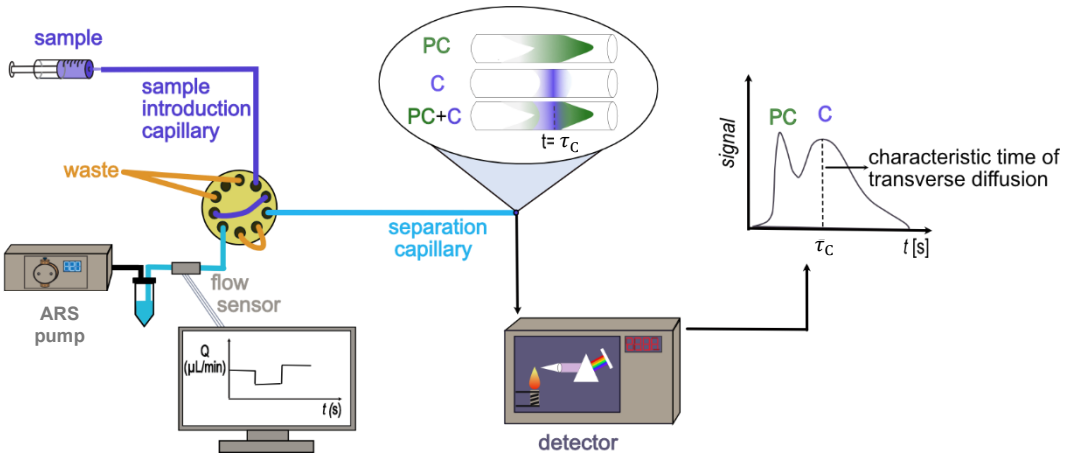

Figure 8: The scheme of ACTIS setup

The following paragraphs provide the explanation of a single ACTIS run. One ACTIS run consists of four steps: 1) sample injection, 2) sample loading, 3) separation, and 4) purge step. A scheme of different valve positions and the flow of ARS and a sample in them is given in appendix, section 1.

For sample injection (step 1) the starting valve position is the position A. In this position, the injection capillary is connected to the waste, while the ARS is directed into the separation capillary. The sample is introduced manually into the injection capillary with a 1 mL syringe (produced by Rays). Simultaneously, the pump fills ARS into the separation capillary at flow rate matching the flow rate used in a separation step, Q_{sep}.

After the injection capillary is purged and filled with the sample, sample loading (step 2) begins by switching the vent to the B position. In the B position the ARS is pumped directly into the injection capillary which is now connected to the separation capillary. At injection flow rate, Q_{inj} the sample is slowly transferred from injection into the separation capillary. This step ensures that the whole sample plug volume is pushed into the separation capillary.

After sample loading step, the flow rate is increased to Q_{sep}. To begin the separation (step 3), the flow rate of the sample plug through the separation capillary is chosen to ensure that TIS occurs at the end of the capillary. As already mentioned, the choice of the duration time and flow rates of single steps plays a crucial role in one ACTIS run. The injection step was performed at flow rate of 20 µL min^{-1} for 20 s. The volume of the injection capillary V_{inj} can be calculated as follows:

$$\boldsymbol{V_{\text{inj}} = \pi \times r^2 \times l} \qquad (11)$$

The r is the inner radius of injection capillary (51 µm) and l refers to its length (15.6 cm). Inserting these values in the formula results in V_{inj} of 1.2 µL. At the flow rate of 20 µL min^{-1} the time needed to push this volume twice through the injection capillary is:

$$\boldsymbol{t_{\text{inj}} = \frac{3 \times 1.2\ \mu L}{15\ \mu L\ min^{-1}} = 0.24\ min = 14.4\ s} \qquad (12)$$

In order to simplify the automatization of the valve and the pump switch, the duration of the sample loading step was set to 15 s.

The duration of the separation step was set twice as long as the characteristic transverse diffusion time of compound, τ_{C}. By setting the duration of separation step longer we are able to see the full peaks. As described in introduction part, the τ_{C} is calculated from the inner radius r, and diffusion constant of the compound, μ_C (see equation 6). We estimated diffusion constant of the FeQ_2 complex, μ_{FeQ2}, to be similar to the Fe (III) diffusion constant of 0.604 × 10^{-9} m² s^{-1} [40]. The calculation of the flow rate in the separation step, Q_{sep} is given in the equation 7. Here, τ_{FeQ2} was 26.7 s and l was 60 cm, and Q_{sep} amounted 68 µL min^{-1}, respectively. Same values of Q_{sep} and t_{inj} were applied in measurements of both

model systems to keep processes consistent. On the other hand, the acquisition time was much longer then the estimated τ_C and the evaluation included finding the maximum of diffusion peak. Since the Q_{inj} and the Q_{sep} varied depending on the used pump during the ACTIS run and the delay of valve switching affected the timing, we determined the real τ_C during the evaluation.

In the last step, high flow rates (Q_{purge} > 100 µL min^{-1}) were used to purge the setup with ARS. For this purpose, the pressure on the ARS pump was set to 2 bar and the valve position was switched every 3 seconds for 10 times. Switching of valve positions allowed the effective purge of potential sample residuals out of the valve.

Table 12 provides an overview of the ACTIS measurement steps with respective valve positions and the applied flow rates.

Table 12: Brief overview of ACTIS run steps

Measurement step	Short description	Flow rate	Valve position	Duration
Sample injection	Transfer of sample from syringe into injection capillary;	manually	A	20 s
	Simultaneously filling the separation capillary with the ARS	68 µL min^{-1}		
Sample loading	Transfer of sample plug from injection into separation capillary	20 µL min^{-1}	B	20 s
Separation	Propagation of sample plug through the separation capillary	68 µL min^{-1}	A	120 s
Purge	Purge the capillaries at high flow rates by switching the valve position	100-500 µL min^{-1}	both	60 s

The duration time and respective flow rates of each step in one ACTIS run are presented in Figure 9.

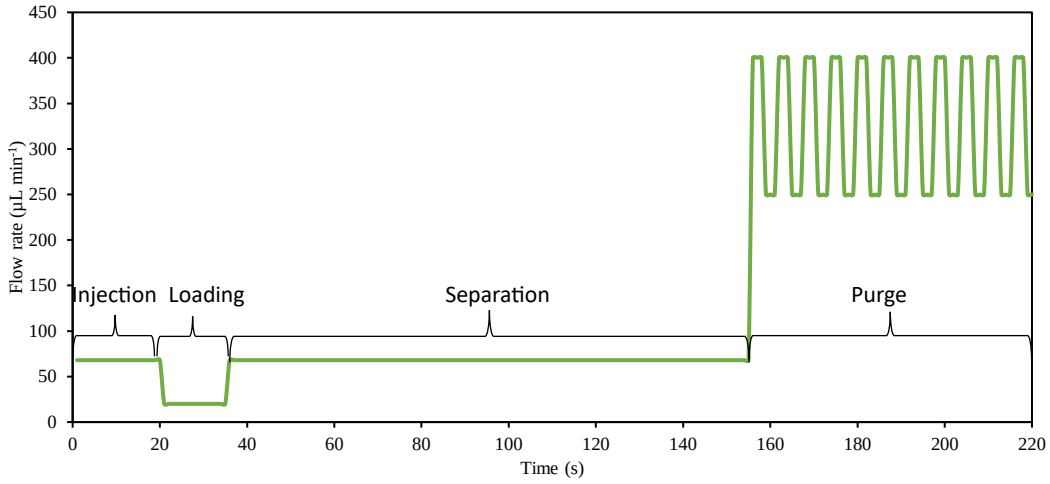

Figure 9: The duration and flow rates of respective steps in one ACTIS run

Even with subsequent τ_C determination, the Q_{inj} and Q_{sep} had to be maintained as constant as possible, because variations would have led to plug distortion.

It is challenging to find a pump that is able to produce constant low flow rates of 20 and 68 µL min^{-1} during separation and valve switching. Three pumps were tested for this purpose: a syringe pump 704806 from Harvard Apparatus, a piezoelectric pump - mp6 liq (Bartels, microfluidic), and a pressure pump - Cobalt (Elveflow). The piezoelectric pump showed the highest flow rate variations. Syringe pump suffered from massive problems caused by air bubbles introduction into the capillary. We found that the most suitable pump for our setup is the pressure pump. The stability of the flow rate was good and the contactless pumping of ARS was also a beneficial characteristic.

However, we found additional concerns that should also be addressed. Namely, the position of the pressure pump relative to the detector position affected its performance due to syphon effects. Because of that, the pressure set on the pump produced different flow rates depending of the pump position. Because of the nebulizer gas flow in the ICP-MS device, the flow rate of the ARS was higher than needed, even with the pump switched off. In order to solve this issue, a 15 cm long capillary with 102 µm inner radius was attached between the flow rate sensor and the valve. This set up modification was applied only to the coupling ACTIS with ICP-MS.

To ensure consistent and repeatable measurements, it is necessary to switch the valve and change the flow rate at predefined time points for each measurement step as described above. At the beginning of the separation step these changes have to be done simultaneously. It is possible for one person to conduct the measurements and manually switch the valve and the pressure. Due to practical precision problems, shifts on the time axis are possible. For the ACTIS-AES measurements of BLG-FeQ_2 model and ACTIS-FLD measurements of HSA-FLC model, manual switching was performed. For all other measurements, a small Python program named *automACTIS*, implemented with the help of Dr. Sven

Kochmann was implemented. This program enabled synchronization of the pump, the valve, and in the case of FLD, also the detector. The source code can be found in the appendix, section 2.

2.4 Detection methods

The ACTIS setup was coupled to four different detectors by directly connecting the separation capillary: fluorescence detection (FLD), time-of-flight mass spectrometry (TOF-MS), inductively coupled plasma mass spectrometry (ICP-MS) and atomic emission spectroscopy (AES). Two of them, FLD and TOF-MS have suitable capillary connection, while ICP-MS and AES required an additional capillary connector. However, very robust and stable coupling with ACTIS characterises all four methods.

The FLD detector UltiMate 3000 by Dionex with a flow cell of 8 µL volume was used. The ACTIS-FLD is the only technique which was employed for both investigated model systems. For the HSA-FLC system measurements the excitation wavelength was set to 300 nm and emission wavelength to 350 nm. The acquisition was performed with a sensitivity of 1. For the BLG-FeQ_2system measurements excitation wavelength was 423 nm, emission 515 nm, and sensitivity was set to 4. The flow cell temperature was set to 25 ^{o}C and the lamp mode to long life lamp for both systems. The overview of FLD parameters applied for HSA-FLC and BLG-FeQ_2 experiments is given in Table 13. ACTIS-FLD coupling is presented in Figure 10.

Table 13: The overview of FLD parameters

Parameter	HSA-FLC experiments	BLG-FeQ_2 experiments
Excitation wavelength (nm)	300	423
Emission wavelength (nm)	350	515
Sensitivity	1	4
Flow Cell Temperature (^{o}C)	25	25
Lamp Mode	Long Life Mode	Long Life Mode

The main advantages of FLD as an ACTIS detector include high sensitivity and specificity due to high extinction coefficient of fluorophore. On the other hand, FLD can only be applied on PC systems with a fluorescent compound. This serious limitation did not had an impact in this study since both compounds, FLC and FeQ_2 are fluorophores. [41-42]

Our FLD device had an integrated flow cell of 8 µL volume with a small detection window. If the separation flow rate for our systems is 68 µL min^{-1}, the flow cell content will be completely replaced in about 7 s. That implies that the detected signal at a specific time point represents a cumulative signal of the past 7 s. This results in signal overlapping, which impacts its resolution and intensity.

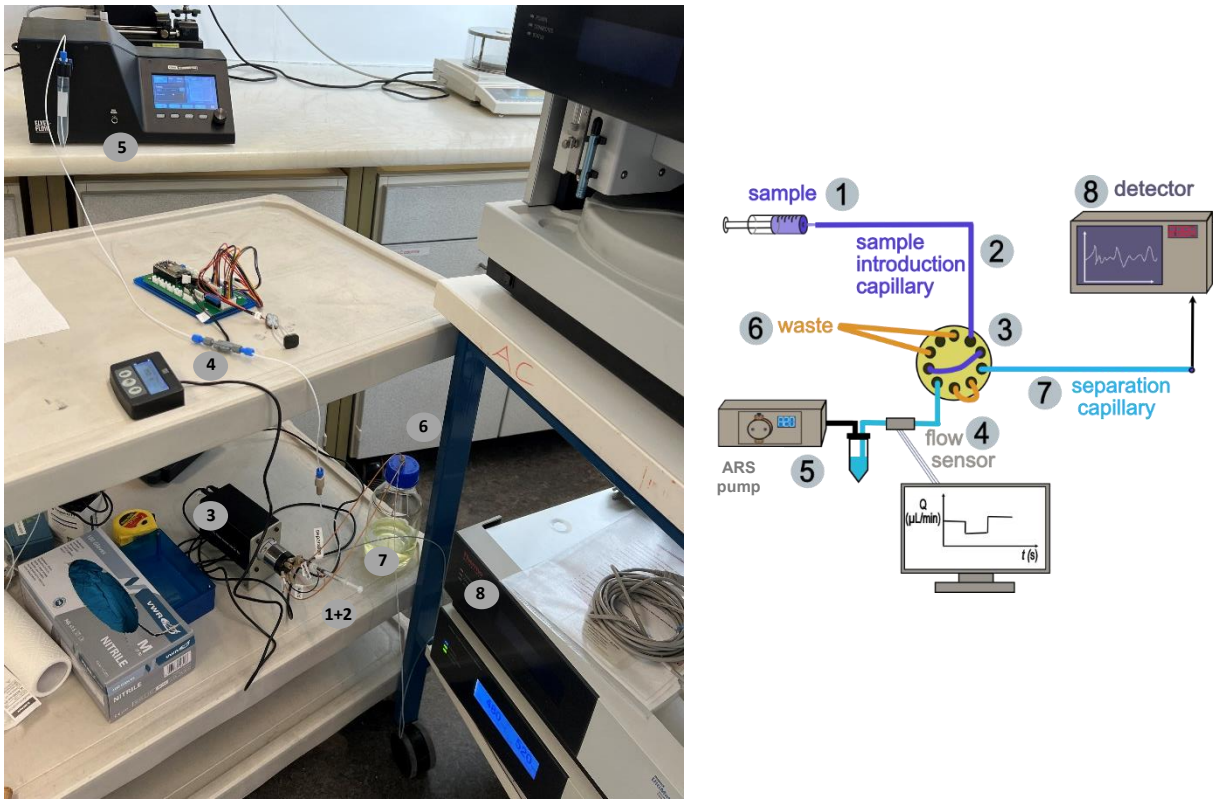

Figure 10: ACTIS setup coupled to FLD

An Agilent 6230 LC TOF MS was used with electrospray ionisation (ESI), as the organic MS detector. The instrument and scan source parameters parameter applied for all ACTIS-TOF-MS measurements are presented in Table 14. The ACTIS experiments were performed in positive mode. According to the molecular structure of quercetin, we assumed that the TOF-MS acquisition in negative mode would be more successful. However, the total ion content was very low in negative mode and no specific quercetin peaks could be determined in this mode. Therefore, the positive mode was selected for actual ACTIS experiments. The ACTIS-TOF-MS coupling is shown in Figure 11.

Table 14: Overview of TOF-MS method parameters

Instrument parameters		Scan Source Parameter	
Gas temperature (°C)	120	**Nozzle voltage (V)**	1000
Gas flow (L min^{-1})	10	**Fragmentor voltage (V)**	120
Nebulizer (psig)	35	**Skimmer1 voltage (V)**	60
Sheath Gas temperature	350	**Octopole RF Peak (V)**	750
Sheath Gas flow	11	**Average Scans**	1
Source Voltage (V)	+3500	**Detection Window (ppm)**	100
		Min Height (counts)	100

Compared to FLD, TOF-MS has a higher acquisition speed since the capillary content comes straight to ESI source. The wide m/z range of TOF-MS is beneficial for the application as ACTIS detector since it allows the observation of protein signals in theory.

After measurements of pure Q and FeQ_2 solutions in the concentration range of prepared BLG-FeQ_2 mixtures, the qualitative data analysis in MS Dial was done. This analysis yielded a list of relevant m/z values, associated with FeQ_2 complex. These m/z values were later used in MS Qual to extract the ion chromatograms out of total ion chromatograms originated from ACTIS measurements.

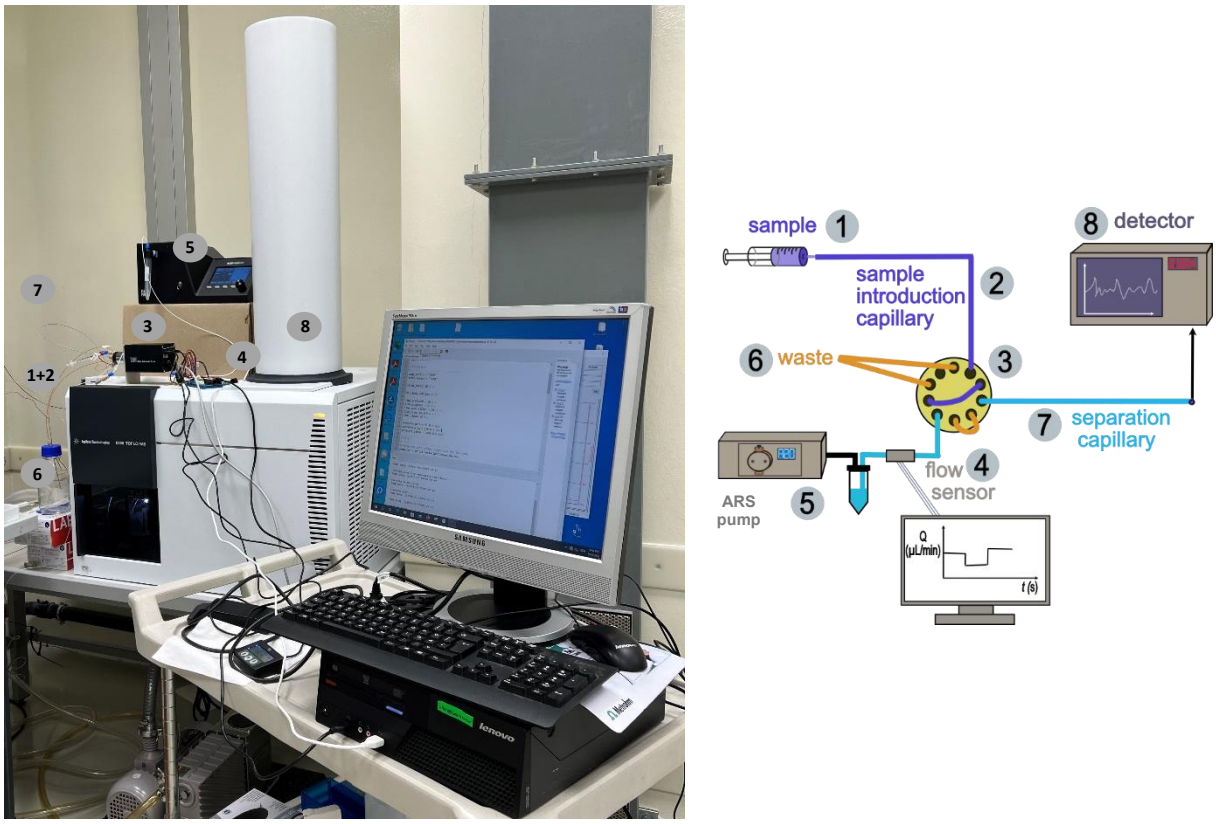

Figure 11: ACTIS-TOF-MS

An ICP-MS with collision/reaction cell (NexION 2000 from PerkinElmer) was utilized as an elemental detector. The acquisitions were performed in kinetic energy discrimination (KED) mode with He as collision gas with cell flow of 7 mL min^{-1}. The Rpq parameter was set to 0.4. The method optimization was performed by using a quality control solution containing 10 ng g^{-1} Fe in 2% HNO_3. The perfluoroalkoxy (PFA) micro flow nebulizer ST-5898 from Perkin Elmer was used to convert the liquid sample into an aerosol, which was further introduced into the ICP-MS. Before each first measurement after device started up, plasma was warmed up for 15 minutes. All ACTIS-ICP-MS measurements were carried out in a clean room laboratory (ISO class 7) with the setup shown in Figure 12.

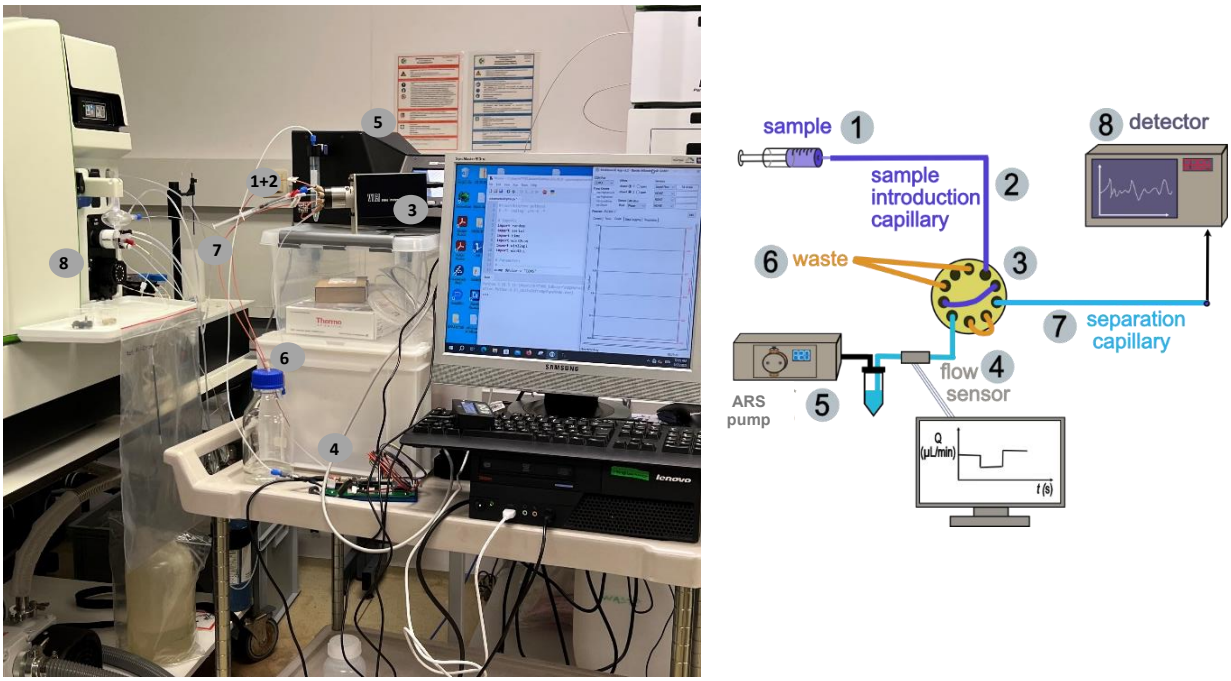

Figure 12: ACTIS-ICP-MS

The last detection method evaluated in this work was ICP-AES, for which the device AVIO 220Max from Perkin Elmer was used. The separation capillary was connected to a ST-9400 PFA microflow nebulizer from Perkin Elmer. The wavelength was set to 238.204 nm for Fe. Before each first measurement after device started up, plasma was warmed up for 10 minutes.

Since this ICP-AES was not designed for transient measurements, direct signal extraction over time was not possible in its software. Therefore, an additional PowerShell "hack" script was needed to copy the signal values and save them in separate text file. This "hack" script is given in the appendix, section 3.

2.5 Data evaluation

One ACTIS run result in a separagram. Depending on the employed detector, the intensity of compound signal as well as acquisition rate can vary. It is imperative that properties of the detector remain consistent for one ACTIS experiment. In the evaluation process the relative signal intensities among the mixtures are used to find K_d based on the principles explained in section 1.3.

The data evaluation can be performed in a calculation program such as Microsoft Excel. Alternatively, automated evaluation is possible by applying the prACTISed workflow; prACTISed is a collection of Python scripts which is designed for the analysis of ACTIS experimental data. [44]

In order to validate the prACTISed workflow results, we performed the data evaluation of initial experiments in Excel. The raw data was imported into Excel and replicates of one PC working solution were organized within one Excel sheet. Subsequently, individual diagrams were generated for each

mixture separately. These diagrams aided in selecting the appropriate cutting points to extract the compound peak for each measurement. It was required to adjust the peaks positions slightly, if the measurements were performed without using automACTIS. The adjustment involved the removing of datapoints prior the non-diffusive peak, to ensure that all the peaks have the same starting timepoint. When applying automACTIS, only slightly shifted peaks positions were observed due to minor changes of flow rates. In this case no peak time corrections were applied. Note that this might have introduced small errors in subsequent evaluation steps.

All peaks were cut and aligned, and the background was removed by subtracting the absolute intensity value at the starting region of each separagram. The next step involved the peak normalization to unity which was followed by averaging over all separagrams (from the same $[P]_0$). The averaged separagrams were used for further analysis. Initially, the τ_C was found as the time point where the mixture with lowest protein concentration reached its maximum. The signal value at determined τ_C were further used to find R_{exp} values, as shown in Equation (). The signals at the $t = \tau_C$ in other separagrams were used to find corresponding R_{exp} values. This resulted in one R_{exp} value for each measured working solution. The R_{exp} values were used to fit R_{theo} of each mixture by applying the Equation (10). Finally, the K_d value was determined as the fitting parameter of R_{theo}.

The described data evaluation workflow is time-consuming and prone to errors, particularly when handling larger data sets. The prACTISed workflow represents the set of open-source Python scripts which enable automated ACTIS data evaluation [44]. Raw separagrams were stored in .csv or .txt formats depending on the detector used. The data had to be compiled into an Excel input file consisting of a data worksheet for each working solution as well as a specific worksheet with experimental parameters such as flow rate and capillary dimensions. In this work, the aligned separagrams used for evaluation in Excel were copied into this input file. The width of the window for detection the corresponding signals at τ_C was set to 2%. For the data resulting from ACTIS-TOF-MS experiments, compensation procedure was applied. The compensation procedure refers to signal-unmasking of the compound which either can be suppressed or increased in the presence of protein.

The analysis of 60 separagrams took about 10 seconds using prACTISed. The output resulted in .xlsx working file containing all analysed separagrams, as well as graphical representation of separagrams and binding isotherm as PNG-files. The example of separagrams and corresponding binding isotherm is given in Figure 13.

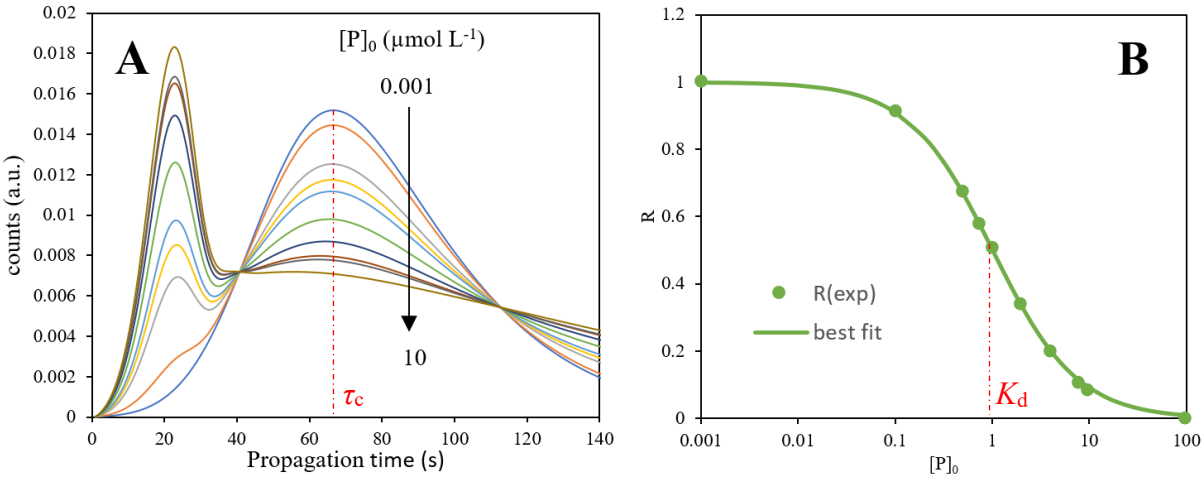

Figure 13: Example of resulting separagrams (A) and binding isotherm (B)

2.6 Computer simulations

To test the impact of the transfer capillary (nebulizer capillary) on the assessed K_d, the computer simulations were performed. For this purpose, the ElmerGUI program using Elmer FEM software for simulations of multi-physics problems was used [45]. The geometry of separation capillary connected to a transfer capillary was submitted as text file and the corresponding 2D mesh was constructed using gmsh.exe program. The example of geometry text file is given in appendix, section 4.

The radius (r_1) and the length (l_1) of the separation capillary and the radius (r_2) and length (l_2) of transfer capillary were selected to align with the real characteristics. In this work, one set of ACTIS virtual experiments was conducted with the variations of r_2 in the range of 50 - 1250 µm. In all virtual experiments, the inflow velocity (v) of sample plug was set to 0.029, the sample plug length (l_{sp}) corresponds to 10 % of l_1. All input values were given in arbitrary units. The diffusivity of the compound (μ_C) was established at 5×10^4, which corresponds to 500 µm s^{-1}. The protein's diffusivity (μ_P) was set to 5×10^3, which corresponds to 50 µm s^{-1}. Experimental and simulation parameters are given in Table 15. We decided to exclude steady state in these simulations. The dimensions were scaled in x-direction (along the capillary) in order to save simulation time and to improve convergence.

Table 15: Real and simulated ACTIS – detector characteristics

characteristics	experimental	unscaled	simulation (scaled)
l_1	600 mm	600	3
r_1	0.25 mm	0.25	0.25
l_2	80 mm	80	0.8
r_2	0.05 mm	0.05 - 1.250	0.05 - 1.250
l_{sp}	5 mm	5	0.1

v	346 mm min^{-1}	346	0.029
μ_C	500 µm s^{-1}	500	5×10^4
μ_P	50 µm s^{-1}	50	5×10^3
Mesh size	-	-	0.01
Timestep interval	-	-	300
Timestep sizes	-	-	1

The geometry of the separation and transfer capillary with their mesh is presented in Figure 14.

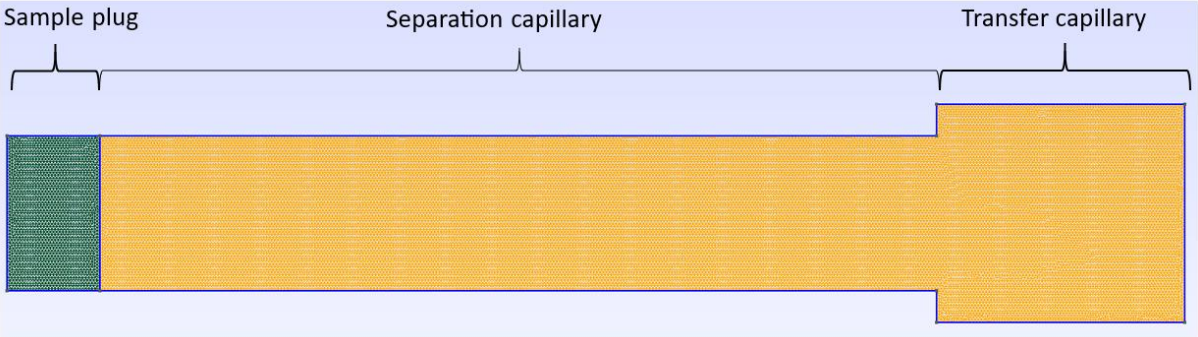

Figure 14: The geometry of separation and transfer capillary with integrated mesh used for computer simulations

Two simulations were carried out for each compound and the protein for every value of r_2. This resulted in total of 20 simulations. Each simulation resulted in time-based compound concentration.

The evaluation of computer simulations involved following steps: 1) normalisation of the functions; 2) calculation of [PC], [P], and [C] for 10 different $[P]_0$ values; 3) calculation of coefficients for compound and protein functions for each $[P]_0$; 4) calculation of resulting functions of low and high diffuse functions by multiplication of normalized functions with respective coefficients; and 5) finding the K_d value by applying prACTISed algorithm. The evaluation resulted in 10 K_d values, for each r_2 value. For the calculation of [PC], [P], and [C], beside the 10 specified $[P]_0$ values, the value for $[C]_0$ and arbitrary K_d are also required. When selecting these values it is important to consider the criteria for K_d /$[C]_0$ to accurately assess K_d [31]. K_d was set to 1000 nmol L^{-1} and the $[C]_0$ to 10 nmol L^{-1}. The range of $[P]_0$ included 10 concentrations from 1 to 2000 nmol L^{-1}.

3 Results and discussion

3.1 Validating ACTIS-setup with HSA-FLC model system

The initial experiments aimed at the validation of our ACTIS setup, testing its functionality, and its ability to accurately determine K_d value of a protein-metal complex. The functionality of the setup includes different aspects. First we wanted to ensure the absence of leaks in the valve, especially during experimental runs. Besides that, we wanted to achieve reproducible flow stability and sample transfer. We implemented data logging of the flow rate over time to assess the repeatability of ARS pump's performance and flow rate stability. In the context of ACTIS-FLD experiments, we considered consistent peak form during the separation step as an indicator of proper sample loading and transfer. Furthermore, the performance of the detector was evaluated based on the repeatability and reproducibility of the separation peaks in terms of their form and intensity. Finally, we confirmed the suitability of our setup for further experiments by K_d assessment of a model system comparable to one that had previously been investigated using ACTIS.

We chose HSA-FLC model system and FLD as appropriate detection method for evaluating our ACTIS setup. This decision was inspired by a similar ACTIS experiment, which was reported previously. Namely, a study which assessed bovine serum albumin (BSA) binding to FLC using ACTIS-FLD method yielded K_d of 28 ± 6 µmol L^{-1} [31]. Since BSA and HSA are similar in terms of their binding affinities [46], we consider the comparison of the obtained results to be reasonable. An additional advantage of HSA-FLC model system is a relatively high expected K_d value (in µmol L^{-1} range) . Higher K_d allows higher $[C]_0$ in working solutions which improves the quantification with chosen detection method and the accuracy [47]. On the other hand, K_d in µmol L^{-1} range refers to unspecific molecular binding. Therefore, deviations of observed K_d values are more likely compared to ones observed in highly specific molecular binding (pmol L^{-1} – nmol L^{-1} range).

First experiment conducted aiming at the validation of our ACTIS setup included ACTIS-FLD measurements of pure FLC solutions. We prepared six solutions with [FLC] in range of 0.025 - 0.5 µmol L^{-1} and measured six runs per solution. Due to high fluorescence of FLC and good sensitivity of used FLD, intense signals were obtained in separation step of each run. Average maximal signals with corresponding standard deviations are given in Table 16. The corresponding standard deviations reveal excellent repeatability of peak intensity, particularly for [FLC] within the range of 0.025 - 0.1 µmol L^{-1}.

Table 16: Average Peak Maximums and Standard Deviation of FLC measurements using ACTIS-FLD

[FLC] (µmol L^{-1})	Average peak maximum (a.u.)	Relative standard deviation (%)
0.025	$8.6 \times 10^6 \pm 5.8 \times 10^5$	0.067
0.075	$2.4 \times 10^7 \pm 1.4 \times 10^6$	0.058

0.050	$1.6 \times 10^7 \pm 9.7 \times 10^5$	0.060
0.100	$3.4 \times 10^7 \pm 3.1 \times 10^6$	0.091
0.230	$7.5 \times 10^7 \pm 1.0 \times 10^7$	0.133
0.500	$1.1 \times 10^8 \pm 6.3 \times 10^5$	0.005

The calibration curve of fluorescein measured using ACTIS-FLD setup is illustrated in Figure 15. Considering the wide range of [FLC] measured and injection via ACTIS setup, we consider $R^2 > 0.9$ as acceptable. The resulting R^2 value of 0.9474 demonstrates a good level of linearity in this experiment. The FLC concentration of 0.05 µmol L^{-1} for HSA-FLC working solutions was selected for ACTIS setup evaluation.

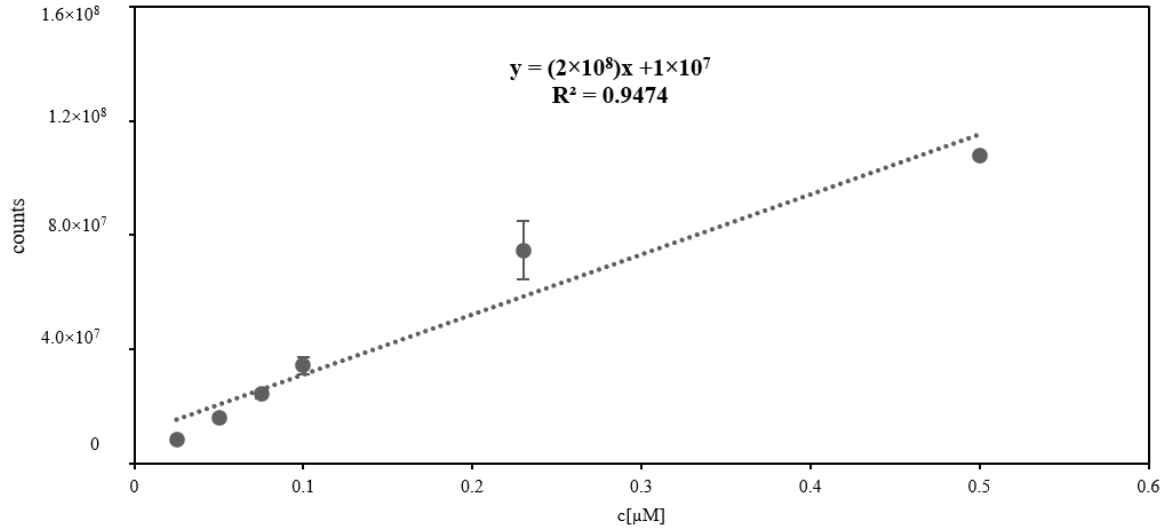

Figure 15: FLC calibration curve

After positive evaluation of the ACTIS-FLD instrumentation for measuring the FLC, the first ACTIS experiment was conducted. The primary objective was to determine if the measurements of HSA-FLC would mirror those of pure FLC from previous assessments. Therefore, only three runs per working solution were performed. In section 2.2.1, the preparation process of all mixtures analysed in the first ACTIS-FLD experiment is given.

Separation peaks cut from normalized average separagrams, as well as resulting binding isotherm are presented in Figure 16A and 16B. Since this was the first ACTIS experiment conducted in this work, we conducted the evaluation using both Excel and the prACTISed script. The evaluation using Microsoft Excel revealed a K_d value of 93.7 ± 34.3 µmol L^{-1}. The evaluation with prACTISed revealed a K_d value of 97.3 ± 22.2 µmol L^{-1}. Evaluated K_d value aligns with the one reported in the literature for BSA-FLC model system.

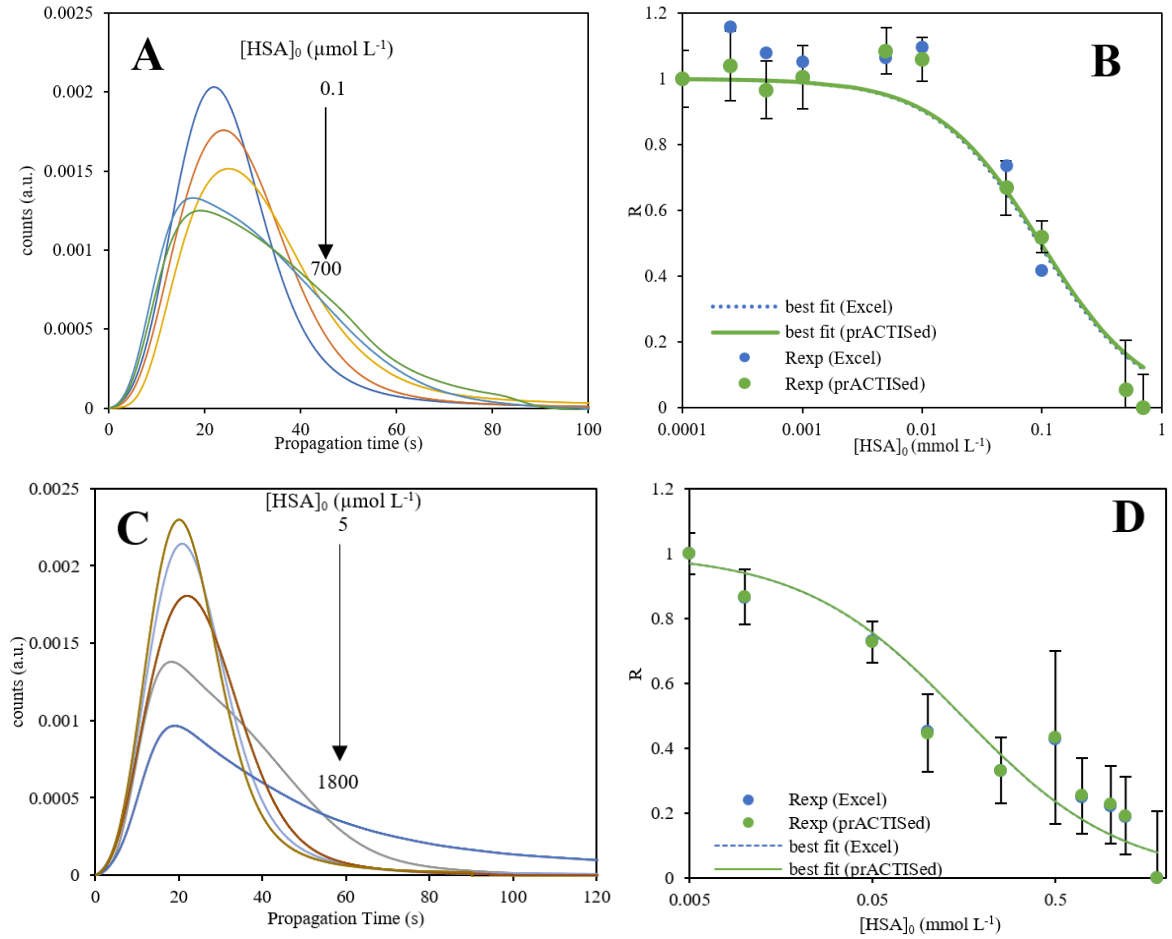

Figure 16: Separation peaks of five HSA-FLC working solution measured in the first ACTIS-FLD experiment (A) and the corresponding binding isotherm (B); Separation peaks (C) and binding isotherm (D) resulted from second ACTIS-FLD experiment of HAS-FLC.

The initial ACTIS-FLD experiment demonstrated good repeatability. As expected, with increased $[HSA]_0$, the form and intensity of the separation peak changed. The intensity of diffuse peak decreased and the frontal part of the peak enhanced with rising $[HSA]_0$ and constant $[FLC]_0$. This appearance validates the fundamental thesis of TIS. However, to determine K_d value of this system more precisely using ACTIS-FLD, a second experiment was conducted with an adjusted range of $[HSA]_0$.

Evaluation of second experiment (Figure 14C and 14D) using Excel gained K_d value of 153.4 ± 40.2 µmol L^{-1} while prACTISed yielded K_d of 154.6 ± 33.8 µmol L^{-1}. Increasing of $[HSA]_0$ in working solutions affected the shift of binding isotherm and its deflection point to higher $[HSA]_0$. Consequently, we observed higher K_d value compared to first experiment.

Now let`s discuss the differences of Excel and prACTISed evaluation approaches. The greatest difference between those two evaluation approaches lies in the width of the data points range used to determine τ_C. In Excel, only one data point was used to find R_{exp}. On the other hand, prACTISed found the R_{exp} as average from the data range of 2% width around the τ_C. Additionally, the calculation of the

standard deviation was also different. In Excel, the standard deviation values were found for each data point for each working solution separately. The gained standard deviation values were further used to find maximal and minimal K_d values. This calculation was performed analogously to the calculation of K_d value. Finally, the standard deviation of K_d was found as a difference between maximal and minimal K_d values. In prACTISed, the given standard deviation refers to the the precision of the linear regression fitting.

We are uncertain about which values are more in agreement with the real K_d value, but the wider window for signal detection applied in prACTISed might be advantageous comparing to picking a single value. With wider window, the average value is calculated and thus the eventual detection system fluctuations can be diminished. Taking into account all the differences in described evaluation approaches, we consider the gained K_d values similar. Therefore, to simplify and to speed up the evaluation process we decided to exclusively use prACTISed for assessing further experiments.

Both obtained K_d values in ACTIS-FLD experiments performed are in similar range of values compared to the reported value for BSA-FLC. As already mentioned, the dissociation constant in µmol L^{-1} range indicates unspecific binding [46]. Additionally, the previously discussed (Section 2.4) flow cell volume of FLD has also negatively affected the precision of the gained results. Therefore, the obtained values are in agreement with reported value of K_d = 28 ± 35.8 µmol L^{-1} for BSA-FLC model system. We consider the conducted experiments validated the capability of our setup to conduct ACTIS-Experiments. The evaluation data resulting from both experiments is given in appendix, section 5.

3.2 Assessing the feasibility of BLG-FeQ_2 model system for ACTIS experiments

After successful evaluation of the ACTIS setup, we wanted to evaluate its applicability on a metal-protein model system. More specifically, this experiment was conducted to explore the fluorescence intensity, solubility, and stability of the selected model system within the evaluated ACTIS setup.

Our assumption was that the BLG-FeQ_2 is suitable for ACTIS-FLD assessment of K_d due to quercetin fluorescence. It is known that no fluorescence emission of quercetin in aqueous solutions occurs due to intermolecular interaction of quercetin polar groups with H_2O molecules [42]. However, binding to proteins leads to strong quercetin fluorescence. After testing different excitation and emission wavelengths, we found that the excitation at 423 nm and emission at 515 nm resulted in reproducible fluorescence signals.

After initial ACTIS-FLD measurements of 100 µmol L^{-1} quercetin solution in 30 mmol L^{-1} NH_4Ac, we observed insufficient solubility of the quercetin. Consequently, this led to nonrepeatable fluorescence intensity. After closer inspection of the injection capillary and connector, we noticed solid quercetin residuals. These residuals impacted the variations of the amount of quercetin injected. To address this

issue, varying amounts of NaOH solution were added to equal quercetin aliquots, aiming to determine the minimum NaOH concentration required for complete quercetin dissolution. We found that by adding 200 µL of the 1 M NaOH into 4.8 mL of 1 mM Q in 30 mmol L^{-1} solution, the complete dissolving of the quercetin occurs.

After solving the quercetin solubility issue, the preparation of the working solutions was done. According to the literature, K_d value of BLG-FeQ_2 system is approximately 0.11 µmol L^{-1} [39]. For K_d value in this range, the ligand concentration should ideally be maximal 0.01 µmol L^{-1}. However, due to low fluorescence of quercetin, $[FeQ_2]_0$ of 50 µmol L^{-1} was chosen for ACTIS experiments. The high component concentration implies that the conducted experiment was more similar to a titration, which means that the determined K_d will be close to $[FeQ_2]_0$ [32]. Nevertheless, since the primary goal of this experiment was to explore the properties of the BLG-FeQ_2 system and its suitability for ACTIS experiments, we ignored the unsuitable component concentration at this stage. The results of ACTIS-FLD measurements of BLG-FeQ_2 system are shown in Figure 17.

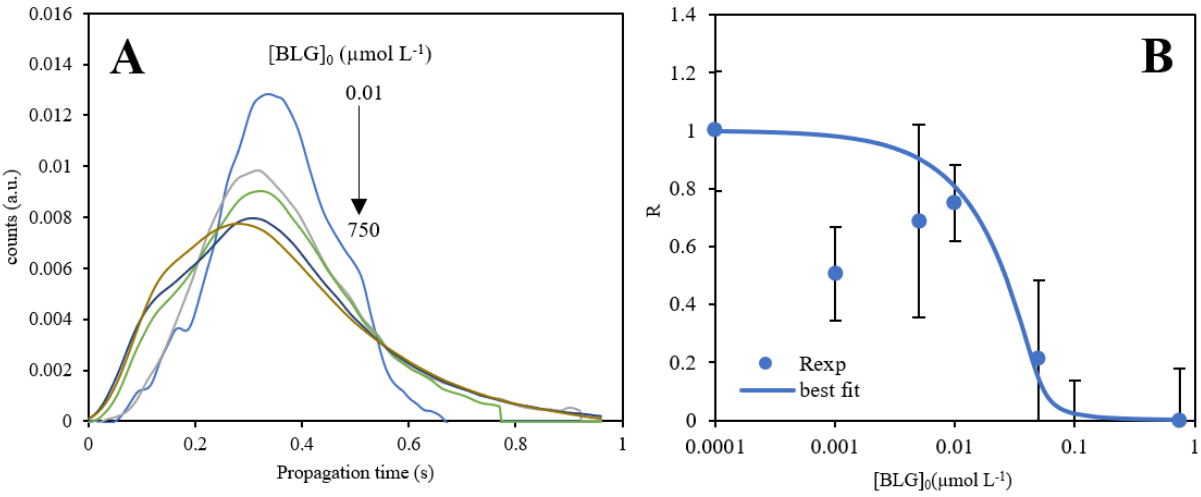

Figure 17: ACTIS-FLD measurements of BLG-FeQ_2 model system

The evaluation of the data yielded a K_d of 1.15 ± 4.14 µmol L^{-1}. The FeQ_2 concentration was constant in all measured working solutions. However, the signal intensity increased with increased $[BLG]_0$. This observation is in agreement with the previously discussed changes of quercetin's fluorescence depending on the binding state. Beside the inappropriate FeQ_2 concentration, this has also contributed to the high standard deviation. Evaluation data from this experiment is given in appendix, section 6.

Despite the high signal increase and consequently high standard deviation, the changed peak form with higher $[BLG]_0$ implies that the ACTIS assessment of K_d of BLG-FeQ_2 is possible. However, we expected that coupling ACTIS to another detector with higher sensitivity and specificity for FeQ_2 to be more successful.

3.3 Assessing K_d of the BLG-FeQ_2 model system

TOF-MS was selected as the detection method for the assessment of K_d of the BLG-FeQ_2 model system by ACTIS. A more precise and more sensitive technique compared to FLD should allow the assessing of accurate K_d value. Same as FLD detection, the TOF-MS compound detection is based on the quercetin signal. The unbounded Fe can not be directly detected with an organic MS method such as TOF-MS, since their m/z exceeds the lower limit of detectable m/z values of TOF-MS [47]. Additionally, the ESI source leads to soft ionisation and iron may not be completely ionised with it. However, we expected TOF-MS to detect FeQ_2 as an intact molecule or to find its fragments [48].

For the BLG-FeQ_2 model system, TOF-MS seems to be an excellent detector choice due to its low LOQ and LOD values. It is important to note that assessing of another metal-protein systems, with no organic molecule incorporated in the complex component, may not be possible by employing organic MS.

The reported m/z value for intact Fe(III)Q_2 complex obtained from ESI-TOF-MS analysis is 658.0049 [49]. According to molecular mass, this m/z value corresponds to $[(2Q\text{-}H)Fe]^+$ ion. According to the same study references [49], depending on further quercetin fragmentation more m/z values are possible, such as: 640, 612, 602, 584, and 465. Notable, this study had different methodology. The FeQ_2 complex was dissolved in methanol to final concentration of 10 µmol L^{-1}. In our work, the relatively high concentration of NH_4Ac and BLG in the working solutions may complicate the identification of 658.0049 m/z value. To be more specific, the presence of multiple positive charges on the $[(2Q\text{-}H)Fe]^+$ ion, or its association with NH_4^+ and/or H_3O^+ ions, can result in another more relevant m/z values for the specific FeQ_2 signal.

BLG-FeQ_2 working solutions were prepared with [FeQ_2] of 5.0×10^{-3} µmol L^{-1} for both experiments. We considered this concentration accessible for TOF-MS measurements and optimal for assessment of K_d. After measurements of pure Q and FeQ_2 solutions in concentration range of prepared BLG-FeQ_2 working solutions, the qualitative data analysis in MS DIAL was done. We applied this algorithm on pure ARS and pure FeQ_2 measurements, aiming to identify the specific m/z for FeQ_2 complex. This analysis in MS DIAL yielded a list of relevant m/z values associated with FeQ_2 complex: 590.9913, 508.9935, 426.9877, 344.9857, 262.9821, 180.9781, 158.9960, and 140.0014. The listed m/z values were used later to extract the ion chromatograms out of total ion chromatograms originated from ACTIS measurements.

Two ACTIS-TOF-MS experiments were carried out on the BLG-FeQ_2 system. The change of total ion content (TIC) during one run indicated if the injection of the sample was done properly. The TIC variations correspond to respective ACTIS steps, as showed in Figure 18.

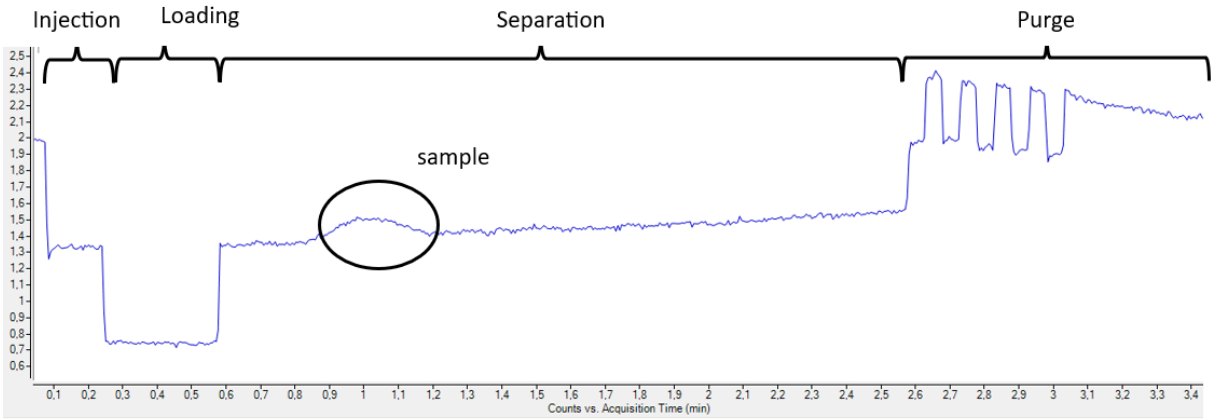

Figure 18: Total ion content (TIC) of one ACTIS–TOF–MS run

The separagrams were gained by extracting ion chromatograms from the TIC for each run. As previously mentioned, eight ions were selected for this purpose.

First experiment resulted in the separagrams and corresponding binding isotherm presented in Figure 19. In contrast to ACTIS-FLD, in ACTIS-TOF-MS signals of FeQ_2 decrease with increasing $[BLG]_0$. The reason for this appearance is the "masking effect" caused by increasing protein concentration. One possible explanation for the occurrence of the "masking effect" is that an increased production of protein fragment ions masks the relevant ions for ion extraction. Therefore, in the evaluation process using prACTISed, the compensation procedure was applied. For this procedure, the computer-simulated separagram of pure protein was necessary.

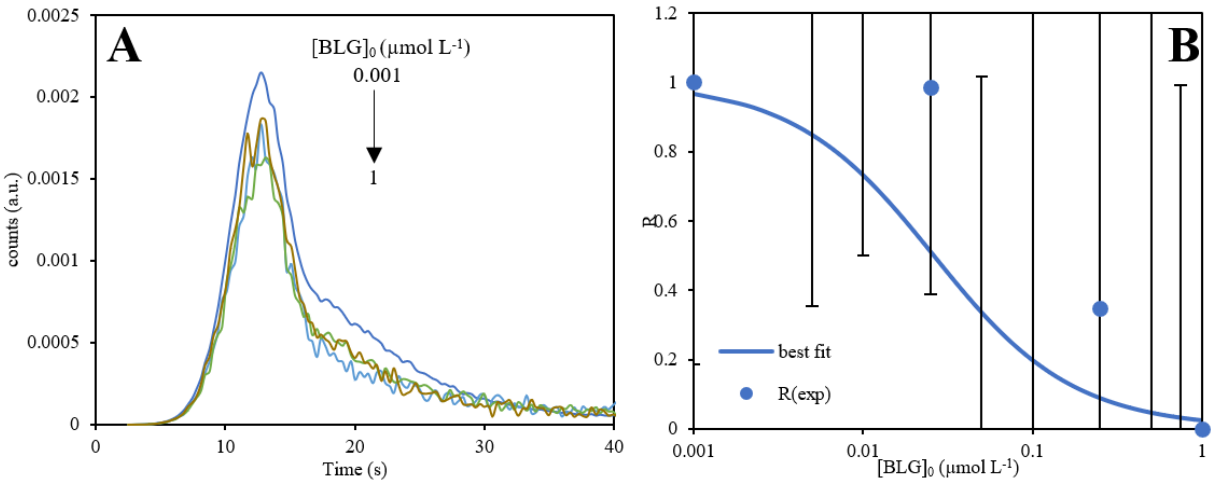

Figure 19: The results of the first ACTIS-TOF-MS experiment. A) The average separagrams of measured mixtures with different $[BLG]_0$; B) The resulting binding isotherm

Even though the compensation procedure proved to be an effective tool to reduce the "masking effect", we decide to change the range of $[BLG]_0$ for the second experiment. The main motivation was to check if this effect will be the same and to test if the precision can be improved. The second ACTIS-TOF-MS

experiment yielded separagrams and binding isotherm presented in Figure 20. Evaluation data from both ACTIS-TOF-MS experiments are given in appendix, sections 7 and 8.

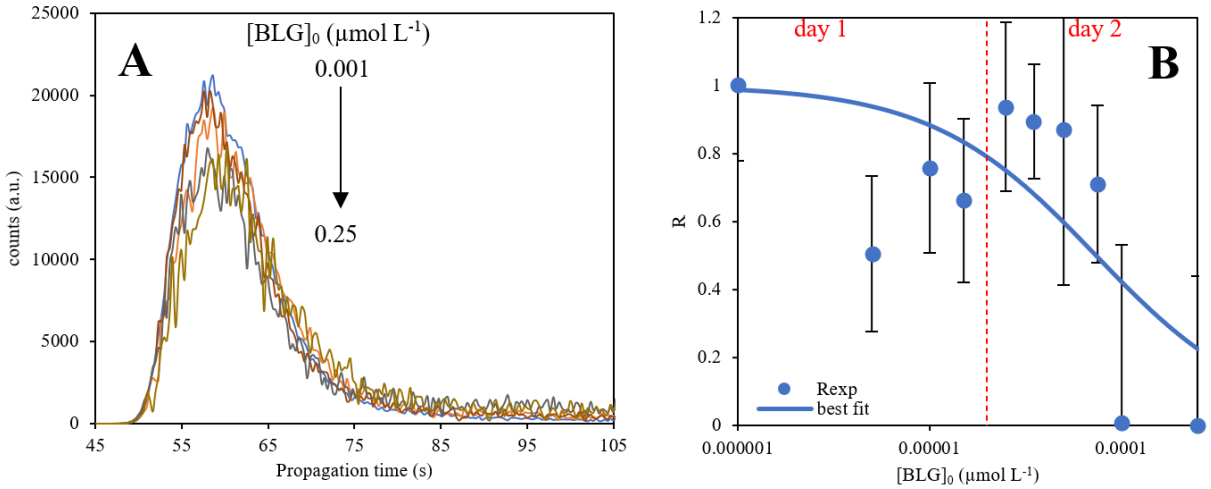

Figure 20: The results of the second ACTIS - MS -TOF experiment. The average separagrams of measured mixtures with different [BLG]0 (A); The resulting binding isotherm (B).

K_d value assessed in the first experiment was 0.0235 ± 0.0037 µmol L^{-1}. The K_d value observed in the second experiment was 0.0709 ± 0.0034 µmol L^{-1}. The reduction of $[BLG]_0$ for the second experiment resulted in a higher K_d value. Closer inspection of the separagrams revealed that the separation peak intensity of the mixtures with the same initial $[BLG]_0$ is higher in the second experiment. For instance, the separagram of $[BLG]_0$ = 0.05 µmol L^{-1} solution reaches its maximum at about 3,000 counts in the first and 18,000 counts in the second experiment. The similar trend is evident for all mixtures with the same $[BLG]_0$ measured in both experiments. Since the device tuning was performed between first and second experiments, this may have caused significant variations. However, since the normalization of the separagrams was done before the actual evaluation, this should not have significantly impacted the assessed K_d values.

Since the resulted distribution of the R values (Figure 18B) in second experiment was inconsistent, the fit of binding isotherm was predictably poor. Consequently, the standard deviation was high compared to gained K_d value. The measurements were performed over two days, namely four working solutions with lowest $[BLG]_0$ on the first and remaining solutions on the second day. The unusual R over $[BLG]_0$ distribution appears to be linked to changes in the day of measurement. Therefore, our assumption was that the TOF-MS conditions were different on each measurement day.

If this assumption is true, this inconsistency of R distribution would be the same for each m/z. Therefore, we checked each EIC for each m/z and found the same unusual R distribution. This distribution was independent of the normalization on the reference 922.0098 m/z. We did not apply

the compensation procedure during the evaluation to exclude the impact of simulated separagram. Resulting K_d values of corresponding m/z used for extraction are presented in Table 17 and Figure 19.

Table 17: K_d values gained by extraction of TICs after corresponding m/z value

m/z	**590.9913**	**508.9935**	**426.9877**	**344.9857**	**262.9821**	**180.9781**	**158.9960**	**140.0014**
K_d	0.0140	0.0153	0.0211	0.0213	0.0191	0.0171	0.0111	0.0224
Std. dev.	0.0088	0.0091	0.0111	0.0124	0.0111	0.0102	0.0076	0.0108

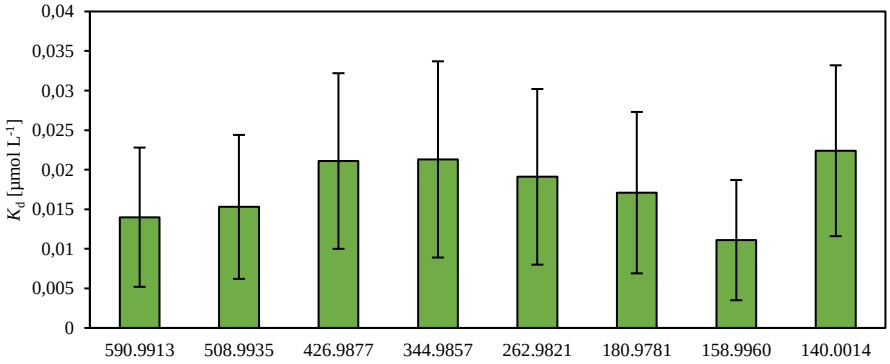

Figure 21: K_d values gained by extraction of TICs after corresponding m/z value

Resulting binding isotherms of all selected m/z values have similar *R* over $[BLG]_0$ distribution. Figure 21 represents binding isotherms of 140.0014 and 590.9913 m/z.

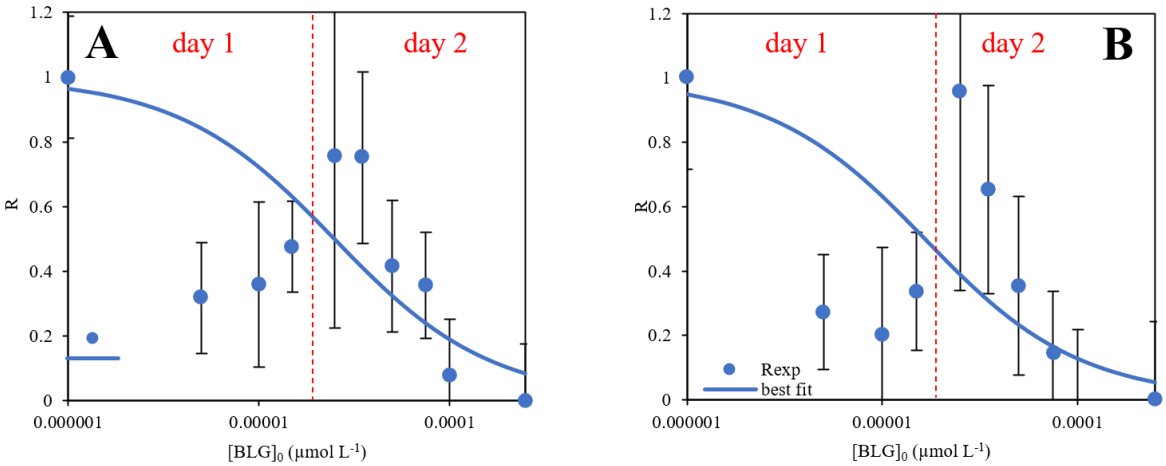

Figure 21: Binding isotherms resulted from TICs extractions after m/z = 140.0014 (A) and 590.9913 (B)

The reason for this unusual R distribution may lie in a device problem but more likely it is caused due to different measurement days and possible calibration of the device in between. To avoid this issue in the future, all measurement in frame of one ACTIS experiment should be performed on the same day in one session.

Despite many challenges in terms of precision and concentration limits, to the best of our knowledge, K_d values obtained with the ACTIS-TOF-MS technique represent the lowest values found for BLG-FeQ_2 complex. These values highlight the advantages and potentials of the ACTIS method. However, the determination of accurate K_d requires systematic studies and method optimization, which were beyond the scope of this work.

3.4 Exploring the application of ICP detection methods for ACTIS

ICP based detection methods are promising techniques for elemental analysis in combination with ACTIS. Particularly the assessment of the metal-protein binding may be achieved by metal detection over the time. ICP is widely used as ionization source in ICP-MS and as excitation source in ICP-AES [50]. The main advantages of ICP based detection techniques are high sensitivity and possibility to couple the instrument with ACTIS setup. These properties may play a crucial role in accurate assessment of K_d.

However, some ICP methods are not intended to perform transient measurements. For instance, sensitivity of ICP-AES and ICP-MS are related to area-based evaluation of the time-dependent signal. This represents a disadvantage for the application as an ACTIS detector because the transient evaluation is a crucial requirement for ACTIS. On the other hand, the optimization of measurement parameters may improve its ability to measure transient signals more precisely.

To explore the applicability of ICP-MS and ICP-AES for ACTIS experiments, we used the BLG-FeQ_2 model system. In contrast to previously performed ACTIS-FLD and ACTIS-TOF-MS, the detection of the compound was based on Fe detection here. The main goal of these experiments was to assess the compatibility of the specified detection methods with ACTIS. In addition to this, the optimal Fe concentration for ACTIS working solutions which can be accurately detected with these techniques should be estimated. Furthermore, the evaluation of impact of Fe binding to Q and to BLG on the Fe signal is also a part of these experiments.

ACTIS-ICP-MS

To test the background of Fe, the ARS (30 mmol L^{-1} NH_4Ac; pH=7.2) was prefilled in ACTIS setup and injected as a sample. In addition to this, the same ARS was also directly injected into the ICP-MS. The average of three measurements each showed similar noise level calculated as 3.5 × Std. dev., as well as similar intensity of about 150 counts. These results are given in appendix, section 9.

When we directly injected pure 5 µmol L^{-1} Fe solution, made by diluting the Fe II stock solution with ARS, unusual peaks appeared. We observed signal fluctuations and many spikes up to 2×10^5 counts. Results of three measurements are presented in Figure 22A. Our initial assumption was that the iron may not remain stable at the pH of 7.2 and the precipitation in solution causes huge signal fluctuations.

However, no precipitation was observed in either the stock solution or any of the analysed solutions. Very high noise level and considerable signal fluctuations indicated that the solution may have an issue.

To test this assumption, we prepared another 5 µmol L^{-1} Fe solution analogously to previous one. However, a different stock solution was used for the preparation in this case. The key difference of this stock solution compared to Fe II stock solution, was in its preparation - diluting Fe in sub-boiled H_2O with 2% HNO_3 and 0.1% HCl. This stock solution is further denoted as "new stock solution". The signals obtained after direct injection of this 5 µmol L^{-1} Fe solution showed reduced signal fluctuations (Figure 22B). This led us to conclusion that the solvent used to prepare the stock solution play a crucial role in the Fe measurement with ICP-MS.

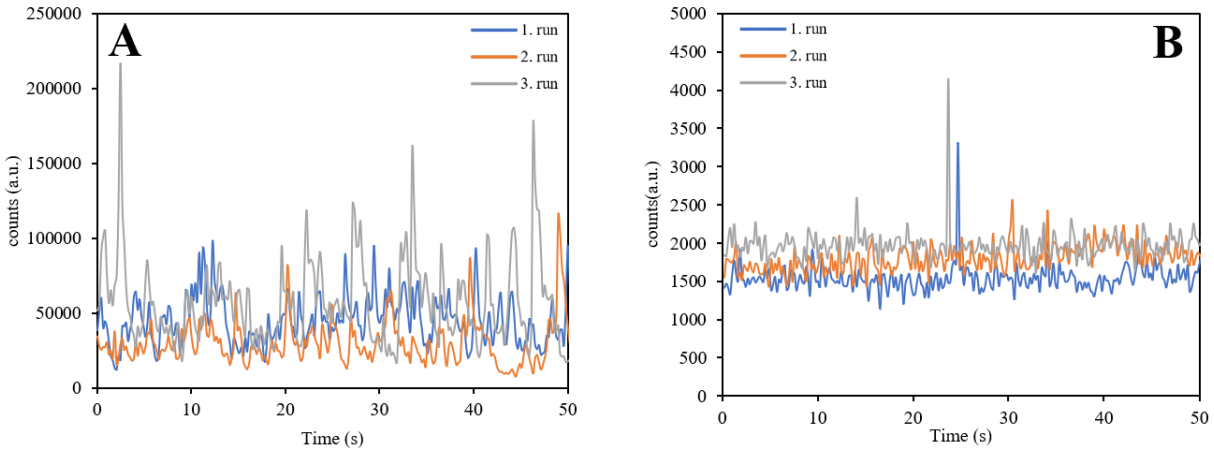

Figure 22: Three direct injections of 5 µmol L^{-1} Fe solution made by dilution of Fe II stock solution with 30 mmol L^{-1} NH_4Ac solution with pH = 7.2 (A); Three direct injections of 5 µmol L^{-1} Fe solution made by dilution of 1000 ng g^{-1} Fe stock solution with 30 mmol L^{-1} NH_4Ac solution with pH = 7.2 (B). The stock solution was prepared in sub-boiled H_2O with 2% HNO_3 and 0.1 % HCl.

The possible explanation for these differences might be the pH value. It is known that iron hydrolysation occurs in the aqueous solution depending on the pH value [51]. At higher pH, the hydrolysation process is more pronounced due to higher availability of OH^- ions. The hydrolysed Fe species can aggregate and especially at higher pH form various polynuclear complex polymers. The presence of Fe aggregates might explain the spikes observed during the measurements of Fe solutions made from stock solution with NH_4Ac. The lower pH and high concentration of NH_4Ac might resulted in dissolved polynuclear complexes.

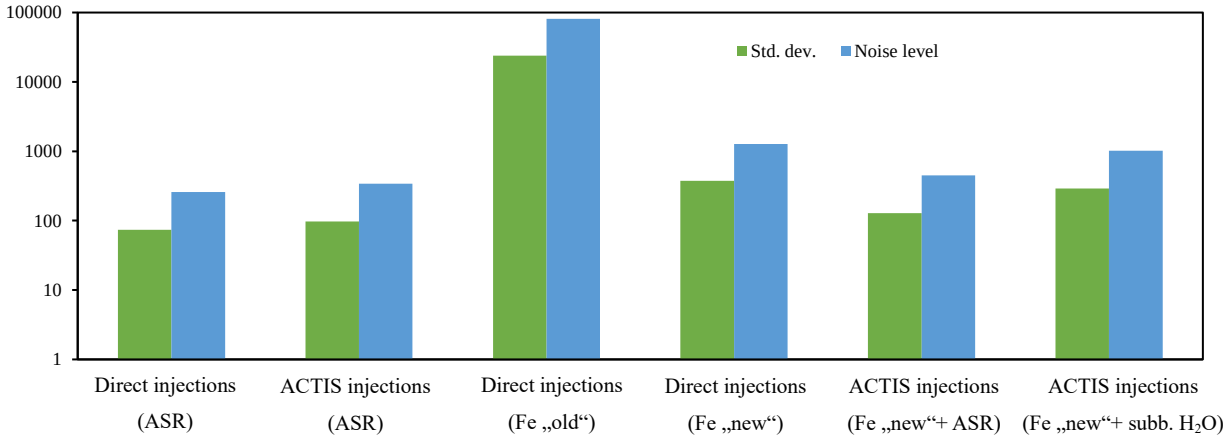

Figure 24: Standard deviations and noise calculated for different direct and ACTIS injections of NH_4Ac and Fe solutions. "Old" refers to Fe solution made by diluting Fe II stock solution and "new" refers to 1000 ng g^{-1} Fe stock solution made by diluting Fe in the 2% HNO_3 and 0.1 % HCl. The number values are given in appendix, section 9.

The standard deviations and noise calculated for different injection of NH_4Ac and Fe solutions are presented in Figure 24. The noise of the measurements of NH_4Ac injected directly or via ACTIS is comparable. The 1.3 times higher noise in the NH_4Ac signals when injected through ACTIS is caused due to longer time for transfer to ICP-MS through ACTIS setup compared to direct injections through autosampler needle. As discussed before, solutions of same [Fe] cause different noise levels depending on solution used in preparation of stock solutions. 30 mmol L^{-1} NH_4Ac with pH=7.2 in stock solution cause 60-times higher noise level comparing to sub-boiled H_2O with 2% HNO_3 and 0.1% HCl.

Iron is a one of the most abundant metals found in fine atmospheric particles [52]. The valve itself contains iron internally. Additionally, polyatomic interferences such as $^{40}Ar^{16}O^+$ and $^{40}Ca^{16}O^+$ can increase the background signals despite the KED mode applied [53]. Based on this data, we consider a background signal of around 150 counts without Fe in NH_4Ac solution added, acceptable.

Even though the 5 µmol L^{-1} Fe solution made from stock solution with sub-boiled H_2O with 2% HNO_3 and 0.1% HCl is theoretically not suitable for our working solutions for assessment of BLG-FeQ_2, we wanted to test if this solution can be potentially measured using ACTIS. Therefore, this Fe solution was injected into ICP-MS through ACTIS setup and the corresponding separagram is presented in Figure 23A. In addition to this, the same stock solution was diluted with sub-boiled H_2O to reach the same concentration and injected via ACTIS (Figure 23B). Notable, in all ACTIS runs, the 30 mmol L^{-1} NH_4Ac with pH=7.2 was employed as an ARS.

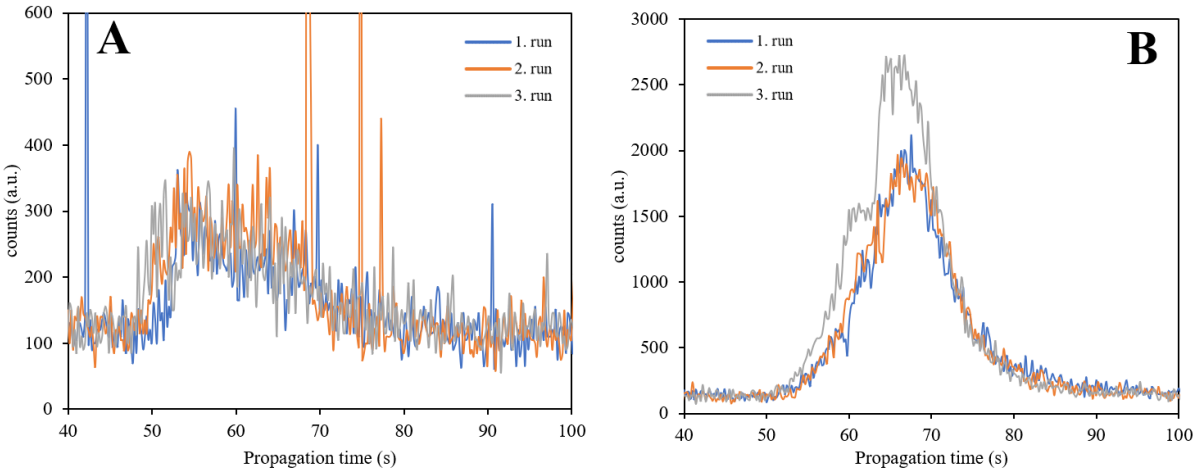

Figure 25: Three ACTIS runs of 5 µmol L^{-1} Fe solution, made by diluting Fe stock solution in sub-boiled H_20, 2% HNO_3 and 0.1% HCl with the NH_4Ac (A). Due to high signal fluctuations, the y-axis is reduced here to better observe the signals. The whole signals are given in appendix, section 8; Three ACTIS runs of the 5 µmol L^{-1} Fe solution made by diluting Fe stock solution in sub-boiled H_20, 2 % HNO_3 and 0.1 % HCl with the sub-boiled H_2O (B) The corresponding noise levels are given in Figure 22

The ACTI-ICP-MS measurement presented in Figure 25 revealed that not only the solvent in the stock solution but also the solvent used for preparing of working solutions affects outcoming signals strongly. We see that the NH_4Ac suppress the signals up to 5 times compared to signals of solutions made with sub-boiled H_2O. Beside the lower intensity, the NH_4Ac solution exhibits much more single distinct peaks, which potentially suggest the presence of Fe agglomerates. The noise is similar in both cases (Figure 22), but the signal-to-noise level is much better in the second case.

In all ACTIS-ICP-MS runs in the time range when the rinsing step occurs, including valve switching, we see that the distinct peaks are more frequent. This appearance is analogous to the signals in purge steps observed in ACTIS-FLD and ACTIS-TOF-MS techniques. However, good repeatability of the measurements supports the idea that the chosen purge time is acceptable for this technique.

The conducted experiments have shown that the coupling of ACTIS to ICP-MS theoretically can be used for the assessment of the metal-protein binding. We found that the preparation of stock solution as well as choice of the solvent play a crucial role for the Fe signal intensity and signal-to-noise ratio. For instance, the Fe concentration of 5 µmol L^{-1} is too low for the accurate measurements if the NH_4Ac is used as a solvent. If the H_2O is used as a solvent instead, even lower Fe concentrations might be considered for the ACTIS working solutions. Our assumption is that the pH value causes the forming of the Fe polynuclear complexes, which further cause higher signal fluctuations. The solvent for our ACTIS experiments was done according to optimal conditions for BLG-FeQ_2 complex. However, the conditions needed for stabile iron in solutions are different. These are important parameters that need to be studied more thoroughly to adjust this model system for ACTIS-ICP-MS assessment. However, this was beyond the scope of this study.

ACTIS-ICP-AES

To test the applicability of ICP-AES as a detector for ACTIS measurements, we first analysed the NH_4Ac solution (30 mmol L^{-1}; pH=7.2). The initial measurement performed to test this technique was the ICP-AES measurement of the pure NH_4Ac solution. The obtained Fe signals in NH_4Ac solution injected through ACTIS injections into ICP-AES are presented in Figure 26.

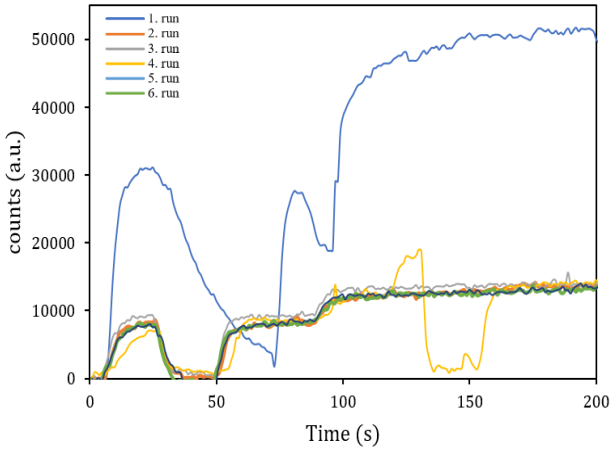

Figure 26: Six ACTIS-ICP-AES runs of NH_4Ac solution injected as a sample. The wavelength was set to 238.204 nm for Fe

Among the six measurements, two showed variations in forms and intensity, namely the first and the fourth run. It is important to highlight that during these measurements a syringe pump was used instead of pressure pump and no flow sensor was utilized. Consequently, these deviations may have been caused due to potential flow rate problems.

Even if we ignore the repeatability issue, it becomes evident that the signal intensity is significantly influenced by the flow rate of injected solution. With the flow rate of about 68 µL min^{-1}, the background signal stabilizes at around 10,000 counts. With the constant flow rate, the signals are steady but when the flow rate is changed, the signal also changes immediately. For example, after valve switch between sample loading and separation step, the signal takes 6 seconds to reach its stable value.

Despite the low repeatability of the Fe signals, we decided to explore the effects of Fe concentration on them. Therefore, Fe solutions of 0.01 µmol L^{-1}, 1 µmol L^{-1}, and 10 µmol L^{-1} were injected into ACTIS-ICP-AES. The repeatability of these measurements was poor. Three of four runs of 10 µmol L^{-1} solutions and only four of six runs of 1 µmol L^{-1} solutions showed similar signal intensity. In contrast to this, all four measurements of 0.01 µmol L^{-1} Fe solutions were similar.

To be able to compare the effects of different Fe concentrations, we decided to consider only the measurements which resulted in similar intensity and shape (± 10% variations). The similarity was checked after normalisation of each separagram. All normalised measurements are added in appendix, section 10. The separation step was cut and normalised to surface of 1. Due to high dependency of the signal on the flow rate, an alignment of the base lines became necessary. We used a linear function

defined by the points marking the start and the end of the separation peak for the alignment. More precisely, the y-values calculated from the resulting function were subtracted from the signal values. The averages of aligned separation peaks are presented in Figure 27.

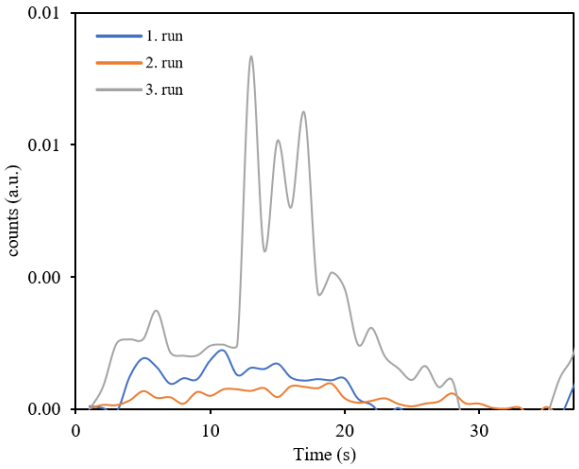

Figure 27: Average signals of normalized separations steps of similar 0.01 µmol L^{-1}, 1 µmol L^{-1}, and 10 µmol L^{-1} measurements

In contrast to 0.01 µmol L^{-1} and 1 µmol L^{-1}, 10 µmol L^{-1} Fe solution exhibit peaks during the separation step (Figure 25). Three peaks observed in 10 µmol L^{-1} Fe solution are very narrow and consist of only few signals, but the peak shape resembles to the flow injection peaks observed in ICP-MS. Namely, the sharp rise and flatter descending are characteristic for ACTIS-ICP-MS injection peaks (Figure 25). However, it is very complicated to determine the time length of this signal.

To check if the Fe binding in BLG-FeQ_2 complex will affect the ACTIS separagrams, we decided to measure BLG-FeQ_2 working solutions. Fe concentration of 1 µmol L^{-1} was selected for BLG-FeQ_2 working solutions. Even though no Fe signals were observed when injected into ACTIS-ICP-AES, using this concentration enabled us to directly assess whether binding to Q or BLG would alter the absence of Fe signals.

10 working solutions of BLG-FeQ_2 were prepared and only one run per mixture was performed. All the aligned peaks were normalized to the surface value of one. The Figure 28 displays peaks gained by correction of whole separation step with the linear function. The solutions with $[BLG]_0$ of 0.25 µmol L^{-1} and 50 µmol L^{-1} exhibited separagrams with significant deviations. They are not presented here to allow for a clearer observation of other separagrams, but they are given in the appendix, section 10.

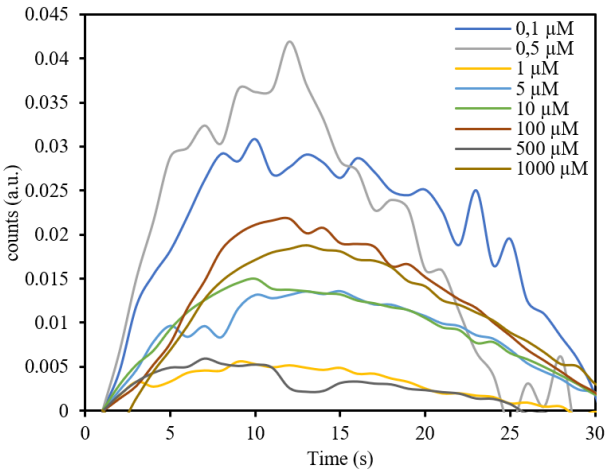

Figure 28: Aligned and normalized separagrams of 8 different working solutions measured using ACTIS-ICP-AES

The different $[BLG]_0$ in working solutions caused different slopes of the separation peak. Since the same flow rate was used for all performed runs, the changes of the slope implicate that the binding of FeQ_2 to BLG affects it.

The increased stability of the Fe in ASR caused by the binding to Q may explain this appearance. It is known that the complexation of Fe in extraction process with chelating agents having a high affinity for Fe can improve its determination [54]. To the best of our knowledge, there have been no studies investigating how the binding of iron to another molecule can affect its quantification by ICP based techniques. Based on performed experiments, the binding to Q and BLG improves iron detection. However, further studies are necessary to validate this observation and more importantly to eliminate the potential influence of flow rate on the signals.

It is evident that the increasing of the $[BLG]_0$ caused the general reduction in maximal signal intensity and changed separagram forms (Figure 28). This pattern is not the same across all mixtures. For instance, the maximum of working solution with $[BLG]_0$ = 0.5 µmol L^{-1} is higher than the maximum of working solution with $[BLG]_0$ = 0.1 µmol L^{-1} mixture, yet the trend remains evident.

The prACTISed evaluation of gained separagrams yielded K_d of 0.208 ± 0.5 µmol L^{-1}. This value is in the same range as K_d yielded from ACTIS-TOF-MS measurements for this model system. However, since only one run per working solution was performed and by strong signal dependence on flow rate, we would not consider gained results as accurate and precise. Despite that, the reduced signal intensity with increased $[BLG]_0$ proves the possibility of K_d assessment using this method. The evaluation data is given in appendix (section 10).

The fluctuations in the Fe signal, even at the constant flow rate, cannot be explained by the apparent impact of the flow rate. This leads us to consider the potential influence of the nebulizer configuration. As already mentioned, µflow nebulizer was used for both ACTIS-ICP-MS and ACTIS-ICP-AES methods.

As the nebulizer is positioned between the separation capillary and the actual detection, the length and geometry of the nebulizer may affect the characteristic flow profile. In order to further explore the impact of the transfer capillary on the characteristic flow profile and consequently the accuracy of the K_d, computer simulations were performed.

3.5 Exploring the detector transfer capillary effects

One of the key advantages of ACTIS is its foundation in a deterministic process. The deterministic process can be computer-simulated, which allows the assessing of K_d in silico. These simulations can be used to evaluate the accuracy of performed ACTIS measurements, but also to examine the influence of physical factors on K_d accuracy. In order to understand the complexity of coupling ACTIS to ICP-AES, computer-simulations provide a valuable opportunity.

The linkage of ACTIS to a detection system is carried out through direct connection of the separation capillary to the detection system. The form of the detector injection system (nebulizer transfer capillary) can possibly have an influence on the K_d accuracy. Depending on the length and the width of the transfer capillary, the form of flow profiles may change after the transition of sample from separation capillary to detector. For example, introduction of the sample from ACTIS to ICP-AES includes the transition from separation capillary through the connector into a nebulizer. The inner radius of nebulizer capillary as well as its length can vary depending on a model used. In order to explore if the sample flow profile and consequently the K_d accuracy are affected by the transfer capillary inner radius, the computer simulations were employed.

Nine different inner radius of transfer capillary were tested using computer simulations. Alignment of the obtained separagrams was necessary due to variations in the starting time points. The shift in peak start positions is emerged due to lower mesh and time resolution with increasing nebulizer radius. The aligned and normalized separagrams of pure PC complex and pure C are displayed in Figure 29.

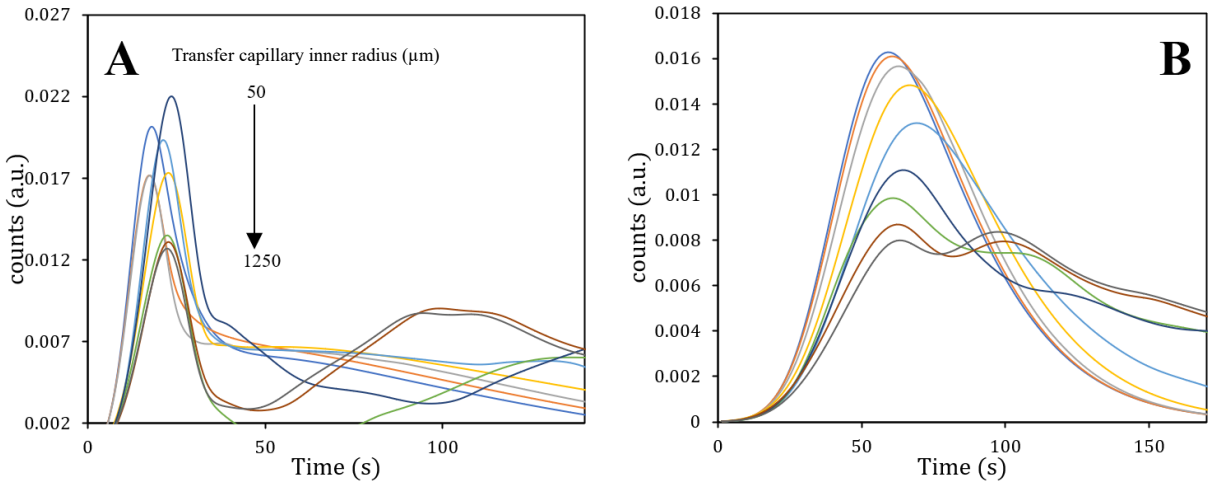

Figure 29: Separagrams made by computer simulations for PC (A) and C (B)

The lower diffusivity of PC complex caused more narrow peaks which arise earlier compared to the low diffusive C peaks. In the simulated separagrams an observable effect is that an increased inner radius decreases peak intensity while simultaneously raising post-peak signals. This signal changes suggest that the later portions of the PC flow profile spent more time in the wider nebulizer and therefore elute later. This caused lower intensity of the initially eluted molecules. The similar trend is observed in the separagrams for high diffusive C.

Let´s examine the appearance of the separagrams of systems with both PC and C. Figure 30 represents the separagrams of both extremes, 50 and 1250 µm nebulizer diameter. These separagrams illustrate the negative effects of the wider transfer capillary. Due to higher signals of later portions of molecules in a flow profile, the diffusive peak is strongly reduced and the new, third peak is formed. Additionally, the dynamic range is reduced about 30% with wider transfer capillary.

Furthermore, a wider nebulizer results in a broader and more intense PC peak at the front of the flow profile. The black arrows clearly show how the working range is reduced in the wider transfer capillary.

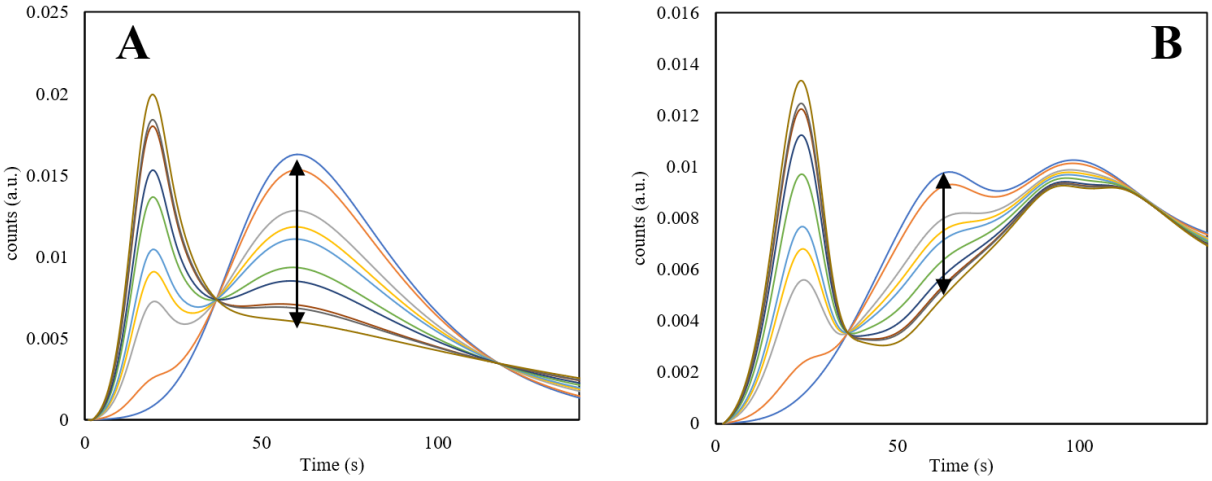

Figure 30: Normalized separagrams for transfer capillary inner radius of 50 µm (A), and 1250 µm (B) and corresponding working range

To estimate the influence of transfer capillary inner radius, the normalized separagrams for each tested nebulizer inner diameter, were put into the prACTISes for the assessing of the K_d values. The assessed K_d values as well as respective standard deviations are displayed in Figure 31. Separagrams and corresponding binding isotherms are given in appendix, section 11.

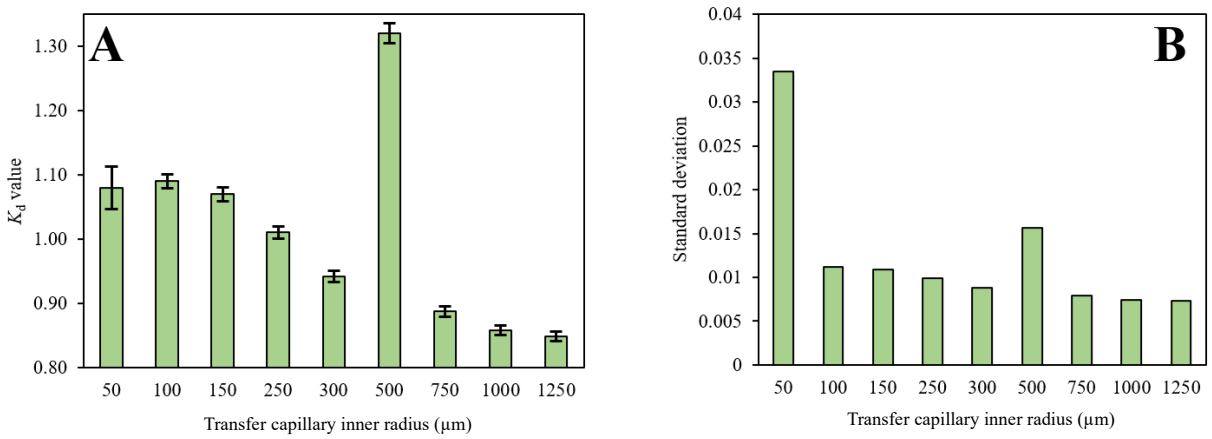

Figure 31: K_d values (A) and respective standard deviations (B) resulted from computer simulations.

K_d value which was used to calculate the R and the separagrams was set to 1 µmol L^{-1}. Therefore, the simulations of ideal transfer capillary inner radius should result in this value. Notably, the nebulizer inner radius of 250 µm gave the closest value to the expected one. The inner radius of the separation capillary was set to 250 µm in all simulations. This implicates, that the most accurate K_d value can be assessed if the nebulizer inner radius matches the separation capillary inner radius. With the exception of the 500 µm transfer capillary radius, assessed K_d values as well as corresponding standard deviations decrease with increasing the nebulizer inner radius (Figure 31). This result is in agreement with the observation of the separagrams, which showed lower values and lower changes of the diffusive peak intensity with wider transfer capillary radius.

In order to explore the effects of noise on resulting K_d values, we added noise to the separagrams of 50, 250 and 1250 µm simulations. The added noise (10-15 s/n) was comparable to the noise observed in conducted ICP-AES and ICP-MS measurements (14 s/n). A random number in range from -0.001 to 0.001 was added to every signal in each simulated separagram. Subsequently, separagrams were normalized and evaluated using prACTISed. The resulting K_d values and corresponding standard deviations are given in Figure 32. Further data is given in appendix, section 12.

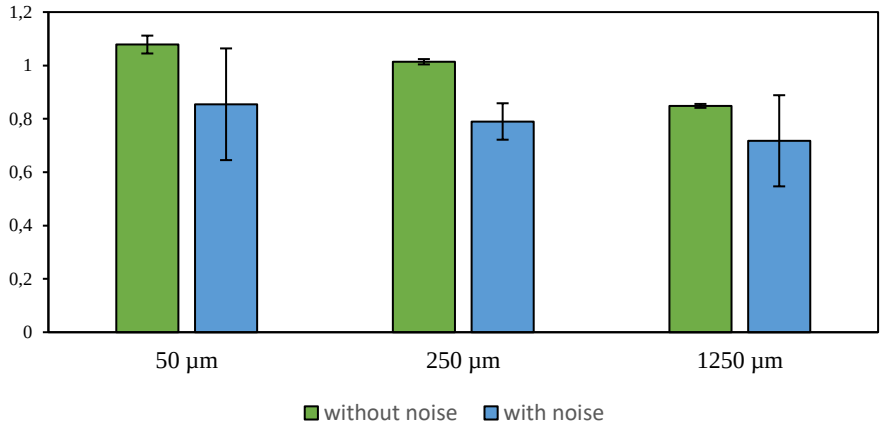

Figure 32: K_d values and corresponding standard deviations of noise-modified and original separagrams for transfer capillary inner radius of 50, 250, and 1250 µm

We see that noise greatly affected the accuracy of gained results independently of transfer capillary inner radius. On the other hand, the standard deviation is lowest for the inner radius of transfer capillary matching the inner radius of separation capillary (250 µm). A requirement for accurate K_d assessment is a high s/n ratio. Based on these simulations, we recommend at least 10 s/n ratio. The computer simulations have shown that the matching inner radii of separation and transfer capillary yield in the most accurate K_d.

3.6 Limitations and challenges

While our ACTIS experiments yielded compelling results, we found different limitation and challenges that we want to discuss here. These challenges and limitations can be categorized as instrumental or as methodological.

In all conducted experiments, we identified a technical challenge related to introduction of air bubbles into ACTIS capillary system. This problem was very characteristic for initial runs following a change of working solutions. Due to air bubble introduction into the injection capillary, the resulting signal was either lost or significantly changed compared to signals from other runs. Consequently, first runs yielded much lower or much higher signal intensity. To address this instrumentation issue, the employing of isopropanol between each sample change can be beneficial. Due to its lower viscosity, compared to aqueous solution of NH_4Ac, it could push air bubbles out of the capillary [55]. In addition

to this, a pump which can set higher pressure to the setup can be also helpful in terms of air bubble reduction.

The methodological limitations refer to the coupling of ACTIS to a detection system. The main limitation of ACTIS-FLD is its applicability on systems which have fluorescence active compound only. Furthermore, the flow cell volume affects the precision of transient measurement. To improve the precision, the FLD with lower flow cell volume should be used.

Even though very low K_d values can be assesses using ACTIS-TOF-MS, we are aware that this method may have few limitations. The investigation of lower binding affinities is limited by the protein concentration. The protein concentration that can be introduced into the TOF-MS device is limited. The protein fragment ions are masking the ligand ions and affects negatively the ion extracting process. The signal-masking effects can be compensated during the evaluation process. Nevertheless, the protein concentration range for working solutions should be selected so, to ensure that no signal overlapping occurs. The investigation of less complex PC system of only two molecules would also greatly improve the process of finding specific m/z values for the extracting of ion chromatograms.

By coupling the ACTIS to ICP based detection systems (ICP-MS and ICP-AES), few points need to be considered. The concentrations of metals are limited by the [C]/K_d ratio in order to achieve accurate K_d values. The injected metal quantity is additionally diluted by the ARS in the separation capillary. Thus, in regard to the BLG-FeQ_2 model system, more sensitive Fe detection would be of advantage.

In the ACTIS-AES, the strong influence of the flow rate on signal represents the main challenge. This can compromise the sensitivity and accuracy of the measurement. Therefore, future experiments on this technique should reduce flow rates in separation steps. Moreover, the assessing of K_d using ACTIS-ICP-MS is strongly affected by the chosen stock solution. The preparation of freshly made Fe solutions in NH_4Ac and the preparation of Fe stock using sub-boiled H_2O in 2% HNO_3 and 0.1% HCl greatly improve the signals intensity and stability.

Since ACTIS is a novel method, it is currently under-explored within the research community, resulting in a limited pool of researchers actively investigating it. This may be challenging in terms of exchange of experiences. On the other hand, the research of this novel method can stimulate innovation and creativity.

4 Summary and conclusion

In conclusion, this work showed that assessing the K_d of metal-protein systems is possible using ACTIS. The conducted ACTIS-FLD measurements on HSA-FLC model system validated the capability of our setup to conduct ACTIS experiments. K_d values in µmol L^{-1} range found in both ACTIS-FLD experiments align with literature value for BSA-FLC model system. This showed that the chosen ACTIS instrumentation is suitable for further experiments.

The validated ACTIS-FLD system was subsequently employed to explore the feasibility of assessing K_d of a specific metal-protein system (BLG-FeQ_2). Challenges related to solubility and signal intensity were effectively addressed during this stage. Although the ability of K_d estimation of this model system using ACTIS-FLD was verified, the necessity for a more sensitive detection system became evident.

To our knowledge, the assessment of BLG-FeQ_2 binding using ACTIS-TOF-MS represents the lowest K_d values found for this complex. K_d value assessed in both ACTIS-TOF-MS experiments were in nmol L^{-1} range. Despite the relatively high standard deviations, these values highlight the potential of the ACTIS method to assess low K_d values. Additionally, we found that it is crucial to perform one experiment within a single day, to eliminate potential variations in device properties that can greatly impact the results.

Coupling of ACTIS to ICP-MS showed promising results when investigating higher K_d values where higher iron concentrations need to be measured. We found that the pH value and the solvent used influence the obtained Fe signal. Transient measurements of Fe concentrations in nmol L^{-1} to µmol L^{-1} range are the base for the assessing accurate K_d of BLG-FeQ_2 model system. The present capability of ICP-MS was not sufficient for this. Therefore, the method optimization through systematic studies is required.

Exploration of ACTIS-ICP-AES system revealed issues caused by flow rate - dependent signal change in transient Fe signal. Additionally, the binding of Fe to Q and BLG affected changes in Fe signal compared to signals of pure Fe solutions. This indicates that the complexation of iron positively affects its detection with this technique. More precise transient metal detection would allow assessing of metal-protein binding affinities using this method.

We must note that the chosen protein-metal model system posed challenges for the ACTIS exploration. The main reason for this is the strong binding that requires low metal concentrations for working solutions. In the separation step of an ACTIS run, this concentration is additionally diluted. Therefore, very low LOQ of detection method is required. Additionally, having three compounds in this model makes the assessment even more complicated.

Finally, we made additional important discoveries by employing computer simulations. In silico simulating of ACTIS experiments with different transfer capillary inner radius proved that the same capillary inner radii of separation and transfer capillary yield the most accurate K_d values. Moreover, the increasing of transfer capillary inner radius induces more turbulence of molecules and destroys the characteristic flow profiles. Additionally, we found that the noise about 15 counts can greatly affects the accuracy of the gained results independently of transfer capillary inner radius. On the other hand, best precision was found for the inner radius of transfer capillary matching the inner radius of separation capillary. A high signal-to-noise ratio is an important requirement for accurate K_d assessment. Based on these simulations, we recommend at least 10 signal-to-noise.

ACTIS proved to be a challenging method to handle. The estimated time for one ACTIS experiment is about 8 h, and the experimenter must be present the whole time. Automated valve and pump switching between the steps, greatly reduces the need of the experimenter to be present, but it is still necessary for sample injection and tracking the sample loading. We found the evaluation of the results also demanding. The actual evaluation using prACTISed take only few seconds, but the preparation of the results for the evaluation is time-consuming since the cut of the separation peaks and their normalization must be done manually in Excel or related software before input into prACTISed.

In summary, the ACTIS method shows great promise for accurately determining K_d of protein-metal complexes. It can assess a wide range of K_d values, depending on the detection system used. By implementing the recommendations given in the next section and addressing the minor technical issues, ACTIS has the potential to become a widely accepted standard for K_d assessment. Additionally, the method's capability for computer simulations is a significant advantage.

5. Outlook

This work is the first step towards enhancing the assessing of metal-protein binding constants. The present findings may help to better design the future ACTIS experiments. Therefore, here are few recommendations for this purpose.

The applying of ACTIS-TOF-MS has a great potential to become main ACTIS detector for assessing PC binding, especially when C is an organic molecule. To further investigate this method, few interesting model systems can be used. For example, binding of an anti-cholesterol drug Rosuvastatin (ROS) to HSA was recently investigated using SPR and K_d value of 1.55 × 10^{-2} µmol L^{-1} was found [56]. If we assume that the real value is in this scale, the $[ROS]_0$ for working solution should be around 1.55 × 10^{-4} µmol L^{-1}. Even though very low concentrations needed for this experiment, the molecule structure of ROS might have a characteristic sulfur containing fragment that represents a specific m/z value for tracking [ROS] over the time [57]. Furthermore, the binding of BSA to Acetazolamide (AZA) was also investigated using SPR and K_d of 67.72 µmol L^{-1} was assessed [58]. K_d in this range enables higher compound concentrations for ACTIS experiments. Since the AZA is a small organic molecule of molecule of mass of 222.25 g mol^{-1} with ESI as a soft ionization technique, theoretically the intact molecules could be used for tracking [AZA] over time.

The employing of MS devices with higher resolution compared to TOF devices, such as Orbitrap, could also improve ACTIS. More specifically, the typical TOF-MS resolution is in the range of 10,000-100,000 compared to Orbitrap which possesses resolutions of 100,000 up to 1,000,000 [59]. Lower resolution may be challenging in evaluation of ACTIS measurements, especially in complex mixtures with higher protein content.

Future experiments of ACTIS coupling to ICP techniques should consider protein-metal model systems including less abundant metals than Fe. Theoretically, precious metals such as Gold (Au), Platinum (Pt), Palladium (Pd) or heavy metals Cadmium (Cd), Lead (Pb), Mercury (Hg) can be effectively and more precisely determined using ICP-MS. HSA and hemoglobin (HG) have a high affinity to Hg with K_d of about 1 × 10^{-7} µmol L^{-1} [60]. Moreover, the investigation of Pt binding peptides would be also suitable for further experiments [61].

5 References

[1] I. Yu *et al.*, 'Biomolecular interactions modulate macromolecular structure and dynamics in atomistic model of a bacterial cytoplasm', *eLife*, vol. 5, p. e19274, doi: 10.7554/eLife.19274.

[2] R. J. Woosley, 'Evaluation of the temperature dependence of dissociation constants for the marine carbon system using pH and certified reference materials', *Mar. Chem.*, vol. 229, p. 103914, 2021, doi: 10.1016/j.marchem.2020.103914.

[3] Department of Chemistry, Federal University of Technology, Owerri, Nigeria, O. V. Ogechi, O. A. Ikejiofor, and Department of Chemistry, Chukwuemeka Odumegwu Ojukwu University, Uli Campus Anambra, Nigeria, 'A Review of the Essence of Stability Constants in the Thermodynamic Assessments of Chemical Compounds', *J. Mater. Sci. Manuf. Res.*, pp. 1-8, 2023, doi: 10.47363/JMSMR/2023(4)150.

[4] N. A. Meanwell, 'Improving Drug Candidates by Design: A Focus on Physicochemical Properties As a Means of Improving Compound Disposition and Safety', *Chem. Res. Toxicol.*, vol. 24, no. 9, pp. 1420–1456, 2011, doi: 10.1021/tx200211v.

[5] J. Carrasco *et al.*, 'In Situ and Theoretical Studies for the Dissociation of Water on an Active Ni/CeO2 Catalyst: Importance of Strong Metal–Support Interactions for the Cleavage of O–H Bonds', *Angew. Chem. Int. Ed.*, vol. 54, no. 13, pp. 3917–3921, 2015, doi: 10.1002/anie.201410697.

[6] J. C. Meier *et al.*, 'Design criteria for stable Pt/C fuel cell catalysts', *Beilstein J. Nanotechnol.*, vol. 5, no. 1, pp. 44–67, 2014, doi: 10.3762/bjnano.5.5.

[7] 'Chemical equilibrium | Definition, Equation, & Facts | Britannica'. Accessed: Oct. 11, 2023. [Online]. Available: https://www.britannica.com/science/chemical-equilibrium

[8] P. Schuck, 'Use of Surface Plasmon Resonance to Probe the Equilibrium and Dynamic Aspects of Interactions Between Biological Macromolecules', *Annu. Rev. Biophys. Biomol. Struct.*, vol. 26, no. 1, pp. 541–566, 1997, doi: 10.1146/annurev.biophys.26.1.541.

[9] K. Kaastrup, L. Chan, and H. D. Sikes, 'Impact of Dissociation Constant on the Detection Sensitivity of Polymerization-Based Signal Amplification Reactions', *Anal. Chem.*, vol. 85, no. 17, pp. 8055–8060, Sep. 2013, doi: 10.1021/ac4018988.

[10] G. G. Ferenczy and G. M. Keserű, 'The impact of binding thermodynamics on medicinal chemistry optimizations', *Future Med. Chem.*, vol. 7, no. 10, pp. 1285–1303, Jul. 2015, doi: 10.4155/fmc.15.63.

[11] L. Fielding, 'NMR methods for the determination of protein–ligand dissociation constants', *Prog. Nucl. Magn. Reson. Spectrosc.*, vol. 51, no. 4, pp. 219–242, Nov. 2007, doi: 10.1016/j.pnmrs.2007.04.001.

[12] F. Bottari *et al.*, 'Do Aptamers Always Bind? The Need for a Multifaceted Analytical Approach When Demonstrating Binding Affinity between Aptamer and Low Molecular Weight Compounds', *J. Am. Chem. Soc.*, vol. 142, no. 46, pp. 19622–19630, Nov. 2020, doi: 10.1021/jacs.0c08691.

[13] H. Wätzig *et al.*, 'Data quality in drug discovery: the role of analytical performance in ligand binding assays', *J. Comput. Aided Mol. Des.*, vol. 29, no. 9, pp. 847–865, 2015, doi: 10.1007/s10822-015-9851-6.

[14] B. Pathare, V. Tambe, and V. Patil, 'A review on various analytical methods used in determination of dissociation constant', *Int. J. Pharm. Pharm. Sci.*, vol. 6, pp. 26–34, 2014.

[15] V. K. Srivastava and R. Yadav, 'Chapter 9 - Isothermal titration calorimetry', in *Data Processing Handbook for Complex Biological Data Sources*, G. Misra, Ed., Academic Press, 2019, pp. 125–137. doi: 10.1016/B978-0-12-816548-5.00009-5.

[16] A. K. Dutta, J. Rösgen, and K. Rajarathnam, 'Using Isothermal Titration Calorimetry to Determine Thermodynamic Parameters of Protein–Glycosaminoglycan Interactions', in *Glycosaminoglycans*, vol. 1229, K. Balagurunathan, H. Nakato, and U. R. Desai, Eds., in Methods in Molecular Biology, vol. 1229. , New York, NY: Springer New York, 2015, pp. 315–324. doi: 10.1007/978-1-4939-1714-3_25.

[17] S. Grüner *et al.*, 'Impact of protein and ligand impurities on ITC-derived protein–ligand thermodynamics', *Biochim. Biophys. Acta BBA - Gen. Subj.*, vol. 1840, no. 9, pp. 2843–2850, 2014, doi: 10.1016/j.bbagen.2014.04.018.
[18] D. Prozeller, S. Morsbach, and K. Landfester, 'Isothermal titration calorimetry as a complementary method for investigating nanoparticle–protein interactions', *Nanoscale*, vol. 11, no. 41, pp. 19265–19273, Oct. 2019, doi: 10.1039/C9NR05790K.
[19] Y. Tang, X. Zeng, and J. Liang, 'Surface Plasmon Resonance: An Introduction to a Surface Spectroscopy Technique', *J. Chem. Educ.*, vol. 87, no. 7, pp. 742–746, 2010, doi: 10.1021/ed100186y.
[20] L. zu externer W. (Anzeige in neuem Fenster), 'Gold-Film-Thickness Dependent SPR Refractive Index and Temperature Sensing with Hetero-Core Optical Fiber Structure', 2019, doi: 10.3390/s19194345.
[21] P. Pattnaik, 'Surface Plasmon Resonance: Applications in Understanding Receptor–Ligand Interaction', *Appl. Biochem. Biotechnol.*, vol. 126, no. 2, pp. 079–092, 2005, doi: 10.1385/ABAB:126:2:079.
[22] R. Bakhtiar, 'Surface Plasmon Resonance Spectroscopy: A Versatile Technique in a Biochemist's Toolbox', *J. Chem. Educ.*, vol. 90, no. 2, pp. 203–209, Feb. 2013, doi: 10.1021/ed200549g.
[23] G. Xu *et al.*, 'Structural Insights into the Mechanism of High-Affinity Binding of Ochratoxin A by a DNA Aptamer', *J. Am. Chem. Soc.*, vol. 144, no. 17, pp. 7731–7740, 2022, doi: 10.1021/jacs.2c00478.
[24] N. Sisavath *et al.*, 'Transient Incomplete Separation Facilitates Finding Accurate Equilibrium Dissociation Constant of Protein–Small Molecule Complex', *Angew. Chem. Int. Ed.*, vol. 58, no. 20, pp. 6635–6639, 2019, doi: 10.1002/anie.201901345.
[25] J.-L. Rukundo *et al.*, 'Template Instrumentation for "Accurate Constant via Transient Incomplete Separation"', *Anal. Chem.*, vol. 93, no. 34, pp. 11654–11659, 2021, doi: 10.1021/acs.analchem.1c02007.
[26] A. Griffiths, 'On the Movement of a Coloured Index along a Capillary Tube, and its Application to the Measurement of the Circulation of Water in a Closed Circuit', *Proc. Phys. Soc. Lond.*, vol. 23, no. 1, pp. 190–197, 1910, doi: 10.1088/1478-7814/23/1/316.
[27] Ch.-H. Fischer and M. Giersig, 'Analysis of colloids', *J. Chromatogr. A*, vol. 688, no. 1–2, pp. 97–105, 1994, doi: 10.1016/0021-9673(94)00962-7.
[28] R. Umehara, H. Miyahara, A. Okino, M. Harada, and T. Okada, 'Wide-Bore Capillary Hydrodynamic Chromatography with ICP-MS Detection for Evaluation of Lanthanide Uptake by Molecular Aggregates', *Anal. Sci.*, vol. 28, no. 4, pp. 359–365, 2012, doi: 10.2116/analsci.28.359.
[29] M. Pelcová, R. Řemínek, F. A. Sandbaumhüter, R. A. Mosher, Z. Glatz, and W. Thormann, 'Simulation and experimental study of enzyme and reactant mixing in capillary electrophoresis based on-line methods', *J. Chromatogr. A*, vol. 1471, pp. 192–200, 2016, doi: 10.1016/j.chroma.2016.10.002.
[30] T. Y. Wang *et al.*, 'Transient Incomplete Separation of Species with Close Diffusivity to Study the Stability of Affinity Complexes', *Anal. Chem.*, vol. 94, no. 44, pp. 15415–15422, 2022, doi: 10.1021/acs.analchem.2c03313.
[31] T. Wang *et al.*, 'What Does the Accuracy of the Equilibrium Dissociation Constant of Affinity Complexes Depend on Fundamentally?', Chemistry, preprint, 2023. doi: 10.26434/chemrxiv-2023-wkjt4.
[32] I. Jarmoskaite, I. AlSadhan, P. P. Vaidyanathan, and D. Herschlag, 'How to measure and evaluate binding affinities', *eLife*, vol. 9, p. e57264, 2020, doi: 10.7554/eLife.57264.
[33] J.-L. Rukundo, J. C. Y. Le Blanc, S. Kochmann, and S. N. Krylov, 'Assessing Accuracy of an Analytical Method In Silico: Application to "Accurate Constant via Transient Incomplete Separation" (ACTIS)', *Anal. Chem.*, vol. 92, no. 17, pp. 11973–11980, 2020, doi: 10.1021/acs.analchem.0c02405.
[34] N. Sisavath *et al.*, 'Transient Incomplete Separation Facilitates Finding Accurate Equilibrium Dissociation Constant of Protein–Small Molecule Complex', *Angew. Chem. Int. Ed.*, vol. 58, no. 20, pp. 6635–6639, 2019, doi: 10.1002/anie.201901345.

[35] H. Diehl and R. Markuszewski, 'Studies on fluorescein—II2The solubility and acid dissociation constants of fluorescein in water solution', *Talanta*, vol. 32, no. 2, pp. 159–165, 1985, doi: 10.1016/0039-9140(85)80049-7.
[36] M. A. Masuelli, 'Study of Bovine Serum Albumin Solubility in Aqueous Solutions by Intrinsic Viscosity Measurements', *Adv. Phys. Chem.*, vol. 2013, pp. 1–8, 2013, doi: 10.1155/2013/360239.
[37] H. E. Hajji, E. Nkhili, V. Tomao, and O. Dangles, 'Interactions of quercetin with iron and copper ions: Complexation and autoxidation', *Free Radic. Res.*, vol. 40, no. 3, pp. 303–320, 2006, doi: 10.1080/10715760500484351.
[38] N. R. Perron and J. L. Brumaghim, 'A review of the antioxidant mechanisms of polyphenol compounds related to iron binding', *Cell Biochem. Biophys.*, vol. 53, no. 2, pp. 75–100, 2009, doi: 10.1007/s12013-009-9043-x.
[39] F. Roth-Walter *et al.*, 'Cow's milk protein β-lactoglobulin confers resilience against allergy by targeting complexed iron into immune cells', *J. Allergy Clin. Immunol.*, vol. 147, no. 1, pp. 321-334.e4, 2021, doi: 10.1016/j.jaci.2020.05.023.
[40] 'Table of Diffusion Coefficients'. Accessed: Oct. 16, 2023. [Online]. Available: https://www.aqion.de/site/diffusion-coefficients
[41] K. G. Romanchuk, 'Fluorescein. Physicochemical factors affecting its fluorescence', *Surv. Ophthalmol.*, vol. 26, no. 5, pp. 269–283, 1982, doi: 10.1016/0039-6257(82)90163-1.
[42] B. Mishra, A. Barik, K. I. Priyadarsini, and H. Mohan, 'Fluorescence spectroscopic studies on binding of a flavonoid antioxidant quercetin to serum albumins', *J. Chem. Sci.*, vol. 117, no. 6, pp. 641–647, Nov. 2005, doi: 10.1007/BF02708293.
[43] 'Avio-220-Max-ICP-OES-Specifications.pdf'. Accessed: Oct. 21, 2023. [Online]. Available: https://perkinelmer.com.ar/wp-content/uploads/sites/3/2018/05/Avio-220-Max-ICP-OES-Specifications.pdf
[44] J.-L. Rukundo, J. Latimer, S. Jain, S. Kochmann, and S. N. Krylov, 'Streamlined Data Processing for Determination of Kd with "Accurate Constant via Transient Incomplete Separation" (ACTIS)'. ChemRxiv, 2022. doi: 10.26434/chemrxiv-2022-ct450.
[45] 'Elmer FEM – open source multiphysical simulation software'. Accessed: Oct. 26, 2023. [Online]. Available: https://www.elmerfem.org/blog/
[46] A. Frutiger, A. Tanno, S. Hwu, R. F. Tiefenauer, J. Vörös, and N. Nakatsuka, 'Nonspecific Binding—Fundamental Concepts and Consequences for Biosensing Applications', *Chem. Rev.*, vol. 121, no. 13, pp. 8095–8160, 2021, doi: 10.1021/acs.chemrev.1c00044.
[47] C. S. Mallis *et al.*, 'Development of native MS capabilities on an extended mass range Q-TOF MS', *Int. J. Mass Spectrom.*, vol. 458, p. 116451, 2020, doi: 10.1016/j.ijms.2020.116451.
[48] H. Manman, C. Weilan, L. Zhimin, P. Liang, H. Lixia, and C. Min, 'ESI-TOF MS analysis of complexes formed between quercetin and five metal ions in hot water and a study into their DNA cleavage activity', *J. Inorg. Biochem.*, vol. 195, pp. 13–19, 2019, doi: 10.1016/j.jinorgbio.2019.03.004.
[49] Y. Liu and M. Guo, 'Studies on Transition Metal-Quercetin Complexes Using Electrospray Ionization Tandem Mass Spectrometry', *Molecules*, vol. 20, no. 5, pp. 8583–8594, May 2015, doi: 10.3390/molecules20058583.
[50] Y. Deng, X. Wu, Y. Tian, Z. Zou, X. Hou, and X. Jiang, 'Sharing one ICP source for simultaneous elemental analysis by ICP-MS/OES: Some unique instrumental capabilities', *Microchem. J.*, vol. 132, pp. 401–405, 2017, doi: 10.1016/j.microc.2017.02.024.
[51] A. N. Pham, A. L. Rose, A. J. Feitz, and T. D. Waite, 'Kinetics of Fe(III) precipitation in aqueous solutions at pH 6.0–9.5 and 25°C', *Geochim. Cosmochim. Acta*, vol. 70, no. 3, pp. 640–650, 2006, doi: 10.1016/j.gca.2005.10.018.
[52] L. Liu *et al.*, 'Variations in concentration and solubility of iron in atmospheric fine particles during the COVID-19 pandemic: An example from China', *Gondwana Res.*, vol. 97, pp. 138–144, 2021, doi: 10.1016/j.gr.2021.05.022.
[53] M. Segura, Y. Madrid, and C. Cámara, 'Elimination of calcium and argon interferences in iron determination by ICP-MS using desferrioxamine chelating agent immobilized in sol–gel and cold plasma conditions', *J Anal Spectrom*, vol. 18, no. 9, pp. 1103–1108, 2003, doi: 10.1039/B301719M.

[54] M. Borzoei, M. A. Zanjanchi, H. Sadeghi-aliabadi, and L. Saghaie, 'Optimization of a methodology for determination of iron concentration in aqueous samples using a newly synthesized chelating agent in dispersive liquid-liquid microextraction', *Food Chem.*, vol. 264, pp. 9–15, 2018, doi: 10.1016/j.foodchem.2018.04.135.
[55] M. Magnini, 'Bubbles in capillaries: Relaxing traditional assumptions', *Sci. Talks*, vol. 2, p. 100020, 2022, doi: 10.1016/j.sctalk.2022.100020.
[56] S. Afkham, J. Hanaee, M. Zakariazadeh, F. Fathi, S. Shafiee, and S. Soltani, 'Molecular mechanism and thermodynamic study of Rosuvastatin interaction with human serum albumin using a surface plasmon resonance method combined with a multi-spectroscopic, and molecular modeling approach', *Eur. J. Pharm. Sci.*, vol. 168, p. 106005, 2022, doi: 10.1016/j.ejps.2021.106005.
[57] N. Mostafa, A. Badawey, L. Nesrine, and A. El-Aleem, 'Selective chromatographic methods for the determination of Rosuvastatin calcium in the presence of its acid degradation products', *J. Liq. Chromatogr. Relat. Technol.*, vol. 37, 2014, doi: 10.1080/10826076.2013.828305.
[58] E. A. Türkoğlu and F. G. Aydin, 'Surface Plasmon Resonance Binding Study on the Interaction of Acetazolamide and Bovine Serum Albumin', *Clin. Exp. Health Sci.*, vol. 13, no. 4, Art. no. 4, doi: 10.33808/clinexphealthsci.1218956.
[59] C. Li *et al.*, 'Towards Higher Sensitivity of Mass Spectrometry: A Perspective From the Mass Analyzers', *Front. Chem.*, vol. 9, p. 813359, 2021, doi: 10.3389/fchem.2021.813359.
[60] Y. Li *et al.*, 'Characterization of mercury-binding proteins in human neuroblastoma SK-N-SH cells with immobilized metal affinity chromatography', *Talanta*, vol. 178, pp. 811–817, 2018, doi: 10.1016/j.talanta.2017.10.028.
[61] N. Pramounmat, K. Yan, J. Wolf, and J. N. Renner, 'Platinum-binding peptides: understanding of selective binding and multifunctionality', *Multifunct. Mater.*, vol. 5, no. 1, p. 012002, 2022, doi: 10.1088/2399-7532/ac4a86.

Appendix

Section 1: Scheme of valve position

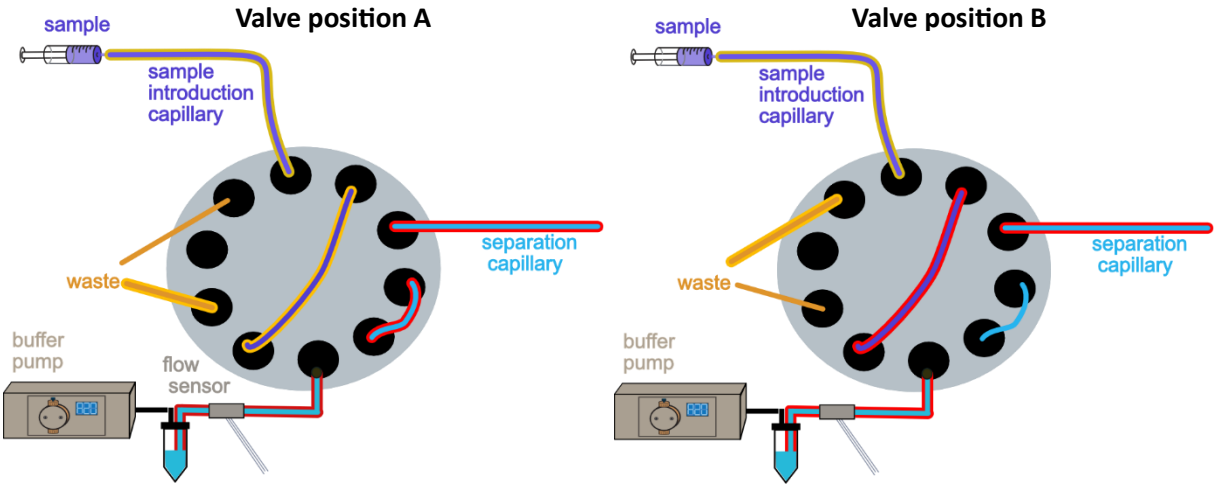

Section 2: Python script "automACTIS"

```
#!/usr/bin/env python3
# -*- coding: utf-8 -*-
# Imports
import random
import serial
import time
import win32con
import win32api
import win32ui
# Parameters
# ----------------------------------
pump_device = "COM5"
valve_device = "COM1"
chrom_button_ID = 2
no_clean_switches = 10
time_preflush = 10 # s
time_plugpush = 20 # s
time_acquisition = 180 # s
time_clean_switch = 5 # s
time_clean= 60 # s
pressure_main = 135.0 # mbar
pressure_plug = 230.0 # mbar
pressure_clean = 2000.0 # mbar

# Init
# ----------------------------------
# Setup and open serial connection for the pump
pump_ser = serial.Serial(port=pump_device,
                    baudrate=115384,
                    bytesize=serial.EIGHTBITS,
                    parity=serial.PARITY_NONE,
                    stopbits=serial.STOPBITS_ONE,
                    rtscts=True,
                    dsrdtr=True,
                    timeout=2
                    )
# Setup and open serial connection for the valve
valve_ser = serial.Serial(port=valve_device,
                    baudrate=9600,
```

```
                    bytesize=serial.EIGHTBITS,
                    parity=serial.PARITY_NONE,
                    stopbits=serial.STOPBITS_ONE,
                    rtscts=False,
                    dsrdtr=False,
                    timeout=2
                    )
def pump_send(ser, text):
    sendbytes = (text + "\n").encode()
    ser.write(sendbytes)

def valve_send(ser, text):
    sendbytes = (text + "\r").encode()
    ser.write(sendbytes)

def recv(ser):
    readbytes = ser.read_until()
    return readbytes.decode(errors='replace')

def chrom_start_acquisition():
    try:
        pyCWnd = win32ui.FindWindow("#32770", "Chromeleon")
    except Exception as a:
        print("Error finding Chromeleon window", a)

    print("Chromeleon window found:", pyCWnd, "0x%x" % (pyCWnd.GetSafeHwnd()))

    try:
        # Control ID for the "OK"-Button in the Chromeleon dialog box is "2"
        pyCWnd.SendMessage(win32con.WM_COMMAND, chrom_button_ID, 0)
    except Exception as a:
        print("Error sending Chromeleon the OK-command", a)

# Pre-program
# ----------------------------------
# Valve: set to initial position A
print("Set valve position to A...")
valve_send(valve_ser, "1GOA")

# Pump
print("Initialising pump...")
pump_send(pump_ser, "/startpcmode")
pump_send(pump_ser, "/getpid")
pid = recv(pump_ser)
print("Pump ID: ", pid)
pump_send(pump_ser, "/setp1 %.2f" % pressure_main)
time.sleep(time_preflush)
pump_send(pump_ser, "/ping")
print("Pump pong:", recv(pump_ser))

# Program
# ----------------------------------
# Push plug into capillary
print("Pushing plug into separation capillary...")
valve_send(valve_ser, "1GOB")
pump_send(pump_ser, "/setp1 %.2f" % pressure_plug)
time.sleep(time_plugpush)
pump_send(pump_ser, "/ping")
print("Pump pong:", recv(pump_ser))

# Acquisition (main part)
print("Starting acquisition...")
valve_send(valve_ser, "1GOA")
chrom_start_acquisition()
pump_send(pump_ser, "/setp1 %.2f" % pressure_main)
time.sleep(time_acquisition)
pump_send(pump_ser, "/ping")
print("Pump pong:", recv(pump_ser))

# Post-program
# ----------------------------------
print("Cleaning valve...")
pump_send(pump_ser, "/setp1 %.2f" % pressure_clean)
for i in range(no_clean_switches):
    valve_send(valve_ser, "1TO")
    time.sleep(time_clean_switch)
pump_send(pump_ser, "/ping")
print("Pump pong:", recv(pump_ser))
```

```
pump_send(pump_ser, "/setp1 %.2f" % pressure_main)
pump_send(pump_ser, "/ping")
print("Pump pong:", recv(pump_ser))

# Push plug into capillary
print("Cleaning valve...")
valve_send(valve_ser, "1GOA")
pump_send(pump_ser, "/setp1 %.2f" % pressure_clean)
time.sleep(time_clean)
pump_send(pump_ser, "/ping")
print("Pump pong:", recv(pump_ser))
print("Program finished.")
pump_ser.close()
valve_ser.close()
```

Section 3: The "hack" script for the extraction of ICP-AES transient Fe signals

```
# This is the handle you want to check
$handle = 0x205BA
# Maximum points you want to collect
$maxpoints = 5000

# Import GetWindowText
Add-Type @"
  using System;
  using System.Runtime.InteropServices;
  public class UserWindows {
    [DllImport("user32.dll")]
    public static extern IntPtr GetWindowText(IntPtr hWnd, System.Text.StringBuilder text, int
count);
}
"@

$str = New-Object System.Text.StringBuilder 256

$n = 0
"Time (s)`tValue"
for($i = 0; $i -le $maxpoints; $i++) {
    # Receive Window-Text
    $ret = [UserWindows]::GetWindowText($handle, $str, 256)

    "$($i+1)`t$($str.ToString())"

    # Sleep one second
```

Section 4: Text file for capillary geometry

```
        /*********************************************************************
  Geometry for a 2D cross section of two capillaries for ACTIS.
  Geometry includes a plug-region in the beginning for propagation
  of (non-)diffusive species.
  Created by Dr. Sven Kochmann, 2023.07.20
  Modified by ...
  Manual: https://gmsh.info/doc/texinfo/gmsh.html#Geometry-scripting-commands
*********************************************************************/

/* Definitions: all sizes are in mm */
cap_length  = 3.8;
cap_radius  = 0.25;
plug_length = 0.3;


/* Mesh size should be a bit smaller than the smallest
   dimension above */
mesh_size   = 0.01;

/* Points { x, y, z, mesh } */
Point(1) = { 0.0, -cap_radius, 0.0, mesh_size };
Point(2) = { 0.0, +cap_radius, 0.0, mesh_size };
```

```
Point(3) = { plug_length, -cap_radius, 0.0, mesh_size };
Point(4) = { plug_length, +cap_radius, 0.0, mesh_size };

Point(5) = { cap_length, -cap_radius, 0.0, mesh_size };
Point(6) = { cap_length, +cap_radius, 0.0, mesh_size };



/* Curves { p1, p2 } */
Line(1) = {1, 2};
Line(2) = {2, 4};
Line(3) = {4, 3};
Line(4) = {3, 1};

Line(5) = {3, 5};
Line(6) = {5, 6};
Line(7) = {4, 6};


/* Loops: first one for the plug; second one for the capillaries */
Curve Loop(1) = {1, 2, 3, 4};
Curve Loop(2) = {3, 5, 6, -7};

/* Will be grouped boundaries for Elmer */
Physical Curve("walls") = {2, 4, 7, 5};
Physical Curve("inlet") = {1};
Physical Curve("outlet") = {6};

/* Surfaces: Plug + capillaries */
Plane Surface(1) = { 1 };
Plane Surface(2) = { 2 };

Physical Surface("plug") = { 1 };
Physical Surface("capillary") = { 2 };
```

Section 5: Assessing of HSA-FLC binding; ACTIS-FLD experiments

HSA-FLC first experiment normalized

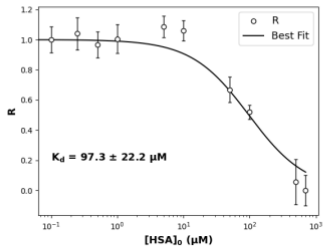

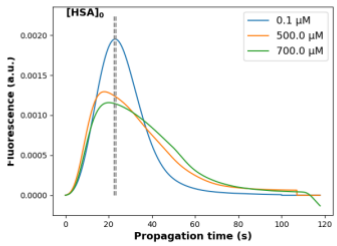

Propogation flow rate	68
Injection flow rate	0
Injection time (s)	0
Separation capillary length	60
Separation capillary diameter	127
Injection loop length	13
Injection loop diameter	50
Protein name	HSA
Ligand name	Fluorescein
Number of Concentrations	10
Initial Ligand concentration [L]0 (µM)	0.05
Type of Data	F
Compensation procedure	N
[P]0 reference for MS normalization (µM)	nan
Window width (%)	2
Determination of peak	P
Manually determined peaks	nan
[P]0 to programmaticlly determine peak	0.1

Conc	Avg Sig (S)	S Std Dev	S Rel Std Dev	R value	R Std Dev	R Rel Std Dev
0.1 µM	0.002015706	4.88266e-05	2.422308	1	0.08656556	8.656556
0.25 µM	0.002047313	6.765785e-05	3.304714	1.039625	0.1060751	10.20321
0.5 µM	0.001989812	5.020637e-05	2.523171	0.9675384	0.08645506	8.935569
1.0 µM	0.002020157	6.000851e-05	2.970487	1.00558	0.0972025	9.666308
5.0 µM	0.002083888	1.740985e-05	0.8354503	1.085476	0.07020513	6.467681
10.0 µM	0.002063197	1.178047e-05	0.5709812	1.059537	0.066653	6.290768
50.0 µM	0.001751338	5.464571e-05	3.120152	0.6686297	0.08327541	12.45464
100.0 µM	0.001632537	8.248854e-06	0.5052782	0.5196433	0.04805605	9.247892
500.0 µM	0.001262834	0.0001064515	8.429573	0.0561682 1	0.149727	266.569
700.0 µM	0.001218013	5.73012e-05	4.704416	0	0.1015903	10159030

Kd: 97.3094 ± 22.1817 µM
R^2: 0.9547
Chi^2: 0.2410

HSA-FLC second experiment -prACTISed

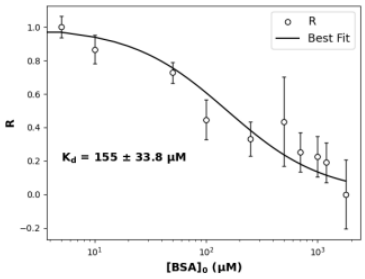

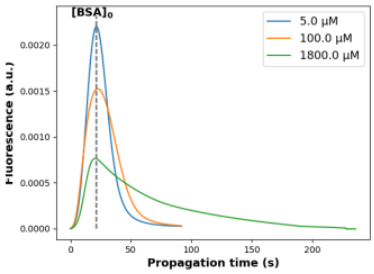

Propogation flow rate	68
Injection flow rate	0
Injection time (s)	0
Separation capillary length	60
Separation capillary diameter	127
Injection loop length	13
Injection loop diameter	50
Protein name	BSA
Ligand name	Fluorescein
Number of Concentrations	10
Initial Ligand concentration [L]0 (µM)	0.05
Type of Data	F
Compensation procedure	N
[P]0 reference for MS normalization (µM)	nan
Window width (%)	2
Determination of peak	P
Manually determined peaks	nan
[P]0 to programmaticlly determine peak	5

Conc	Avg Sig (S)	S Std Dev	S Rel Std Dev	R value	R Std Dev	R Rel Std Dev
5.0 µM	0.002125833	5.300003e-05	2.493142	1	0.0634706	6.34706
10.0 µM	0.001967858	8.576207e-05	4.358144	0.8662263	0.08466273	9.773743
50.0 µM	0.001803558	4.260265e-05	2.362144	0.7270974	0.06290515	8.651544
100.0 µM	0.001471877	0.0001019834	6.928798	0.4462296	0.1200373	26.90034
250.0 µM	0.001335575	2.73844e-05	2.050383	0.3308083	0.1016019	30.71322
500.0 µM	0.001457729	0.0002985591	20.4811	0.4342492	0.26671	61.41866
700.0 µM	0.001243637	4.44489e-05	3.574104	0.2529558	0.1160402	45.87371
1000.0 µM	0.001211006	4.651478e-05	3.841003	0.2253236	0.1202978	53.38889
1200.0 µM	0.001170 33	1.979912e-05	1.691755	0.1908792	0.1197392	62.73038
1800.0 µM	0.000944 9182	0.0001725859	18.26464	0	0.2066816	20668160

Kd: 154.5953 ± 33.7676 µM
R^2: 0.8913
Chi^2: 0.4453

Section 6: Assessing of BLG-FeQ$_2$ binding; ACTIS-FLD experiment

BLGFeQ2 ACTIS-FLD experiment - normalized

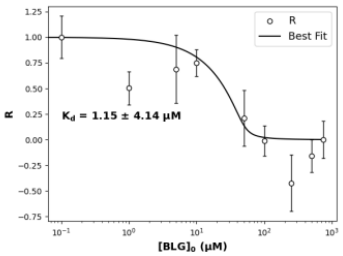

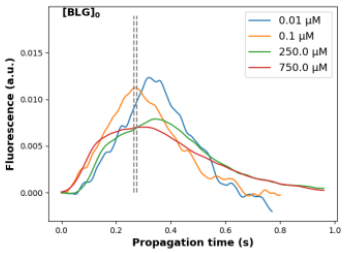

Propogation flow rate	68
Injection flow rate	0
Injection time (s)	0
Separation capillary length	60
Separation capillary diameter	127
Injection loop length	13
Injection loop diameter	50
Protein name	BLG
Ligand name	Quercetin
Number of Concentrations	10
Initial Ligand concentration [L]0 (µM)	50
Type of Data	F
Compensation procedure	N
[P]0 reference for MS normalization (µM)	nan
Window width (%)	2
Determination of peak	P
Manually determined peaks	nan
[P]0 to programmaticlly determine peak	0.1

Conc	Avg Sig (S)	S Std Dev	S Rel Std Dev	R value	R Std Dev	R Rel Std Dev
0.01 µM	0.0100270 3	0.0005412 547	5.397955	nan	nan	nan
0.1 µM	0.0108043 4	0.0004523 885	4.187101	1	0.2068942	20.68942
1.0 µM	0.0092741 03	0.0003980 184	4.291718	0.5051426	0.1613164	31.93483
5.0 µM	0.0098406 7	0.0009703 127	9.86023	0.6883627	0.3319446	48.22234
10.0 µM	0.0100341 3	0.0001994 242	1.987457	0.7509266	0.1313003	17.4851
50.0 µM	0.0083631 1	0.0007803 746	9.331153	0.2105399	0.2734992	129.9037
100.0 µM	0.0076848 59	0.0002273 405	2.958291	-0.008797 125	0.1483466	14834660
250.0 µM	0.0064018 01	0.0006089 892	9.512779	-0.423720 5	0.2751203	27512030
500.0 µM	0.0072276 41	0.0001775 533	2.456587	-0.156655 2	0.1601401	16014010
750.0 µM	0.0077120 62	0.0003949 383	5.121047	0	0.18062	18062000

Kd: 1.1544 ± 4.1424 µM
R^2: 0.7291
Chi^2: 42.4552

Section 7: Assessing of BLG-FeQ_2 binding; first ACTIS-TOF-MS experiment

BLG-FeQ2 first ACTIS-TOF-MS experiment

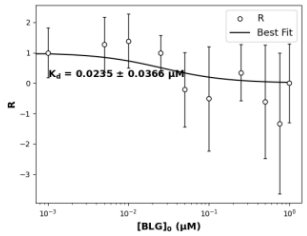

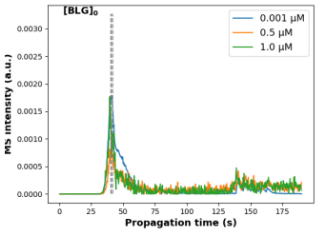

Propogation flow rate	70
Injection flow rate	20
Injection time (s)	20
Separation capillary length	60
Separation capillary diameter	127
Injection loop length	13
Injection loop diameter	50
Protein name	BLG
Ligand name	Quercetin
Number of Concentrations	10
Initial Ligand concentration [L]0 (µM)	0.005
Type of Data	MS
Compensation procedure	Compensated
[P]0 reference for MS normalization (µM)	1.0
Window width (%)	2
Determination of peak	P
Manually determined peaks	nan
[P]0 to programmaticlly determine peak	0.001

Conc	Avg Sig (S)	S Std Dev	S Rel Std Dev	R value	R Std Dev	R Rel Std Dev
0.001 µM	0.001971899	0.000176850 8	8.968554	1	0.8142459	81.42459
0.005 µM	0.002054572	0.000150873 8	7.34332	1.269153	0.914276	72.0383
0.01 µM	0.002091095	4.426416e-05	2.116793	1.388058	0.8863364	63.85444
0.025 µM	0.001967644	5.750024e-05	2.922296	0.9861326	0.5979736	60.63825
0.05 µM	0.001600418	0.000157706 2	9.854064	-0.2094017	1.226051	122605100
0.1 µM	0.001508243	0.000299154	19.83461	-0.5094883	1.71552	171552000
0.25 µM	0.001772	0.000207774 2	11.7254	0.3492059	0.9234279	264.4365
0.5 µM	0.001476923	0.000339716 3	23.00163	-0.6114541	1.876725	187672500
0.75 µM	0.001256223	0.000154022 6	12.26077	-1.329969	2.320493	232049300
1.0 µM	0.001664738	0.000281108 2	16.88603	0	1.294261	129426100

Kd: 0.0235 ± 0.0366 µM
R^2: 0.4712
Chi^2: 75.6142

Section 8: Assessing of BLG-FeQ$_2$ binding; second ACTIS-TOF-MS experiment

BLG-FeQ2 second ACTIS-TOF-MS experiment - all ions

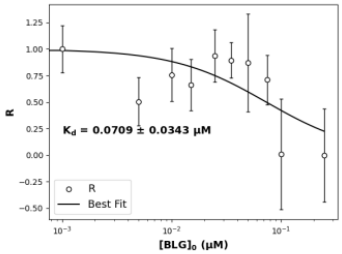

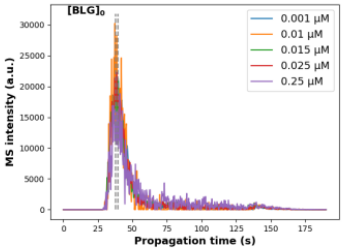

Propogation flow rate	70
Injection flow rate	20
Injection time (s)	20
Separation capillary length	60
Separation capillary diameter	254
Injection loop length	13
Injection loop diameter	113
Protein name	BLG
Ligand name	Quercetin
Number of Concentrations	10
Initial Ligand concentration [L]0 (µM)	0.005
Type of Data	MS
Compensation procedure	Compensated
[P]0 reference for MS normalization (µM)	0.001
Window width (%)	2
Determination of peak	P
Manually determined peaks	nan
[P]0 to programmaticlly determine peak	0.001

Conc	Avg Sig (S)	S Std Dev	S Rel Std Dev	R value	R Std Dev	R Rel Std Dev
0.001 µM	20244.59	740.9369	3.659925	1	0.221256	22.1256
0.005 µM	17901.95	707.8993	3.954315	0.5053415	0.2285744	45.23168
0.01 µM	19097.37	975.0428	5.105639	0.75776	0.2492293	32.89027
0.015 µM	18642.31	908.4146	4.872866	0.6616715	0.242021	36.57722
0.025 µM	19947.01	944.3866	4.734477	0.9371642	0.2482821	26.49291
0.035 µM	19746.96	413.9084	2.096061	0.8949232	0.1682532	18.80086
0.05 µM	19632.91	2067.461	10.53059	0.8708411	0.4590783	52.71665
0.075 µM	18872.49	868.1272	4.599961	0.710275	0.2325177	32.7363
0.1 µM	15544.85	1997.503	12.84994	0.0076309 6	0.522585	6848.221
0.25 µM	15508.71	1472.432	9.494228	0	0.4396924	43969240

Kd: 0.0709 ± 0.0343 µM
R^2: 0.4439
Chi^2: 1.2193

BLG-FeQ2 second ACTIS-TOF-MS experiment - 140.0014 - single ion extraction

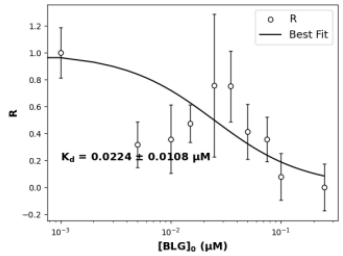

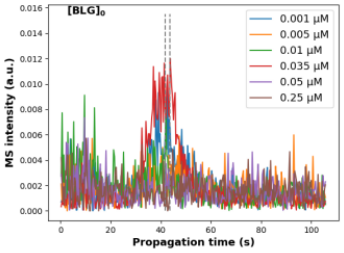

Propogation flow rate	70
Injection flow rate	20
Injection time (s)	20
Separation capillary length	60
Separation capillary diameter	254
Injection loop length	13
Injection loop diameter	113
Protein name	BLG
Ligand name	FeQ2
Number of Concentrations	10
Initial Ligand concentration [L]0 (µM)	0.005
Type of Data	MS
Compensation procedure	N
[P]0 reference for MS normalization (µM)	1.0
Window width (%)	2
Determination of peak	P
Manually determined peaks	nan
[P]0 to programmaticlly determine peak	0.001

Conc	Avg Sig (S)	S Std Dev	S Rel Std Dev	R value	R Std Dev	R Rel Std Dev
0.001 µM	0.007013881	0.000714560 4	10.1878	1	0.1875582	18.75582
0.005 µM	0.003335934	0.000766765 7	22.98503	0.3173665	0.1709106	53.85276
0.01 µM	0.003558158	0.001275519	35.84774	0.3586117	0.2542654	70.90271
0.015 µM	0.004186239	0.000575848 9	13.75576	0.4751847	0.1401498	29.49376
0.025 µM	0.005700669	0.002804639	49.19843	0.7562655	0.5309841	70.21134
0.035 µM	0.005674356	0.001314162	23.15966	0.7513817	0.2652846	35.30624
0.05 µM	0.003861037	0.000980580 7	25.39682	0.4148266	0.2035443	49.06734
0.075 µM	0.003548103	0.000729846 4	20.57005	0.3567454	0.1642219	46.03337
0.1 µM	0.002043893	0.000699413 1	34.21965	0.07756138	0.1734312	223.605
0.25 µM	0.001626002	0.000669066 2	41.14794	0	0.1756169	17561690

Kd: 0.0224 ± 0.0108 µM
R^2: 0.2417
Chi^2: 1.1967

BLG-FeQ2 second ACTIS-TOF-MS experiment - 158.9960 - single ion extractions

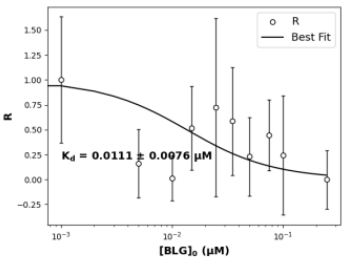

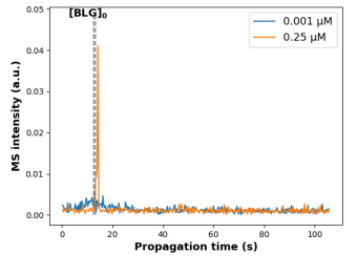

Propogation flow rate	70
Injection flow rate	20
Injection time (s)	20
Separation capillary length	60
Separation capillary diameter	254
Injection loop length	13
Injection loop diameter	113
Protein name	BLG
Ligand name	FeQ2
Number of Concentrations	10
Initial Ligand concentration [L]0 (µM)	0.005
Type of Data	MS
Compensation procedure	N
[P]0 reference for MS normalization (µM)	1.0
Window width (%)	2
Determination of peak	P
Manually determined peaks	nan
[P]0 to programmaticlly determine peak	0.001

Conc	Avg Sig (S)	S Std Dev	S Rel Std Dev	R value	R Std Dev	R Rel Std Dev
0.001 µM	0.003869331	0.001072301	27.71283	1	0.6330142	63.30142
0.005 µM	0.001863151	0.000690005 8	37.03434	0.1625642	0.3442149	211.7409
0.01 µM	0.001502955	0.000229995	15.30285	0.01220816	0.2265071	1855.375
0.015 µM	0.002711025	0.000802376 9	29.59681	0.5164907	0.4191719	81.15769
0.025 µM	0.003209053	0.0019896	61.99959	0.7243815	0.8933985	123.3326
0.035 µM	0.002880586	0.001116523	38.76028	0.58727	0.5419053	92.27532
0.05 µM	0.002027491	0.000826942 3	40.78651	0.2311637	0.3941333	170.4997
0.075 µM	0.002542723	0.000640790 5	25.20095	0.4462367	0.3530746	79.12271
0.1 µM	0.002059386	0.001363676	66.2176	0.2444781	0.6005082	245.6286
0.25 µM	0.001473709	0.000497369 4	33.7495	0	0.2936134	29361340

Kd: 0.0111 ± 0.0076 µM
R^2: -0.1220
Chi^2: 2.8223

BLG-FeQ2 second ACTIS-TOF-MS experiment - 180.9781 - single ion extractions

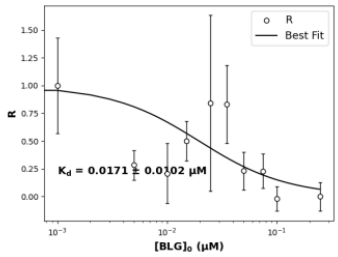

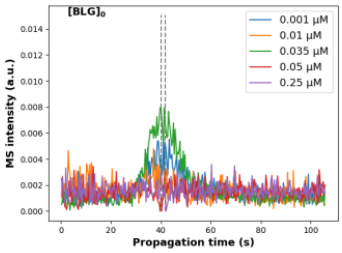

Propogation flow rate	70
Injection flow rate	20
Injection time (s)	20
Separation capillary length	60
Separation capillary diameter	254
Injection loop length	13
Injection loop diameter	113
Protein name	BLG
Ligand name	FeQ2
Number of Concentrations	10
Initial Ligand concentration [L]0 (µM)	0.005
Type of Data	MS
Compensation procedure	N
[P]0 reference for MS normalization (µM)	1.0
Window width (%)	2
Determination of peak	P
Manually determined peaks	nan
[P]0 to programmaticlly determine peak	0.001

Conc	Avg Sig (S)	S Std Dev	S Rel Std Dev	R value	R Std Dev	R Rel Std Dev
0.001 µM	0.005337212	0.001086653	20.35993	1	0.4308392	43.08392
0.005 µM	0.002779249	0.000287869 1	10.3578	0.2828605	0.1344353	47.52707
0.01 µM	0.002516266	0.000899693 4	35.7551	0.2091315	0.2696452	128.9357
0.015 µM	0.003555418	0.000281731	7.923989	0.5004639	0.1774546	35.45803
0.025 µM	0.004772181	0.002665717	55.85951	0.8415902	0.7902328	93.89757
0.035 µM	0.004735139	0.000864540 6	18.25797	0.8312054	0.3508561	42.21052
0.05 µM	0.002594772	0.000499866 3	19.26436	0.2311411	0.1713161	74.11752
0.075 µM	0.002589543	0.000424405 8	16.38921	0.2296753	0.1543459	67.20178
0.1 µM	0.001700616	0.000227616 2	13.38434	-0.019540 54	0.1116346	11163460
0.25 µM	0.001770315	0.000319778	18.06345	0	0.1267873	12678730

Kd: 0.0171 ± 0.0102 µM
R^2: 0.2207
Chi^2: 1.9824

BLG-FeQ2 second ACTIS-TOF-MS experiment - 262.9821 - single ion extractions

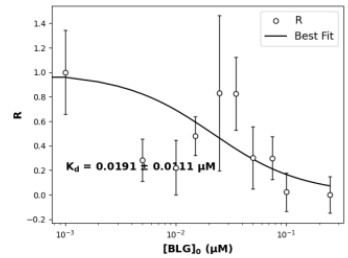

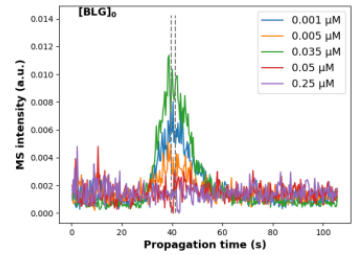

Propogation flow rate	70
Injection flow rate	20
Injection time (s)	20
Separation capillary length	60
Separation capillary diameter	254
Injection loop length	13
Injection loop diameter	113
Protein name	BLG
Ligand name	FeQ2
Number of Concentrations	10
Initial Ligand concentration [L]0 (µM)	0.005
Type of Data	MS
Compensation procedure	N
[P]0 reference for MS normalization (µM)	1.0
Window width (%)	2
Determination of peak	P
Manually determined peaks	nan
[P]0 to programmaticlly determine peak	0.001

Conc	Avg Sig (S)	S Std Dev	S Rel Std Dev	R value	R Std Dev	R Rel Std Dev
0.001 µM	0.007528115	0.001309925	17.40044	1	0.3442461	34.42461
0.005 µM	0.003668419	0.000751855 4	20.49535	0.2827663	0.1734319	61.33401
0.01 µM	0.003345058	0.001076814	32.19118	0.2226774	0.2231933	100.2317
0.015 µM	0.004721659	0.000494086 2	10.46425	0.4784862	0.1583451	33.09293
0.025 µM	0.006608956	0.003230408	48.87926	0.8291959	0.6335809	76.40907
0.035 µM	0.006587661	0.001182747	17.95398	0.8252387	0.2983346	36.15131
0.05 µM	0.003775957	0.001240836	32.86151	0.3027498	0.2531781	83.62618
0.075 µM	0.003758312	0.000765363 5	20.36455	0.2994709	0.1763368	58.88278
0.1 µM	0.002270971	0.000628036 4	27.65498	0.0230835	0.156367	677.3972
0.25 µM	0.002146675	0.000572431 4	26.66503	0	0.150434	15043400

Kd: 0.0191 ± 0.0111 µM
R^2: 0.1752
Chi^2: 1.7638

BLG-FeQ2 second ACTIS-TOF-MS experiment - 344.9857 - single ion extractions

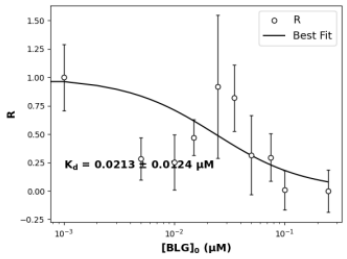

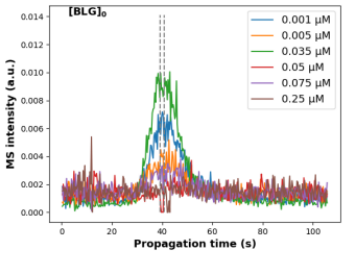

Propogation flow rate	70
Injection flow rate	20
Injection time (s)	20
Separation capillary length	60
Separation capillary diameter	254
Injection loop length	13
Injection loop diameter	113
Protein name	BLG
Ligand name	FeQ2
Number of Concentrations	10
Initial Ligand concentration [L]0 (µM)	0.005
Type of Data	MS
Compensation procedure	N
[P]0 reference for MS normalization (µM)	1.0
Window width (%)	2
Determination of peak	P
Manually determined peaks	nan
[P]0 to programmaticlly determine peak	0.001

Conc	Avg Sig (S)	S Std Dev	S Rel Std Dev	R value	R Std Dev	R Rel Std Dev
0.001 µM	0.007411415	0.001041733	14.05579	1	0.291627	29.1627
0.005 µM	0.003801369	0.000748480 5	19.68976	0.2853899	0.1855187	65.00536
0.01 µM	0.003638686	0.001094218	30.0718	0.2531866	0.2438714	96.32082
0.015 µM	0.004744488	0.000515531 8	10.86591	0.4720806	0.1574917	33.36119
0.025 µM	0.00699036	0.003035113	43.41855	0.916652	0.629933	68.72106
0.035 µM	0.006501892	0.001194274	18.3681	0.8199594	0.2916323	35.56668
0.05 µM	0.003959151	0.001671615	42.22245	0.3166228	0.3492742	110.3124
0.075 µM	0.003848638	0.000894685 1	23.2468	0.2947467	0.20935	71.02709
0.1 µM	0.00240233	0.000553669 6	23.04719	0.008449427	0.1713065	2027.434
0.25 µM	0.002359645	0.000670717 3	28.4245	0	0.1877634	18776340

Kd: 0.0213 ± 0.0124 µM
R^2: 0.1908
Chi^2: 1.7812

BLG-FeQ2 second ACTIS-TOF-MS experiment - 426.9877 - single ion extractions

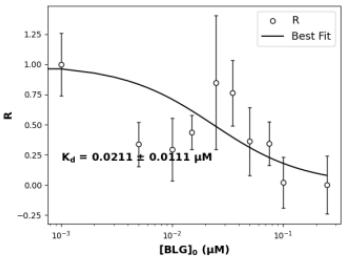

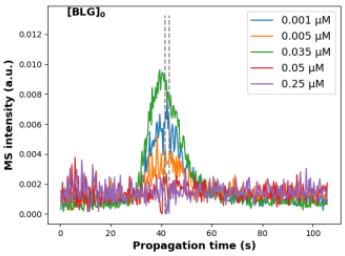

Propogation flow rate	70
Injection flow rate	20
Injection time (s)	20
Separation capillary length	60
Separation capillary diameter	254
Injection loop length	13
Injection loop diameter	113
Protein name	BLG
Ligand name	FeQ2
Number of Concentrations	10
Initial Ligand concentration [L]0 (µM)	0.005
Type of Data	MS
Compensation procedure	N
[P]0 reference for MS normalization (µM)	1.0
Window width (%)	2
Determination of peak	P
Manually determined peaks	nan
[P]0 to programmaticlly determine peak	0.001

Conc	Avg Sig (S)	S Std Dev	S Rel Std Dev	R value	R Std Dev	R Rel Std Dev
0.001 µM	0.006917698	0.000884230 1	12.78214	1	0.2604111	26.04111
0.005 µM	0.003740176	0.000626060 604	16.7388	0.33829	0.1829938	54.09375
0.01 µM	0.003535893	0.001072068	30.31958	0.2957486	0.2590186	87.58064
0.015 µM	0.004214494	0.000340254 9	8.073446	0.4370655	0.1436078	32.85728
0.025 µM	0.006195708	0.002547583	41.1185	0.8496477	0.5537032	65.16857
0.035 µM	0.005781612	0.001100572	19.03573	0.7634133	0.2718479	35.60954
0.05 µM	0.003853447	0.001211051	31.42774	0.3618783	0.2824357	78.04715
0.075 µM	0.003774878	0.000618935 1	16.39616	0.3455165	0.1816471	52.57263
0.1 µM	0.00222266	0.000624147 9	28.08112	0.022271511	0.2108047	946.5217
0.25 µM	0.002115712	0.000814869 3	38.51513	0	0.2399839	23998390

Kd: 0.0211 ± 0.0111 µM
R^2: 0.2326
Chi^2: 1.4899

BLG-FeQ2 second ACTIS-TOF-MS experiment - 508.9935 - single ion extractions

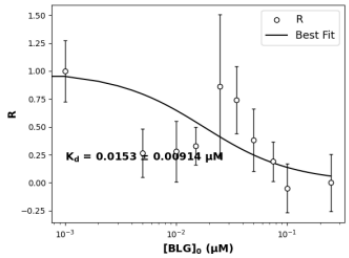

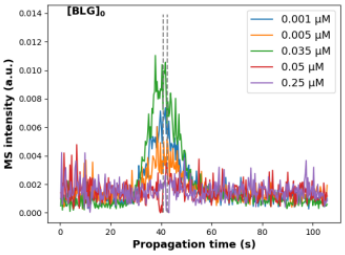

Propogation flow rate	70
Injection flow rate	20
Injection time (s)	20
Separation capillary length	60
Separation capillary diameter	254
Injection loop length	13
Injection loop diameter	113
Protein name	BLG
Ligand name	FeQ2
Number of Concentrations	10
Initial Ligand concentration [L]0 (µM)	0.005
Type of Data	MS
Compensation procedure	N
[P]0 reference for MS normalization (µM)	1.0
Window width (%)	2
Determination of peak	P
Manually determined peaks	nan
[P]0 to programmaticlly determine peak	0.001

Conc	Avg Sig (S)	S Std Dev	S Rel Std Dev	R value	R Std Dev	R Rel Std Dev
0.001 µM	0.00744512	0.00095319	12.80288	1	0.2753861	27.53861
0.005 µM	0.00383996	0.00079744	20.76688	0.2635013	0.2163595	82.10945
0.01 µM	0.00391965	0.00114177	29.12778	0.279781	0.2724645	97.38493
0.015 µM	0.00416947	0.00048257	11.57398	0.3308119	0.1686148	50.96998
0.025 µM	0.00676614	0.00303868	44.90973	0.8612922	0.643512	74.71472
0.035 µM	0.00618053	0.00128038	20.71641	0.7416572	0.3024014	40.77375
0.05 µM	0.00441882	0.00119026	26.93617	0.3817581	0.2776365	72.72577
0.075 µM	0.00348353	0.00045375	13.0256	0.1906865	0.1768359	92.73648
0.1 µM	0.00230336	0.00053745	23.33328	-0.0504099	0.2191609	21916090
0.25 µM	0.00255012	0.00088271	34.61455	0	0.2550247	25502470

Kd: 0.0153 ± 0.0091 µM
R^2: 0.2064
Chi^2: 2.0698

BLG-FeQ2 second ACTIS-TOF-MS experiment - 590.9913 - single ion extractions

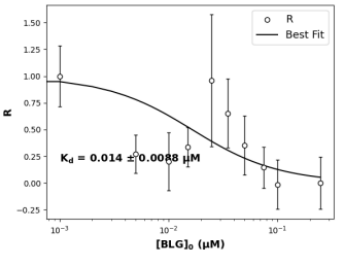

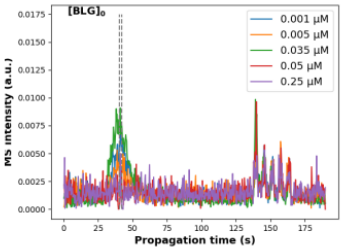

Propogation flow rate	70
Injection flow rate	20
Injection time (s)	20
Separation capillary length	60
Separation capillary diameter	254
Injection loop length	13
Injection loop diameter	113
Protein name	BLG
Ligand name	FeQ2
Number of Concentrations	10
Initial Ligand concentration [L]0 (µM)	0.005
Type of Data	MS
Compensation procedure	N
[P]0 reference for MS normalization (µM)	1.0
Window width (%)	2
Determination of peak	P
Manually determined peaks	nan
[P]0 to programmaticlly determine peak	0.001

Conc	Avg Sig (S)	S Std Dev	S Rel Std Dev	R value	R Std Dev	R Rel Std Dev
0.001 µM	0.00677643	0.00086027	12.69508	1	0.2826478	28.26478
0.005 µM	0.00364291	0.00049287	13.5298	0.2720074	0.1785145	65.62853
0.01 µM	0.00334256	0.00098497	29.46752	0.2022304	0.2701333	133.577
0.015 µM	0.00392546	0.00054215	13.81124	0.3376509	0.1830245	54.20523
0.025 µM	0.00659641	0.00252575	38.28987	0.958176	0.6172947	64.42394
0.035 µM	0.00528599	0.00124889	23.62657	0.6537265	0.3237761	49.52776
0.05 µM	0.00399668	0.00104997	26.27112	0.3541977	0.2773968	78.31692
0.075 µM	0.00309539	0.00052365	16.91713	0.1448067	0.1934989	133.6256
0.1 µM	0.00241694	0.00065659	27.16648	-0.0128145	0.232073	23207300
0.25 µM	0.00247210	0.00074320	30.06363	0	0.2441837	24418370

Kd: 0.0140 ± 0.0088 µM
R^2: 0.1918
Chi^2: 2.1885

Section 9: ACTIS-ICP-MS measurements

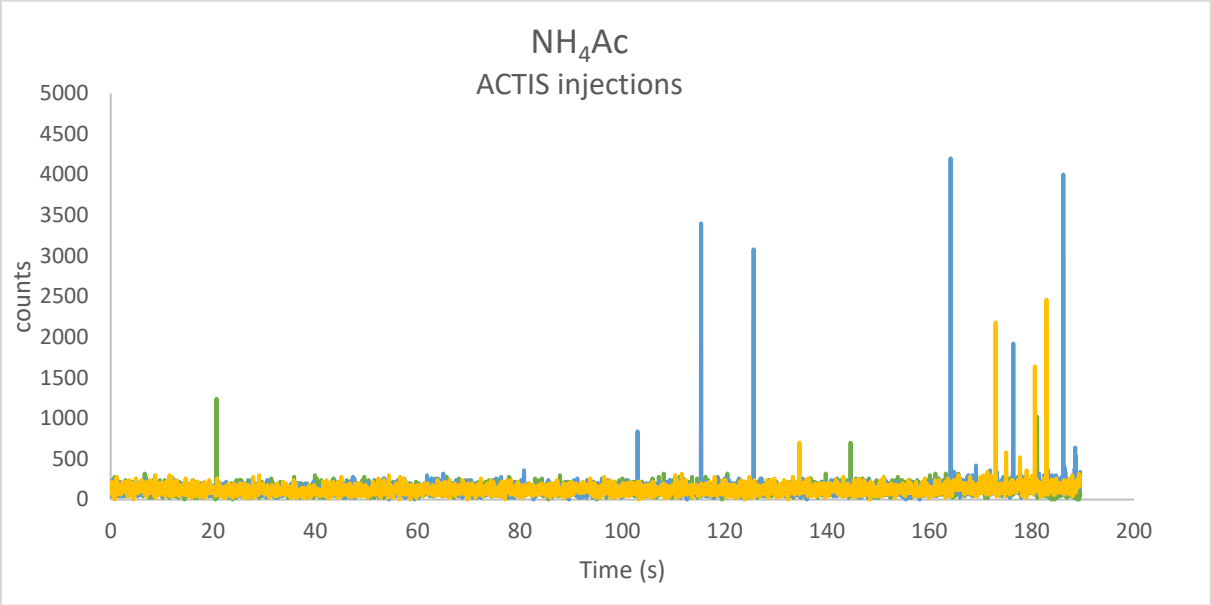

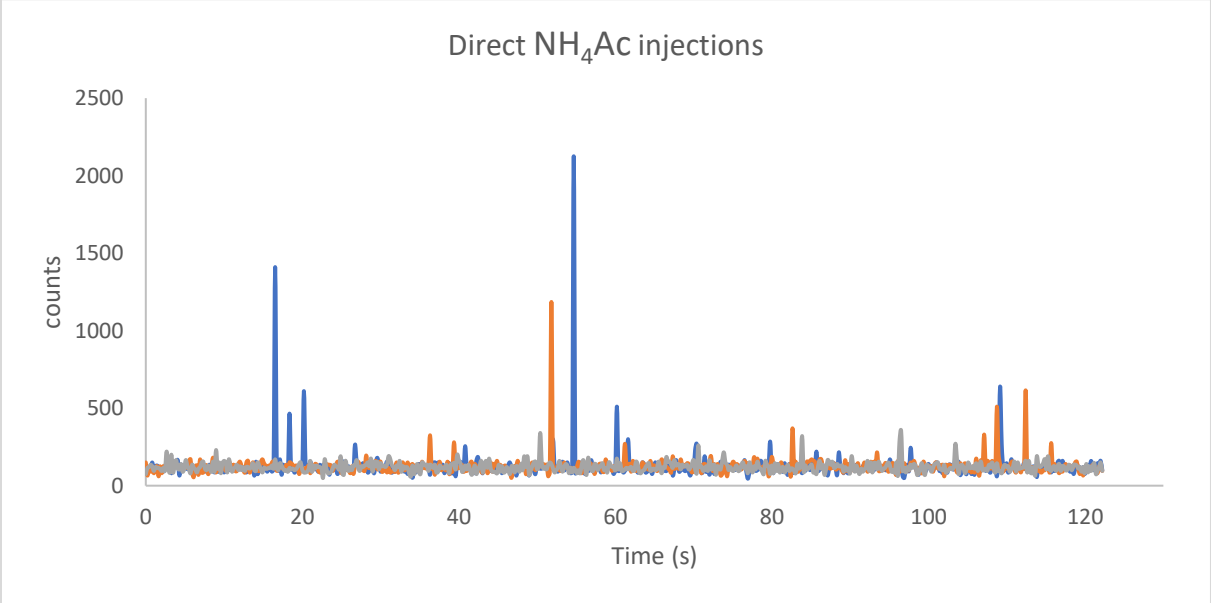

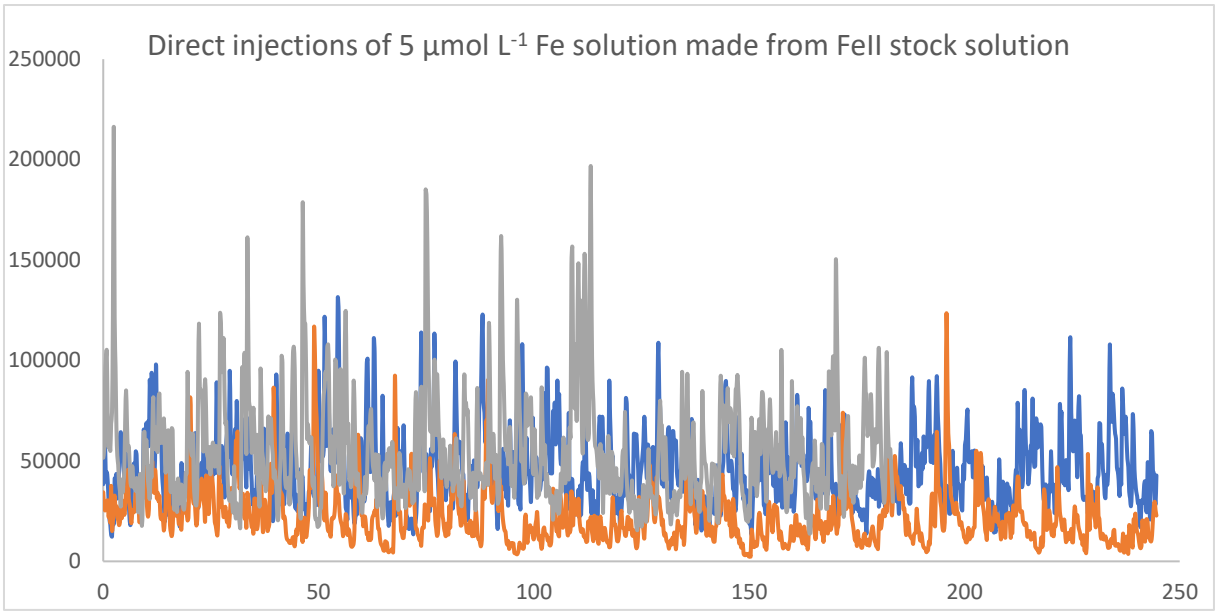

Table 18: Samples, injection methods, corresponding Std. dev, and noise level in ACTIS-ICP-MS measurements

Sample and injection method	**Standard deviation**	**Noise level**
direct injections of NH_4Ac solution	73.8	258.4
NH_4Ac injections through ACTIS	97.6	341.6
direct injections of 5 µM Fe made from Fe II stock solution	23968.4	81492.6
direct injections of 5 µM Fe made from stock solution in subb. H2O with 2% HNO3 and 0.1 % HCl	376.0	1278.3
ACTIS injections of 5 µM Fe made from stock solution in subb, H2O with 2% HNO3 and 0,1 % HCl (diluted with NH_4Ac)	127.7	447.2
ACTIS injections of 5 µM Fe made from stock solution in subb, H2O with 2% HNO3 and 0,1 % HCl (diluted with subb, H2O)	291.4	1019.9

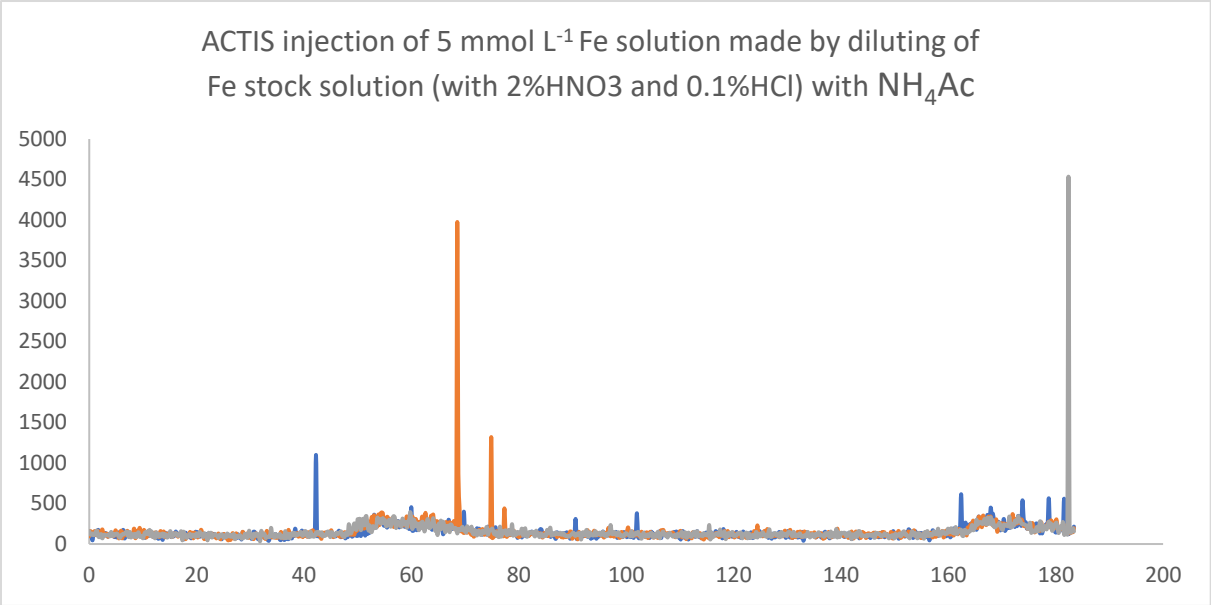
ACTIS injection of 5 mmol L-1 Fe solution made by diluting of
Fe stock solution (with 2%HNO3 and 0.1%HCl) with NH4Ac
5000
4500
4000
3500
3000
2500
2000
1500
1000
500
0
0
20
40
60
80
100
120
140
160
180
200

Section 10: ACTIS-ICP-AES measurements

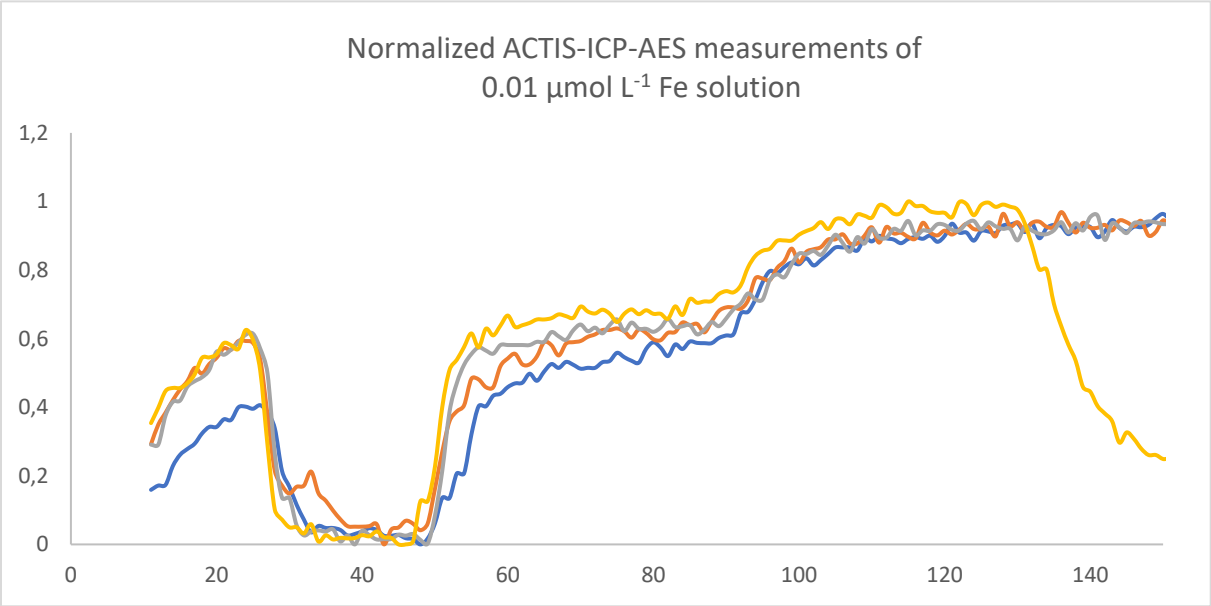

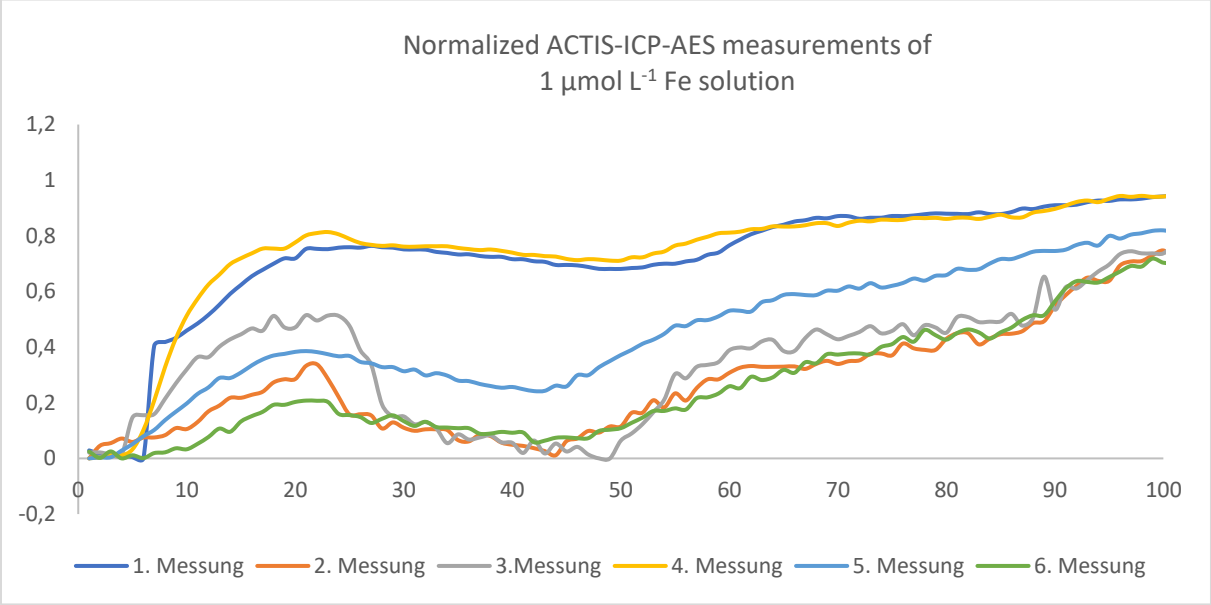

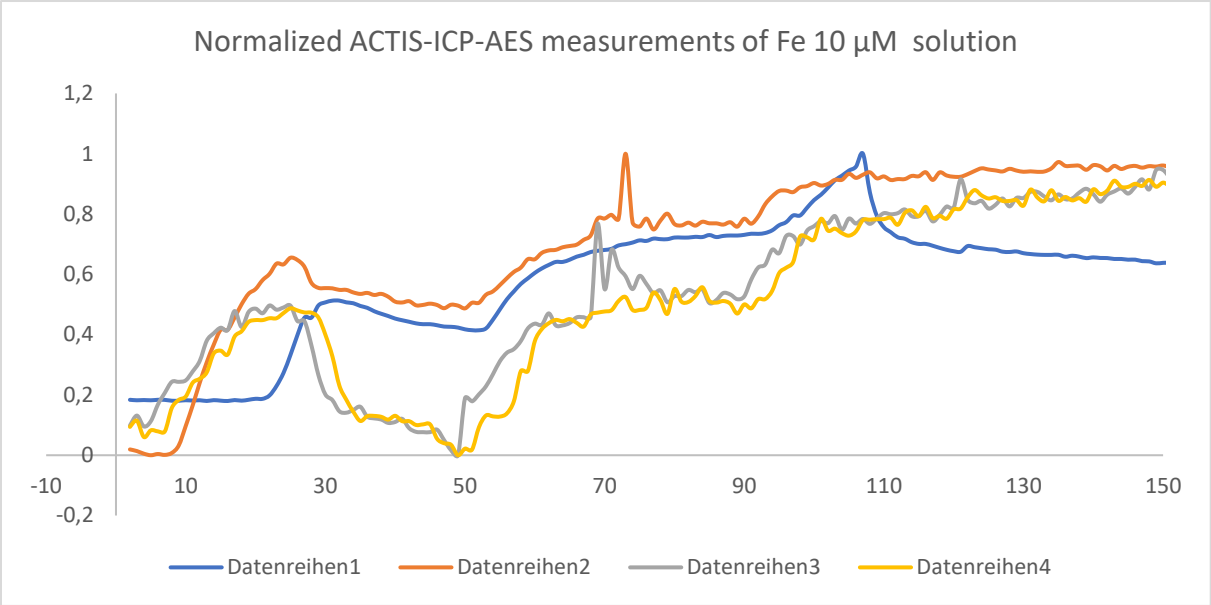
Normalized ACTIS-ICP-AES measurements of Fe 10 µM solution
1,2
1
0,8
0,6
0,4
0,2
0
-0,2
-10
10
30
50
70
90
110
130
150
Datenreihen1
Datenreihen2
Datenreihen3
Datenreihen4

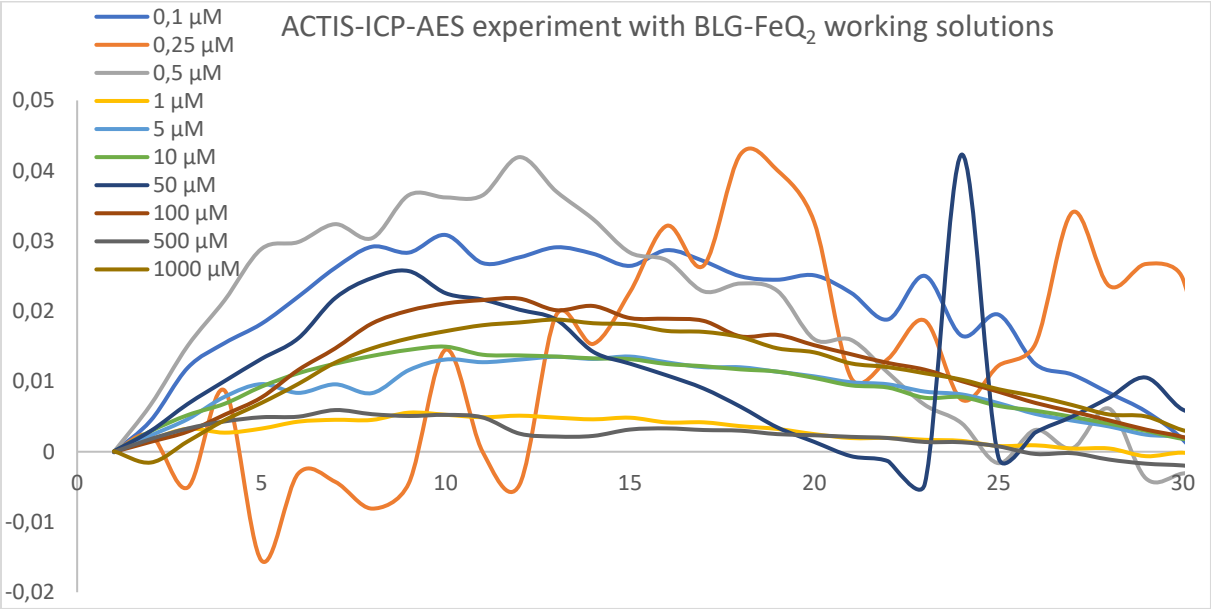
ACTIS-ICP-AES experiment with BLG-FeQ2 working solutions
0,1 µM
0,25 µM
0,5 µM
1 µM
5 µM
10 µM
50 µM
100 µM
500 µM
1000 µM
0,05
0,04
0,03
0,02
0,01
0
-0,01
-0,02
0
5
10
15
20
25
30

$[BLG]_0$

BLG-FeQ2 prACTISed evaluation - without 0.25 and 50 µM

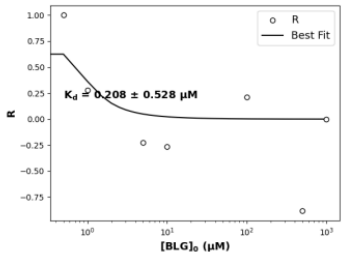

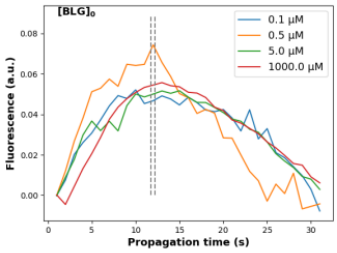

Propogation flow rate	68
Injection flow rate	0
Injection time (s)	0
Separation capillary length	60
Separation capillary diameter	127
Injection loop length	13
Injection loop diameter	50
Protein name	BLG
Ligand name	FeQ2
Number of Concentrations	8
Initial Ligand concentration [L]0 (µM)	1
Type of Data	F
Compensation procedure	N
[P]0 reference for MS normalization (µM)	nan
Window width (%)	2
Determination of peak	P
Manually determined peaks	nan
[P]0 to programmaticlly determine peak	0.5

Conc	Avg Sig (S)	S Std Dev	S Rel Std Dev	R value	R Std Dev	R Rel Std Dev
0.1 µM	0.04670018	0	0	nan	nan	nan
0.5 µM	0.07432935	0	0	1	0	0
1.0 µM	0.06004597	0	0	0.2807535	0	0
5.0 µM	0.04999841	0	0	-0.2251962	0	0
10.0 µM	0.04921969	0	0	-0.2644088	0	0
100.0 µM	0.05863858	0	0	0.209884	0	0
500.0 µM	0.0369122	0	0	-0.884158	0	0
1000.0 µM	0.05447053	0	0	0	0	0

Kd: 0.2080 ± 0.5279 µM
R^2: 0.4412
Chi^2: 1904.3568

Section 12: Computer simulations results

50 µm

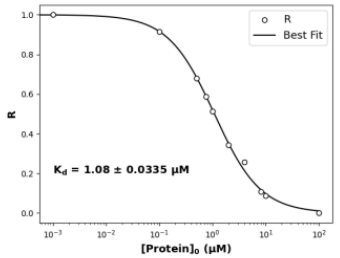

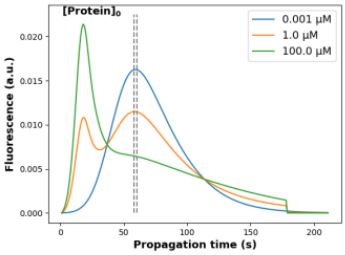

Propogation flow rate	68
Injection flow rate	0
Injection time (s)	0
Separation capillary length	60
Separation capillary diameter	127
Injection loop length	13
Injection loop diameter	50
Protein name	Protein
Ligand name	Compound
Number of Concentrations	10
Initial Ligand concentration [L]0 (µM)	0.01
Type of Data	F
Compensation procedure	N
[P]0 reference for MS normalization (µM)	nan
Window width (%)	2
Determination of peak	P
Manually determined peaks	nan
[P]0 to programmaticlly determine peak	0.001

Conc	Avg Sig (S)	S Std Dev	S Rel Std Dev	R value	R Std Dev	R Rel Std Dev
0.001 µM	0.01624896	0	0	1	0	0
0.1 µM	0.01541895	0	0	0.9153952	0	0
0.5 µM	0.01311756	0	0	0.6808096	0	0
0.75 µM	0.01218852	0	0	0.5861105	0	0
1.0 µM	0.01148269	0	0	0.514163	0	0
2.0 µM	0.00980613	0	0	0.3432647	0	0
4.0 µM	0.00895256	0	0	0.2562613	0	0
8.0 µM	0.00750828	0	0	0.1090165	0	0
10.0 µM	0.00729567	0	0	0.08737033	0	0
100.0 µM	0.00643853	0	0	0	0	0

Kd: 1.0783 ± 0.0335 µM
R^2: 0.9979
Chi^2: 0.0218

100 µm

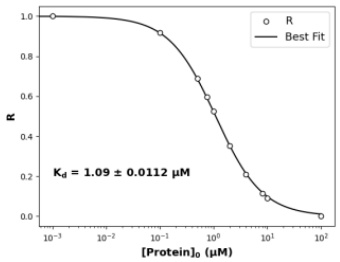

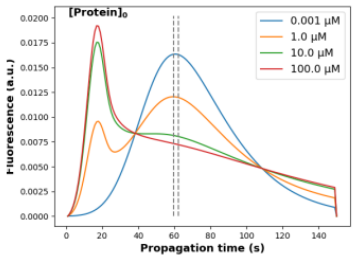

Propogation flow rate	68
Injection flow rate	0
Injection time (s)	0
Separation capillary length	60
Separation capillary diameter	127
Injection loop length	13
Injection loop diameter	50
Protein name	Protein
Ligand name	Compound
Number of Concentrations	10
Initial Ligand concentration [L]0 (µM)	0.01
Type of Data	F
Compensation procedure	N
[P]0 reference for MS normalization (µM)	nan
Window width (%)	2
Determination of peak	P
Manually determined peaks	nan
[P]0 to programmaticlly determine peak	0.001

Conc	Avg Sig (S)	S Std Dev	S Rel Std Dev	R value	R Std Dev	R Rel Std Dev
0.001 µM	0.01633113	0	0	1	0	0
0.1 µM	0.01559172	0	0	0.9183847	0	0
0.5 µM	0.01351606	0	0	0.6892746	0	0
0.75 µM	0.01266736	0	0	0.5955951	0	0
1.0 µM	0.01201834	0	0	0.5239572	0	0
2.0 µM	0.01046195	0	0	0.3521632	0	0
4.0 µM	0.00917406 6	0	0	0.2100075	0	0
8.0 µM	0.00829418 1	0	0	0.1128863	0	0
10.0 µM	0.00809182 1	0	0	0.09054988	0	0
100.0 µM	0.00727147	0	0	0	0	0

Kd: 1.0852 ± 0.0112 µM
R^2: 0.9998
Chi^2: 0.0118

150 µm

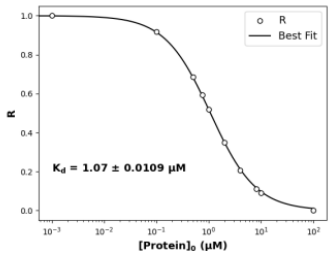

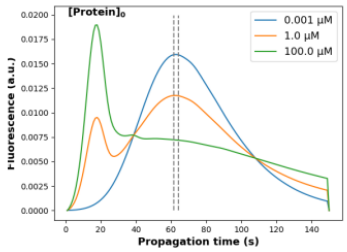

Propogation flow rate	68
Injection flow rate	0
Injection time (s)	0
Separation capillary length	60
Separation capillary diameter	127
Injection loop length	13
Injection loop diameter	50
Protein name	Protein
Ligand name	Compound
Number of Concentrations	10
Initial Ligand concentration [L]0 (µM)	0.01
Type of Data	F
Compensation procedure	N
[P]0 reference for MS normalization (µM)	nan
Window width (%)	2
Determination of peak	P
Manually determined peaks	nan
[P]0 to programmaticlly determine peak	0.001

Conc	Avg Sig (S)	S Std Dev	S Rel Std Dev	R value	R Std Dev	R Rel Std Dev
0.001 µM	0.01592857	0	0	1	0	0
0.1 µM	0.01520697	0	0	0.9172642	0	0
0.5 µM	0.0131907	0	0	0.6860838	0	0
0.75 µM	0.01237024	0	0	0.5920118	0	0
1.0 µM	0.01174436	0	0	0.5202505	0	0
2.0 µM	0.01024887	0	0	0.3487813	0	0
4.0 µM	0.00901713 4	0	0	0.2075534	0	0
8.0 µM	0.00817858 1	0	0	0.1114071	0	0
10.0 µM	0.00798606 67	0	0	0.08933389	0	0
100.0 µM	0.00720692 9	0	0	0	0	0

Kd: 1.0694 ± 0.0109 µM
R^2: 0.9998
Chi^2: 0.0116

250 µm

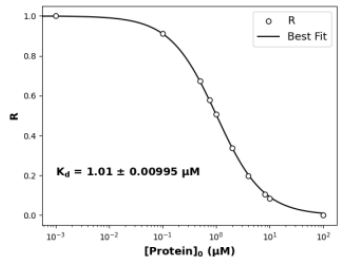

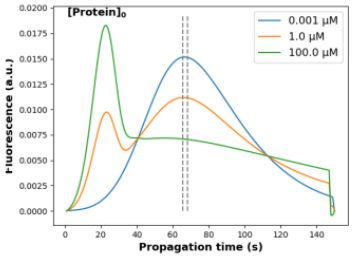

Propogation flow rate	68
Injection flow rate	0
Injection time (s)	0
Separation capillary length	60
Separation capillary diameter	127
Injection loop length	13
Injection loop diameter	50
Protein name	Protein
Ligand name	Compound
Number of Concentrations	10
Initial Ligand concentration [L]0 (µM)	0.01
Type of Data	F
Compensation procedure	N
[P]0 reference for MS normalization (µM)	nan
Window width (%)	2
Determination of peak	P
Manually determined peaks	nan
[P]0 to programmaticlly determine peak	0.001

Conc	Avg Sig (S)	S Std Dev	S Rel Std Dev	R value	R Std Dev	R Rel Std Dev
0.001 µM	0.01516081	0	0	1	0	0
0.1 µM	0.0144576	0	0	0.9130663	0	0
0.5 µM	0.01252638	0	0	0.6743207	0	0
0.75 µM	0.01175442	0	0	0.5788873	0	0
1.0 µM	0.01117082	0	0	0.5067409	0	0
2.0 µM	0.00979451	0	0	0.3366003	0	0
4.0 µM	0.00867983	0	0	0.198799	0	0
8.0 µM	0.00793052	0	0	0.1061648	0	0
10.0 µM	0.00775599	0	0	0.08503083	0	0
100.0 µM	0.00707183	0	0	0	0	0

Kd: 1.0138 ± 0.0100 µM
R^2: 0.9998
Chi^2: 0.0111

300 µm

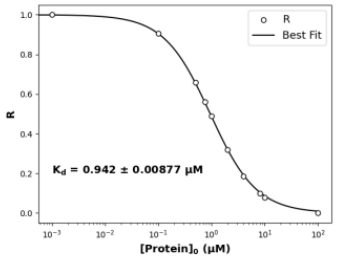

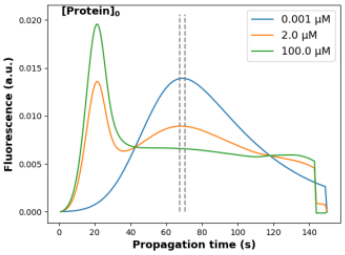

Propogation flow rate	68
Injection flow rate	0
Injection time (s)	0
Separation capillary length	60
Separation capillary diameter	127
Injection loop length	13
Injection loop diameter	50
Protein name	Protein
Ligand name	Compound
Number of Concentrations	10
Initial Ligand concentration [L]0 (µM)	0.01
Type of Data	F
Compensation procedure	N
[P]0 reference for MS normalization (µM)	nan
Window width (%)	2
Determination of peak	P
Manually determined peaks	nan
[P]0 to programmaticlly determine peak	0.001

Conc	Avg Sig (S)	S Std Dev	S Rel Std Dev	R value	R Std Dev	R Rel Std Dev
0.001 µM	0.01391486	0	0	1	0	0
0.1 µM	0.01323294	0	0	0.9069609	0	0
0.5 µM	0.01140622	0	0	0.6577334	0	0
0.75 µM	0.01069433	0	0	0.5606065	0	0
1.0 µM	0.01016288	0	0	0.4880977	0	0
2.0 µM	0.00893194	0	0	0.3201539	0	0
4.0 µM	0.00795735	0	0	0.1871858	0	0
8.0 µM	0.00731313	0	0	0.09929234	0	0
10.0 µM	0.00716737	0	0	0.07940494	0	0
100.0 µM	0.00658537	0	0	0	0	0

Kd: 0.9417 ± 0.0088 µM
R^2: 0.9998
Chi^2: 0.0103

500 µm

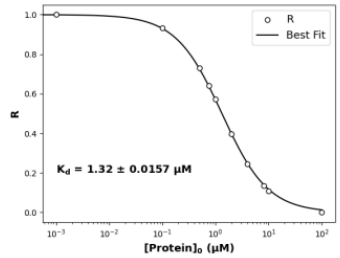

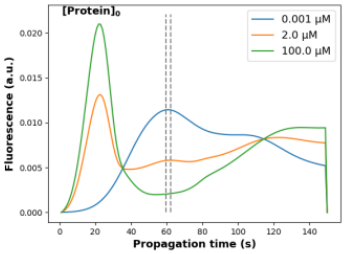

Propogation flow rate	68
Injection flow rate	0
Injection time (s)	0
Separation capillary length	60
Separation capillary diameter	127
Injection loop length	13
Injection loop diameter	50
Protein name	Protein
Ligand name	Compound
Number of Concentrations	10
Initial Ligand concentration [L]0 (µM)	0.01
Type of Data	F
Compensation procedure	N
[P]0 reference for MS normalization (µM)	nan
Window width (%)	2
Determination of peak	P
Manually determined peaks	nan
[P]0 to programmaticlly determine peak	0.001

Conc	Avg Sig (S)	S Std Dev	S Rel Std Dev	R value	R Std Dev	R Rel Std Dev
0.001 µM	0.0114304	0	0	1	0	0
0.1 µM	0.01079336	0	0	0.9319456	0	0
0.5 µM	0.00890015 3	0	0	0.7296992	0	0
0.75 µM	0.00807804 1	0	0	0.641875	0	0
1.0 µM	0.00742911 4	0	0	0.5725517	0	0
2.0 µM	0.00579656 8	0	0	0.3981506	0	0
4.0 µM	0.00435766 2	0	0	0.2444356	0	0
8.0 µM	0.00332477 9	0	0	0.1340952	0	0
10.0 µM	0.00308119 3	0	0	0.1080735	0	0
100.0 µM	0.00206953 1	0	0	0	0	0

Kd: 1.3168 ± 0.0157 µM
R^2: 0.9997
Chi^2: 0.0141

750 µm

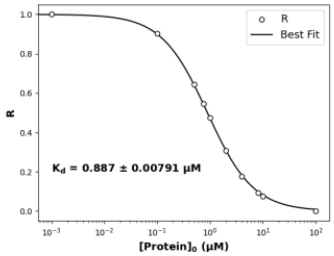

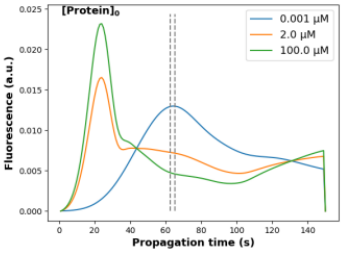

Propogation flow rate	68
Injection flow rate	0
Injection time (s)	0
Separation capillary length	60
Separation capillary diameter	127
Injection loop length	13
Injection loop diameter	50
Protein name	Protein
Ligand name	Compound
Number of Concentrations	10
Initial Ligand concentration [L]0 (µM)	0.01
Type of Data	F
Compensation procedure	N
[P]0 reference for MS normalization (µM)	nan
Window width (%)	2
Determination of peak	P
Manually determined peaks	nan
[P]0 to programmaticlly determine peak	0.001

Conc	Avg Sig (S)	S Std Dev	S Rel Std Dev	R value	R Std Dev	R Rel Std Dev
0.001 µM	0.01296747	0	0	1	0	0
0.1 µM	0.0121512	0	0	0.9017272	0	0
0.5 µM	0.01001032	0	0	0.6439833	0	0
0.75 µM	0.00919353 5	0	0	0.5456499	0	0
1.0 µM	0.00859003 2	0	0	0.4729932	0	0
2.0 µM	0.00721231 9	0	0	0.3071283	0	0
4.0 µM	0.00614101 5	0	0	0.1781525	0	0
8.0 µM	0.00544210 8	0	0	0.09401002	0	0
10.0 µM	0.00528497 4	0	0	0.07509242	0	0
100.0 µM	0.00466123 9	0	0	0	0	0

Kd: 0.8870 ± 0.0079 µM
R^2: 0.9998
Chi^2: 0.0098

1000 µm

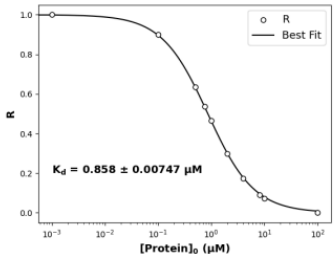

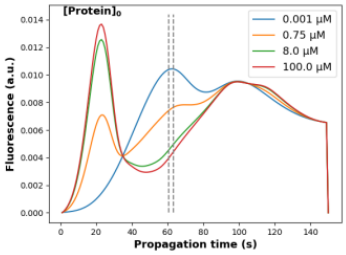

Propogation flow rate	68
Injection flow rate	0
Injection time (s)	0
Separation capillary length	60
Separation capillary diameter	127
Injection loop length	13
Injection loop diameter	50
Protein name	Protein
Ligand name	Compound
Number of Concentrations	10
Initial Ligand concentration [L]0 (µM)	0.01
Type of Data	F
Compensation procedure	N
[P]0 reference for MS normalization (µM)	nan
Window width (%)	2
Determination of peak	P
Manually determined peaks	nan
[P]0 to programmaticlly determine peak	0.001

Conc	Avg Sig (S)	S Std Dev	S Rel Std Dev	R value	R Std Dev	R Rel Std Dev
0.001 µM	0.010421 28	0	0	1	0	0
0.1 µM	0.009790 658	0	0	0.8986847	0	0
0.5 µM	0.008156 74	0	0	0.6361807	0	0
0.75 µM	0.007540 904	0	0	0.5372409	0	0
1.0 µM	0.007088 507	0	0	0.464559	0	0
2.0 µM	0.006064 036	0	0	0.2999683	0	0
4.0 µM	0.005275 281	0	0	0.1732474	0	0
8.0 µM	0.004764 369	0	0	0.0911646 7	0	0
10.0 µM	0.004649 897	0	0	0.0727736 4	0	0
100.0 µM	0.004196 928	0	0	0	0	0

Kd: 0.8577 ± 0.0075 µM
R^2: 0.9998
Chi^2: 0.0095

1250 µm

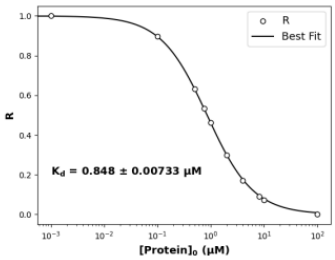

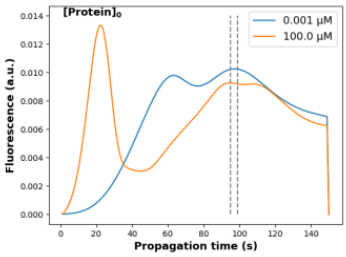

Propogation flow rate	68
Injection flow rate	0
Injection time (s)	0
Separation capillary length	60
Separation capillary diameter	127
Injection loop length	13
Injection loop diameter	50
Protein name	Protein
Ligand name	Compound
Number of Concentrations	10
Initial Ligand concentration [L]0 (µM)	0.01
Type of Data	F
Compensation procedure	N
[P]0 reference for MS normalization (µM)	nan
Window width (%)	2
Determination of peak	P
Manually determined peaks	nan
[P]0 to programmaticlly determine peak	0.001

Conc	Avg Sig (S)	S Std Dev	S Rel Std Dev	R value	R Std Dev	R Rel Std Dev
0.001 µM	0.010248 82	0	0	1	0	0
0.1 µM	0.010145 12	0	0	0.8976748	0	0
0.5 µM	0.009877 522	0	0	0.6336207	0	0
0.75 µM	0.009777 065	0	0	0.5344941	0	0
1.0 µM	0.009703 408	0	0	0.461813	0	0
2.0 µM	0.009537 047	0	0	0.2976544	0	0
4.0 µM	0.009409 374	0	0	0.1716713	0	0
8.0 µM	0.009326 864	0	0	0.0902537 8	0	0
10.0 µM	0.009308 397	0	0	0.0720319 4	0	0
100.0 µM	0.009235 399	0	0	0	0	0

Kd: 0.8484 ± 0.0073 µM
R^2: 0.9998
Chi^2: 0.0094

Section 12: Computer simulations with added noise

50 µm with noise

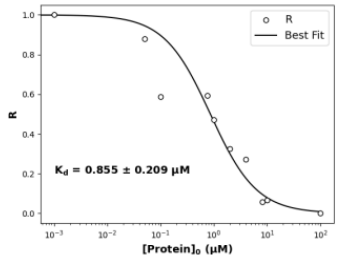

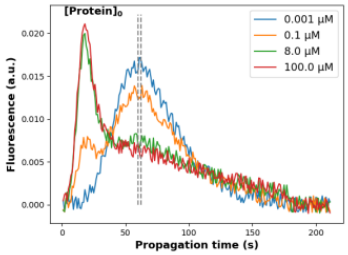

Propogation flow rate	68
Injection flow rate	0
Injection time (s)	0
Separation capillary length	60
Separation capillary diameter	127
Injection loop length	13
Injection loop diameter	50
Protein name	Protein
Ligand name	Compound
Number of Concentrations	10
Initial Ligand concentration [L]0 (µM)	0.01
Type of Data	F
Compensation procedure	N
[P]0 reference for MS normalization (µM)	nan
Window width (%)	2
Determination of peak	P
Manually determined peaks	nan
[P]0 to programmaticlly determine peak	0.001

Conc	Avg Sig (S)	S Std Dev	S Rel Std Dev	R value	R Std Dev	R Rel Std Dev
0.001 µM	0.01665028	0	0	1	0	0
0.05 µM	0.01538978	0	0	0.878497	0	0
0.1 µM	0.01237602	0	0	0.5879912	0	0
0.75 µM	0.01243601	0	0	0.5937741	0	0
1.0 µM	0.01117995	0	0	0.4726988	0	0
2.0 µM	0.00964154	0	0	0.3244067	0	0
4.0 µM	0.00909187 7	0	0	0.271423	0	0
8.0 µM	0.00686726	0	0	0.0569804	0	0
10.0 µM	0.00695409 9	0	0	0.0653563	0	0
100.0 µM	0.00627608	0	0	0	0	0

Kd: 0.8545 ± 0.2093 µM
R^2: 0.8932
Chi^2: 0.1979

250 µm ideal inputs - norm-short - noise

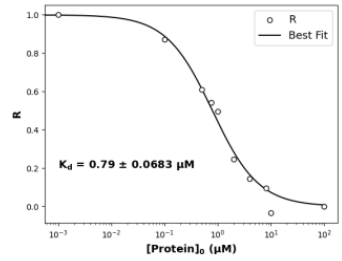

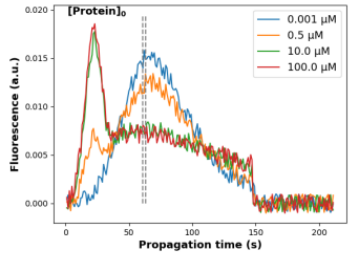

Propogation flow rate	68
Injection flow rate	0
Injection time (s)	0
Separation capillary length	60
Separation capillary diameter	127
Injection loop length	13
Injection loop diameter	50
Protein name	Protein
Ligand name	Compound
Number of Concentrations	10
Initial Ligand concentration [L]0 (µM)	0.01
Type of Data	F
Compensation procedure	N
[P]0 reference for MS normalization (µM)	nan
Window width (%)	2
Determination of peak	P
Manually determined peaks	nan
[P]0 to programmaticlly determine peak	0.001

Conc	Avg Sig (S)	S Std Dev	S Rel Std Dev	R value	R Std Dev	R Rel Std Dev
0.001 µM	0.01487314	0	0	1	0	0
0.1 µM	0.01394203	0	0	0.8725359	0	0
0.5 µM	0.01203475	0	0	0.6114401	0	0
0.75 µM	0.01152612	0	0	0.5418116	0	0
1.0 µM	0.01118683	0	0	0.4953636	0	0
2.0 µM	0.00936572 5	0	0	0.2460643	0	0
4.0 µM	0.00861973 2	0	0	0.1439418	0	0
8.0 µM	0.00827094 3	0	0	0.0961944 5	0	0
10.0 µM	0.00731445 7	0	0	-0.034743 5	0	0
100.0 µM	0.00756825 4	0	0	0	0	0

Kd: 0.7899 ± 0.0683 µM
R^2: 0.9853
Chi^2: 0.1833

1250 µm with noise

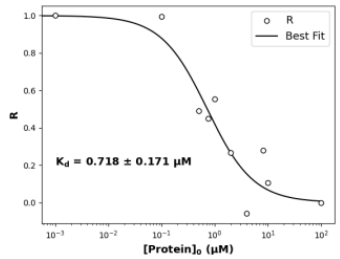

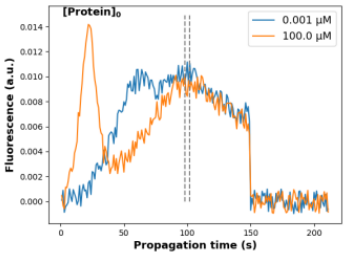

Propogation flow rate	68
Injection flow rate	0
Injection time (s)	0
Separation capillary length	60
Separation capillary diameter	127
Injection loop length	13
Injection loop diameter	50
Protein name	Protein
Ligand name	Compound
Number of Concentrations	10
Initial Ligand concentration [L]0 (µM)	0.01
Type of Data	F
Compensation procedure	N
[P]0 reference for MS normalization (µM)	nan
Window width (%)	2
Determination of peak	P
Manually determined peaks	nan
[P]0 to programmaticlly determine peak	0.001

Conc	Avg Sig (S)	S Std Dev	S Rel Std Dev	R value	R Std Dev	R Rel Std Dev
0.001 µM	0.01024514	0	0	1	0	0
0.1 µM	0.01024131	0	0	0.9964631	0	0
0.5 µM	0.00969268	0	0	0.4895824	0	0
0.75 µM	0.00964780	0	0	0.4481248	0	0
1.0 µM	0.00976043	0	0	0.552185	0	0
2.0 µM	0.00945145	0	0	0.2667109	0	0
4.0 µM	0.00909831	0	0	-0.0595564	0	0
8.0 µM	0.00946657	0	0	0.2806852	0	0
10.0 µM	0.00927808	0	0	0.1065347	0	0
100.0 µM	0.00916277	0	0	0	0	0

Kd: 0.7176 ± 0.1708 µM
R^2: 0.8954
Chi^2: 0.8814

Table 19: K_d values and corresponding standard deviations (all values given in µmol L^{-1}) resulted in evaluation of separagrams with and without noise added. Simulated K_d was set to 1 µmol L^{-1}.

Transfer capillary inner diameter	Without noise		With noise	
	K_d	Std. dev.	K_d	Std. dev.
50 µm	1.0783	0.0335	0.8545	0.2093
250 µm	1.0138	0.0100	0.7899	0.0683
1250 µm	0.8484	0.0073	0.7176	0.1708